(12) INTERNATIONAL APPLICATION PUBLISHED UNDER THE PATENT COOPERATION TREATY (PCT)

(19) World Intellectual Property Organization
International Bureau

(43) International Publication Date
20 February 2025 (20.02.2025)

WIPO | PCT

(10) International Publication Number
WO 2025/035209 A1

(51) International Patent Classification:
G01N 27/26 (2006.01) *G01N 27/327* (2006.01)

(21) International Application Number:
PCT/CA2024/051053

(22) International Filing Date:
09 August 2024 (09.08.2024)

(25) Filing Language: English

(26) Publication Language: English

(30) Priority Data:
63/532,231 11 August 2023 (11.08.2023) US

(71) Applicant: **MCMASTER UNIVERSITY** [CA/CA]; 1280 Main Street West, Hamilton, Ontario L8S 4L8 (CA).

(72) Inventors: **SOLEYMANI, Leyla**; 21 Ennisclare Dr. E., Oakville, Ontario L6J 4N3 (CA). **LI, Yingfu**; 87 Pirie Drive, Dundas, Ontario L9H 6Y2 (CA). **SEN, Payel**; 560 North Service Rd., Grimsby, Ontario L3M 0G1 (CA). **GU, Jimmy**; 4809 Rosebush Road, Mississauga, Ontario L5M 5N2 (CA). **ZHANG, Zijie**; 760 Mohawk Rd. W., Hamilton, Ontario L9C 6P6 (CA). **ADHIKARI, Bal Ram**; 125 Wellington Street North, Hamilton, Ontario L8R 3J4 (CA). **LI, Jiuxing**; 232 Broadway Avenue, Hamilton, Ontario L8S 2W6 (CA).

(74) Agent: **SZWERAS, Melanie** et al.; c/o SMART & BIGGAR LP, Scotia Plaza, 40 King Street West, 40th Floor, Toronto, Ontario M5H 3Y2 (CA).

(81) Designated States *(unless otherwise indicated, for every kind of national protection available)*: AE, AG, AL, AM, AO, AT, AU, AZ, BA, BB, BG, BH, BN, BR, BW, BY, BZ, CA, CH, CL, CN, CO, CR, CU, CV, CZ, DE, DJ, DK, DM, DO, DZ, EC, EE, EG, ES, FI, GB, GD, GE, GH, GM, GT, HN, HR, HU, ID, IL, IN, IQ, IR, IS, IT, JM, JO, JP, KE, KG, KH, KN, KP, KR, KW, KZ, LA, LC, LK, LR, LS, LU, LY, MA, MD, MG, MK, MN, MU, MW, MX, MY, MZ, NA, NG, NI, NO, NZ, OM, PA, PE, PG, PH, PL, PT, QA, RO, RS, RU, RW, SA, SC, SD, SE, SG, SK, SL, ST, SV, SY, TH, TJ, TM, TN, TR, TT, TZ, UA, UG, US, UZ, VC, VN, WS, ZA, ZM, ZW.

(84) Designated States *(unless otherwise indicated, for every kind of regional protection available)*: ARIPO (BW, CV, GH, GM, KE, LR, LS, MW, MZ, NA, RW, SC, SD, SL, ST, SZ, TZ, UG, ZM, ZW), Eurasian (AM, AZ, BY, KG, KZ, RU, TJ, TM), European (AL, AT, BE, BG, CH, CY, CZ, DE, DK, EE, ES, FI, FR, GB, GR, HR, HU, IE, IS, IT, LT, LU, LV, MC, ME, MK, MT, NL, NO, PL, PT, RO, RS, SE, SI, SK, SM, TR), OAPI (BF, BJ, CF, CG, CI, CM, GA, GN, GQ, GW, KM, ML, MR, NE, SN, TD, TG).

Published:
— *with international search report (Art. 21(3))*
— *with sequence listing part of description (Rule 5.2(a))*
— *in black and white; the international application as filed contained color or greyscale and is available for download from PATENTSCOPE*

(54) Title: LABEL-FREE MULTIMERIC APTAMER BIOSENSOR SYSTEM FOR REAL-TIME MONITORING OF TARGET ANALYTES IN A ONE-POT CONFIGURATION

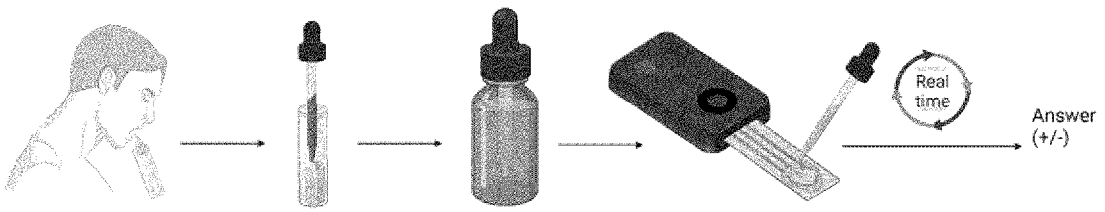

FIG. 3A

(57) Abstract: This disclosure relates to a biosensor for detecting a target analyte in a sample comprising: a) an electrochemical impedance spectroscopy (EIS) module comprising (i) a working electrode, operable at a single frequency for real-time monitoring of aptamer binding to target, aptamer- target dissociation, or aptamer or target degradation on the working electrode, (ii) a counter electrode, (iii) a reference electrode, and (iv) a circuit compatible with potentiostat; b) a multimeric aptamer comprising two or more units for specific target binding and formation of an aptamer-target complex in solution, wherein the target comprises two or more binding sites, wherein the multimeric aptamer has a K_d < about 300 pM; wherein the multimeric aptamer is configured to bind to the surface of the working electrode, and wherein the biosensor system is configured to operate in a wash-free and single-pot format.

WO 2025/035209 A1

LABEL-FREE MULTIMERIC APTAMER BIOSENSOR SYSTEM FOR REAL-TIME MONITORING OF TARGET ANALYTES IN A ONE-POT CONFIGURATION

CROSS-REFERENCE TO RELATED APPLICATION

[0001] This application claims the benefit of United States Provisional Patent Application No. 63/532,231 filed August 11, 2023, herein incorporated by reference in its entirety.

SEQUENCE LISTING

[0002] A computer readable form of the Sequence Listing "3244-P72630PC00_SequenceListing" (13,366 bytes) was created on August 9, 2024, is filed herewith by electronic submission.

FIELD

[0003] The present disclosure relates to biosensor systems, and in particular, to electrochemical biosensor systems, methods, and kits for target analyte detection.

BACKGROUND

[0004] Despite tremendous efforts towards developing rapid infectious disease antigen tests for point-of-need diagnostics, tests that offer high clinical sensitivity and specificity together with simple mix and measure operation remain elusive. Lateral flow assays present a gold standard for easy operation and are amenable to widespread use at the point-of-need; however, they fail to offer reliable results, especially in complex matrices such as saliva[1]. Electrochemical[2] and optical[3] affinity-based assays using nanomaterials[4,5] and nano-confinement[3,6] offer excellent analytical sensitivity; however, they often rely on multi-step sample manipulation or wash steps to maintain their analytical performance in clinical samples. A major obstacle in developing high performance and simple assays for widespread use is the need for wash steps for both removing unreacted reagents and preserving analytical performance in clinical samples such as saliva that contain a large amount of interfering proteins, organics and enzymes.[7] Using peripheral systems that automate or integrate washing steps such as microfluidics, paper-based fluidics, or manual fluidics is one way of reducing the burden of manual washing or sample manipulation; however, these methods add to the assay complexity, scalability, and cost, indicating the need for truly wash-free and single-pot assays.

[0005] In the context of electrochemical biosensing, affinity-based assays based on structure-switching aptamers are capable of overcoming washing and offering single-pot operation. However, a large fraction of aptamers selected through systemic evolution of ligands by exponential enrichment (SELEX), despite high affinity and selectivity, do not present sufficient structure switching to translate target binding to a measurable electrochemical signal change.[8] As such there is an unmet need for universal aptamer-based electrochemical assays, structure-switching or not, that operate in a wash-free and single-pot manner.

[0006] The background herein is included solely to explain the context of the disclosure. This is not to be taken as an admission that any of the material referred to was published, known, or part of the common general knowledge as of the priority date.

SUMMARY

[0007] The present disclosure describes a label-free multimeric aptamer biosensor system for real-time monitoring of target analytes in a one-pot configuration. The present inventors have employed a three-pronged approach that uses: 1) ultra-high affinity aptamers, 2) in-solution target extraction using multimeric aptamers, and 3) real-time signal monitoring, which has provided analytical sensitivity and precision that are necessary for combating signal-loss and signal variability encountered in wash-free and single-pot electrochemical readout. Using this three-pronged approach, it was demonstrated that a range of viral targets and protein biomarkers can be detected using a wash-free and single-pot format in native biological matrices and clinical samples. This approach is versatile and can be applied to a wide range of targets and their aptamers, providing a universal approach for aptamer-based target detection using electrochemical readout.

[0008] Accordingly, herein provided is a biosensor for detecting a target analyte in a sample comprising:

a) an electrochemical impedance spectroscopy (EIS) module comprising (i) a working electrode, operable at a single frequency for real-time monitoring of aptamer binding to target, aptamer-target dissociation, or aptamer or target degradation on the working electrode, (ii) a counter electrode, (iii) a reference electrode, and (iv) a circuit compatible with potentiostat;

b) a multimeric aptamer comprising two or more units for specific target binding and formation of an aptamer-target complex in solution, wherein the target comprises two or more binding sites, wherein the multimeric aptamer has a K_d < about 300 pM;

wherein the multimeric aptamer is configured to bind to the surface of the working electrode, and

wherein the biosensor system is configured to operate in a wash-free and single-pot format.

[0009] In some embodiments, the multimeric aptamer is biotinylated and the surface of the working electrode is coated with streptavidin. In some embodiments, the working electrode is a gold working electrode. In some embodiments, the counter electrode is a gold counter electrode. In some embodiments, the reference electrode is a silver reference electrode. In some embodiments, the biosensor system is configured to operate in a wash-free and single-pot format. In some embodiments, the solution comprises a readout buffer comprising phosphate buffer saline, KCl, and redox reporter. In some embodiments, the redox reporter comprises $K_3[Fe(CN)_6]/K_4[Fe(CN)_6]$, $[Fe(CN)_6]^{3-}/[Fe(CN)_6]^{4-}$, Q/H_2Q, $[Ru(NH_3)_6]^{3+}/[Ru(NH_3)_6]^{2+}$, MB^+/MBH_2, or MV^{2+}/MV^+ redox reporter. In some embodiments, the solution comprises redox reporter at about 2 mM $K_3[Fe(CN)_6]$ and about 2 mM $K_4[Fe(CN)_6]$. In some embodiments, the the solution comprises a blocking buffer comprising biotin-BSA and BSA. In some embodiments, the solution comprises about 0.01 μM biotin-BSA and about 0.1% BSA. In some embodiments, the the solution comprises a binding buffer comprising HEPES, NaCl, KCl, $MgCl_2$, and $CaCl_2$. In some embodiments, the solution comprises about 5 mM HEPES, pH about 7.4, about 15 mM NaCl, about 0.6 mM KCl, about 0.25 mM $MgCl_2$, and about 0.25 mM $CaCl_2$. In some embodiments, the sample is a clinical sample. In some embodiments, the sample is saliva. In some embodiments, the saliva is heat-treated saliva.

[0010] In some embodiments, the target is a protein target, a viral target, or a bacterial target. In some embodiments, the viral target is SARS-CoV-2 or influenza. In some embodiments, the viral target is SARS-CoV-2. In some embodiments, the SARS-CoV-2 is SARS-CoV-2 B.1.1.529 omicron variant. In some embodiments, the protein target is SARS-CoV-2 B.1.1.529 omicron variant spike protein. In some embodiments, the aptamer is a SARS-CoV-2 specific aptamer having the nucleic acid sequence of SEQ ID NO: 6, 7, or 11. In some embodiments, the biosensor system is configured to detect SARS-CoV-2 B.1.1.529 omicron

variant with a limit-of-detection of about 138 copies/mL in the solution comprising the redox buffer, the blocking buffer, and the binding buffer. In some embodiments, the biosensor system is configured to detect SARS-CoV-2 with a limit-of-detection of about 584 copies/mL in heat-treated saliva diluted to about 25% (v/v) in the solution comprising the redox buffer, the blocking buffer, and the binding buffer. In some embodiments, the viral target is influenza. In some embodiments, the aptamer is an influenza specific aptamer having the nucleic acid sequence of SEQ ID NO: 1, 2, or 9. In some embodiments, the protein target is vascular endothelial growth factor (VEGF). In some embodiments, the aptamer is a VEGF specific aptamer having the nucleic acid sequence of SEQ ID NO: 4, 5, or 10. In some embodiments, the biosensor system provides at least 80% sensitivity and at least 99% specificity. In some embodiments, the biosensor system provides at least 93% sensitivity. In some embodiments, the biosensor system provides at least 98% sensitivity. In some embodiments, the biosensor system provides 100% specificity.

[0011] Also provided is a method for detecting a label-free target real-time in a sample, comprising:

a) mixing the sample with a solution comprising a redox readout buffer, a binding buffer, a blocking buffer, and the multimeric aptamer of the biosensor system described herein to provide a mixture,

b) applying the mixture onto the working electrode of the biosensor system described herein,

c) measuring total impedance at a single frequency at real-time for about 30 minutes, and

d) calculating fold change of the total impedance ($\Delta Zt/Zt$),

wherein $\Delta Zt/Zt$ >= about 1.2 at any time from 1 minute to 30 minutes indicates the presence of the target in the sample.

[0012] In some embodiments, the $\Delta Z_t/Z_t$ is >= about 1.2 at about 14 minutes indicates the presence of the target in the sample. In some embodiments, the $\Delta Z_t/Z_t$ is >= about 1.2 at about 20 minutes indicates the presence of the target in the sample. In some embodiments, the $\Delta Z_t/Z_t$ is >= about 1.3 at 26 minutes indicates the presence of the target in the sample. In some embodiments, the single frequency is between about 1 and about 20 kHz. In some

embodiments, the single frequency is between about 12.6 and about 80 Hz. In some embodiments, the single frequency is about 12.6 Hz. In some embodiments, the total impedance is measured at intervals of every 2 minutes.

[0013] Also provided is a kit for detecting a label-free target in a sample, comprising the biosensor system described herein, further comprising at least one of a dropper, a collection tube, a container holding the redox readout buffer, a container holding the binding buffer, a container holding the block buffer, and instruction for use.

[0014] Other features and advantages of the present disclosure will become apparent from the following detailed description. It should be understood, however, that the detailed description and the specific examples, while indicating embodiments of the disclosure, are given by way of illustration only and the scope of the claims should not be limited by these embodiments, but should be given the broadest interpretation consistent with the description as a whole.

BRIEF DESCRIPTION OF THE DRAWINGS

[0015] Certain embodiments of the disclosure will now be described in greater detail with reference to the attached drawings in which:

[0016] **FIG. 1A** shows real-time monitoring of target binding using aptamers and electrochemical readout through electrochemical impedance spectroscopy to determine the frequency for real-time electrochemical readout in an exemplary embodiment of the disclosure. FIG. 1A shows impedance plots generated across a frequency range of 1-20 kHz, and $\Delta Z/Z$ signals obtained for both target (OPV at 10^4 copies/mL) and blank solutions using the monomeric aptamers MSA52 (left panel). Target-to-blank ratio (T/B) analyzed across the frequency range of 1-20 kHz, with particular focus on the frequency range of 12.6-80 Hz, which exhibited the best resolution for maximizing the T/B ratio (right panel).

[0017] **FIG. 1B** shows real-time monitoring of target binding (OPV at 10^4 copies/mL) in BR buffer to monomeric aptamer-modified electrodes without washing in an exemplary embodiment of the disclosure.

[0018] **FIG. 1C** shows real-time monitoring of target (OPV at 10^4 copies/mL) binding in BR buffer solution by monomeric aptamers, followed by target/aptamer complex binding to streptavidin-modified electrode surfaces in an exemplary embodiment of the disclosure.

[0019] **FIG. 1D** shows real-time of target (OPV at 10^4 copies/mL) binding in BR buffer solution by trimeric aptamers, followed by target/aptamer complex binding to streptavidin-modified electrode surfaces in an exemplary embodiment of the disclosure.

[0020] **FIG. 2A** shows the limit-of-detection of the RT-MAP Assay for detecting OPV spiked in buffer and saliva in an exemplary embodiment of the disclosure. FIG. 2A shows real-time signals obtained for 0-10^5 copies/mL of OPV spiked in BBR buffer. The insets demonstrate a schematic depicting the proposed binding mechanism and T/B refers to target-to-blank ratio.

[0021] **FIG. 2B** provides the plot of the peak impedance obtained for each OPV concentration from the corresponding real-time data (FIG. 2A), inferring a limit of detection of 138 copies/mL in buffer in an exemplary embodiment of the disclosure.

[0022] **FIG. 2C** shows the limit-of-detection of the RT-MAP Assay for detecting OPV spiked in buffer and saliva. FIG. 2C shows real-time signals obtained for 0-10^5 copies/mL of OPV spiked in BBR Buffer mixed with 25% heat-treated saliva in an exemplary embodiment of the disclosure. The insets demonstrate a schematic depicting the proposed binding mechanism and T/B refers to target-to-blank ratio.

[0023] **FIG. 2D** provides a plot of the peak impedance obtained for each OPV concentration from the corresponding real-time data (FIG. 2C), inferring a limit of detection of 584 copies/mL in 25% heat treated saliva in an exemplary embodiment of the disclosure.

[0024] **FIG. 3A** shows assay validation for analyzing clinical samples in an exemplary embodiment of the disclosure. FIG. 3A provides a schematic showing the steps followed by the user for clinical diagnosis.

[0025] **FIG. 3B** shows assay validation for analyzing clinical samples in an exemplary embodiment of the disclosure. FIG. 3B shows signals obtained at 2 min of real-time clinical testing for 18 known Negatives and 16 single Blind saliva samples.

[0026] **FIG. 3C** shows assay validation for analyzing clinical samples in an exemplary embodiment of the disclosure. FIG. 3C shows signals obtained at 10 min of real-time clinical testing for 18 known Negatives and 16 single Blind saliva samples.

[0027] **FIG. 3D** shows assay validation for analyzing clinical samples in an exemplary embodiment of the disclosure. FIG. 3D shows signals obtained at 18 min of real-time clinical testing for 18 known Negatives and 16 single Blind saliva samples.

[0028] **FIG. 3E** shows assay validation for analyzing clinical samples in an exemplary embodiment of the disclosure. FIG. 3E shows signals obtained at 26 min of real-time clinical testing for 18 known Negatives and 16 single Blind saliva samples.

[0029] **FIG. 3F** shows assay validation for analyzing clinical samples in an exemplary embodiment of the disclosure. FIG. 3F provides a box plot showing COVID-19 distribution for positive (infected) and negative (healthy) patient saliva samples corresponding to 2 min.

[0030] **FIG. 3G** shows assay validation for analyzing clinical samples in an exemplary embodiment of the disclosure. FIG. 3G provides a box plot showing COVID-19 distribution for positive (infected) and negative (healthy) patient saliva samples corresponding to 10 min.

[0031] **FIG. 3H** shows assay validation for analyzing clinical samples in an exemplary embodiment of the disclosure. FIG. 3H provides a box plot showing COVID-19 distribution for positive (infected) and negative (healthy) patient saliva samples corresponding to 18 min.

[0032] **FIG. 3I** shows assay validation for analyzing clinical samples in an exemplary embodiment of the disclosure. FIG. 3I provides a box plot showing COVID-19 distribution for positive (infected) and negative (healthy) patient saliva samples corresponding to 26 min.

[0033] **FIG. 3J** shows assay validation for analyzing clinical samples in an exemplary embodiment of the disclosure. FIG. 3J provides an Operating Characteristic (ROC) curve obtained for 2 min.

[0034] **FIG. 3K** shows assay validation for analyzing clinical samples in an exemplary embodiment of the disclosure. FIG. 3K provides a Receiver Operating Characteristic (ROC) curve obtained for 10 min.

[0035] **FIG. 3L** shows assay validation for analyzing clinical samples in an exemplary embodiment of the disclosure.

[0036] **FIG. 3M** shows assay validation for analyzing clinical samples in an exemplary embodiment of the disclosure. FIG. 3M provides a Receiver Operating Characteristic (ROC) curve obtained for 26 min.

[0037] **FIG. 4A** shows the limit of detection of the RT-MAP Assay for detecting Influenza A spiked in 25% heat treated saliva + BBR Buffer in an exemplary embodiment of the disclosure FIG. 4A shows real-time signals obtained for 0-10^6 copies/mL of Influenza A.

[0038] **FIG. 4B** shows the limit of detection of the RT-MAP Assay for detecting Influenza A spiked in 25% heat treated saliva + BBR Buffer in an exemplary embodiment of the disclosure. FIG. 4B shows the plot of the peak impedance obtained for each Influenza A concentration from the corresponding real-time data inferring a limit of detection of 408 copies/mL Influenza in 25% heat treated saliva and 0.96 pM $VEGF_{165}$ in buffer.

[0039] **FIG. 4C** shows the limit-of-detection of the RT-MAP Assay for detecting $VEGF_{165}$ spiked in BBR buffer in an exemplary embodiment of the disclosure. FIG. 4C shows real-time signals obtained for 0-2500 pM of $VEGF_{165}$. T/B refers to target-to-blank ratio.

[0040] **FIG. 4D** shows the limit-of-detection of the RT-MAP Assay for detecting $VEGF_{165}$ spiked in BBR buffer in an exemplary embodiment of the disclosure. FIG. 4D shows a plot of the peak impedance obtained for each $VEGF_{165}$ concentration from the corresponding real-time data inferring a limit of detection of 408 copies/mL Influenza in 25% heat treated saliva and 0.96 pM $VEGF_{165}$ in buffer.

[0041] **FIG. 5A** shows selecting the frequency for continuous monitoring in an exemplary embodiment of the disclosure. FIG. 5A shows $\Delta Z/Z$ signals obtained for target and blank using solution binding strategy recorded at single frequency of 12.6 Hz showing a T/B of 2.1 for monomeric aptamer and 3.5 for trimeric aptamer.

[0042] **FIG. 5B** shows selecting the frequency for continuous monitoring in an exemplary embodiment of the disclosure. FIG. 5B shows $\Delta Z/Z$ signals obtained for target and blank using solution binding strategy recorded at single frequency of 65 Hz showing a T/B of 2.2 for monomeric aptamer and 2.9 for trimeric aptamer.

[0043] **FIG. 5C** shows selecting the frequency for continuous monitoring in an exemplary embodiment of the disclosure. FIG. 5C shows $\Delta Z/Z$ signals obtained for target and blank using solution binding strategy recorded at single frequency of 80 Hz showing a T/B of 2.1 for monomeric aptamer and 3.5 for trimeric aptamer.

[0044] **FIG. 6A** shows blocking buffer using concentration of trimeric aptamer at 0.5 μM and frequency of 12.6 Hz in an exemplary embodiment of the disclosure. FIG. 6A shows

the results from varying concentrations of biotin-BSA while maintaining a constant percentage of BSA (0.1%). Among the tested concentrations, 0.01 μM biotin-BSA showed the highest target-to-blank ratio (T/B = 5) and was selected for further experimentations.

[0045] **FIG. 6B** shows blocking buffer using concentration of trimeric aptamer at 0.5 μM and frequency of 12.6 Hz in an exemplary embodiment of the disclosure. FIG. 6B shows the concentration of BSA using the concentration of biotin-BSA at 0.01 μM. A combination of 0.1% BSA and 0.01 μM biotin-BSA resulted in a T/B ratio of 5.

[0046] **FIG. 6C** shows blocking buffer using concentration of trimeric aptamer at 0.5 μM and frequency of 12.6 Hz in an exemplary embodiment of the disclosure. FIG. 6C shows signals obtained using a one-pot system, where the concentrations of BSA (0.1%), biotin-BSA (0.01 μM), and trimeric aptamer (0.5 μM) were sequentially added. This setup allowed for accurate measurement of the signal specifically attributed to target binding.

[0047] **FIG. 7A** shows dilution and pre-treatment of saliva in an exemplary embodiment of the disclosure. FIG. 7A provides a schematic illustrating the percentage dilution and treatment applied to saliva in each experimental setup.

[0048] **FIG. 7B** shows dilution and pre-treatment of saliva in an exemplary embodiment of the disclosure. FIG. 7B shows target (T) and blank (B) signals recorded for 10%, 25% and 50% diluted saliva samples without heat treatment (top) compared with diluted saliva samples with heat treatment at 60 °C for 10 minutes (bottom).

[0049] **FIG. 8A** shows pre-incubation time for clinical diagnosis in an exemplary embodiment of the disclosure. FIG. 8A provides a schematic illustrating an experimental protocol and treatment applied to saliva.

[0050] **FIG. 8B** shows pre-incubation time for clinical diagnosis in an exemplary embodiment of the disclosure. FIG. 8B shows change in $\Delta Z/Z$ signals recorded for 0 min, 5 min, 10 min pre-incubation using one individual COVID positive patient saliva sample.

[0051] **FIG. 9A** shows data processing pipeline for binary classification of clinical dataset in an exemplary embodiment of the disclosure.

[0052] **FIG. 9B** shows curve fitting with validated model for impedance kinetics data from select clinical samples in an exemplary embodiment of the disclosure.

[0053] **FIG. 9C** shows weights for first and second principal components (PC1 and PC2) generated from dimensionality reduction of curve fitting features in an exemplary embodiment of the disclosure.

[0054] **FIG. 9D** shows binary classification of clinical samples through support vector machine analysis. The clinical samples are visualized as a scatterplot with their first two principal components, overlaid with the decision map from support vector machine analysis. The decision map shows the boundaries between positive and negative samples. The inset table shows the confusion matrix of the support vector machine model on the test set of clinical samples.

[0055] **FIG. 10A** shows $\Delta Z/Z$ signals obtained for 19 COVID-negative saliva samples at 2 min to 30 min time points for establishing diagnostic threshold in an exemplary embodiment of the disclosure. The dotted line for each denotes the diagnostic threshold at each time point.

[0056] **FIG. 10B** shows $\Delta Z/Z$ signals obtained for 19 COVID-negative saliva samples at 12 min to 20 min time points for establishing diagnostic threshold in an exemplary embodiment of the disclosure. The dotted line for each denotes the diagnostic threshold at each time point.

[0057] **FIG. 10C** shows $\Delta Z/Z$ signals obtained for 19 COVID-negative saliva samples at 22 min to 30 min time points for establishing diagnostic threshold in an exemplary embodiment of the disclosure. The dotted line for each denotes the diagnostic threshold at each time point.

[0058] **FIG. 11A** shows $\Delta Z/Z$ signals obtained for 19 single-blinded saliva samples at 2 min to 10 min time points in an exemplary embodiment of the disclosure. The dotted line for each denotes the pre-established diagnostic threshold at each time point.

[0059] **FIG. 11B** shows $\Delta Z/Z$ signals obtained for 19 single-blinded saliva samples at 12 min to 20 min time points in an exemplary embodiment of the disclosure. The dotted line for each denotes the pre-established diagnostic threshold at each time point.

[0060] **FIG. 11C** shows $\Delta Z/Z$ signals obtained for 19 single-blinded saliva samples at 22 min to 30 min time points in an exemplary embodiment of the disclosure. The dotted line for each denotes the pre-established diagnostic threshold at each time point.

[0061] **FIG. 12A** shows receiver operating characteristic (ROC) curve obtained for 19 single-blinded saliva samples at 2 min to 10 min time points showing the sensitivity and specificity improvement with time in an exemplary embodiment of the disclosure.

[0062] **FIG. 12B** shows receiver operating characteristic (ROC) curve obtained for 19 single-blinded saliva samples at 12 min to 20 min time points showing the sensitivity and specificity improvement with time in an exemplary embodiment of the disclosure.

[0063] **FIG. 12C** shows receiver operating characteristic (ROC) curve obtained for 19 single-blinded saliva samples at 22 min to 30 min time points showing the sensitivity and specificity improvement with time in an exemplary embodiment of the disclosure.

[0064] **FIG. 13A** shows the assessment of the binding affinity of monomeric (RHA06) and trimeric (TRHA06) for influenza HA proteins using dot blot assay in an exemplary embodiment of the disclosure. FIG. 13A shows representative dot blot results.

[0065] **FIG. 13B** shows the assessment of the binding affinity of monomeric (RHA06) and trimeric (TRHA06) for influenza HA proteins using dot blot assay in an exemplary embodiment of the disclosure. FIG. 13B shows binding curves used to derive the K_d values and affinity enhancement folds. TRHA06 with control protein (BSA) and mutant trimeric aptamer with H3N2 were also included as controls. BA: bound aptamer; UA: unbound aptamer.

[0066] **FIG. 14A** shows a cooperativity assessment of binding trimeric H3N2-HA protein by the three arms of trimeric aptamer (TRHA06) aptamer by adding antisense sequence (AS) of RHA06 (SEQ ID NO: 1) in an exemplary embodiment of the disclosure.

[0067] **FIG. 14B** shows binding curves in an exemplary embodiment of the disclosure. FIG. 14B shows K_d increases indicating reduced affinity. The three arms of TRHA06 were determined bound with the trimeric HA protein.

[0068] **FIG. 15** shows the concentration of Influenza A trimeric aptamer (TRHA06) in an exemplary embodiment of the disclosure. FIG. 15 shows four H1A concentrations tested: 250 nM, 500 nM and 1 μM. Target-to-blank ratio (T/B) ratio obtained for 10^4 copies/mL H3N2 subtype of Influenza A shows that 500 nM of TRHA06 is the selected concentration.

[0069] **FIG. 16A** shows an assessment of the binding affinity of monomeric (H1A) and trimeric (TH1A) aptamers for $VEGF_{165}$ using dot blot assay in an exemplary embodiment of the disclosure. FIG. 16A provides a dot blot of the results.

[0070] **FIG. 16B** shows an assessment of the binding affinity of monomeric (H1A) and trimeric (TH1A) aptamers for $VEGF_{165}$ using dot blot assay in an exemplary embodiment of the disclosure. FIG. 16B shows binding curves used to derive the K_d values. Affinity enhanced ~78-fold.

[0071] **FIG. 17A** shows a cooperativity assessment of binding $VEGF_{165}$ by three arms of trimeric (TH1A) aptamer using antisense sequence (AS) of H1A (SEQ ID NO: 4) in an exemplary embodiment of the disclosure.

[0072] **FIG. 17B** shows binding curves in an exemplary embodiment of the disclosure. FIG. 17B shows K_d increased indicating reduced affinity. The three arms of TH1A were determined bound with VEGF protein, though VEGF was determined a dimeric protein.

[0073] **FIG. 18A** shows the concentration of $VEGF_{165}$ trimeric aptamer (TH1A) at 25 nM in an exemplary embodiment of the disclosure. Four TH1A concentrations were tested 25 nM, 100 nM, 250 nM and 500 nM. Target-to-blank ratio (T/B) ratio obtained for two concentrations (2.5 pM and 250 pM) of $VEGF_{165}$ shows that 250 nM of H1A is the selected concentration.

[0074] **FIG. 18B** shows the concentration of $VEGF_{165}$ trimeric aptamer (TH1A) at 100nM in an exemplary embodiment of the disclosure. Four TH1A concentrations were tested 25 nM, 100 nM, 250 nM and 500 nM. Target-to-blank ratio (T/B) ratio obtained for two concentrations (2.5 pM and 250 pM) of $VEGF_{165}$ shows that 250 nM of H1A is the selected concentration.

[0075] **FIG. 18C** shows the concentration of $VEGF_{165}$ trimeric aptamer (TH1A) at 250 nM in an exemplary embodiment of the disclosure. Four TH1A concentrations that were tested: 25 nM, 100 nM, 250 nM and (500 nM. Target-to-blank ratio (T/B) ratio obtained for two concentrations (2.5 pM and 250 pM) of $VEGF_{165}$ shows that 250 nM of H1A is the selected concentration.

[0076] **FIG. 18D** shows the concentration of $VEGF_{165}$ trimeric aptamer (TH1A) at 500nM in an exemplary embodiment of the disclosure. Four TH1A concentrations were tested: 25 nM, 100 nM, 250 nM and 500 nM. Target-to-blank ratio (T/B) ratio obtained for two concentrations (2.5 pM and 250 pM) of $VEGF_{165}$ shows that 250 nM of H1A is the selected concentration.

[0077] **FIG. 19A** shows the evaluating of analytical specificity in buffer and saliva samples in an exemplary embodiment of the disclosure. FIG. 19A shows signals obtained for 10^4 copies/mL of OPV and non-binding respiratory viruses spiked in BBR buffer.

[0078] **FIG. 19B** shows the evaluating of analytical specificity in buffer and saliva samples in an exemplary embodiment of the disclosure. FIG. 19B shows signals obtained for COVID assay in presence of specific (10^4 copies/mL OPV) target, non-binding target (10^4 copies/mL Influenza A) and a mixture of specific and non-binding target (10^4 copies/mL each of OPV + Influenza A) and Influenza assay in presence of specific (10^4 copies/mL Influenza A) target, non-binding target (10^4 copies/mL OPV) and a mixture of specific and non-binding target (10^4 copies/mL each of Influenza A + OPV) in BBR buffer. The insets show simple schematics to explain the experimental protocol.

[0079] Further aspects and features of the example embodiments described herein will appear from the following description taken together with the accompanying drawings.

DETAILED DESCRIPTION

I. Definitions

[0080] Unless otherwise indicated, the definitions and embodiments described in this and other sections are intended to be applicable to all embodiments and aspects of the present disclosure herein described for which they are suitable as would be understood by a person skilled in the art. It is also to be understood that the terminology used herein is for the purpose of describing particular aspects only and is not intended to be limiting.

[0081] The term "sample" or "test sample" as used herein refers to any material in which the presence or amount of a target analyte is unknown and can be determined in an assay. The sample can be from any source, for example, any biological (e.g. human or animal samples, including clinical samples), environmental (e.g. water, soil or air) or natural (e.g. plants) source, or from any manufactured or synthetic source (e.g. food or drinks). The sample can be comprised or is suspected of comprising one or more analytes. The sample can be a "biological sample" comprising cellular and non-cellular material, including, but not limited to, tissue samples, urine, blood, serum, other bodily fluids and/or secretions. The sample can be in its undiluted form or diluted in an appropriate diluent, for example, a buffer or an aqueous solution known in the art. In some embodiments, the sample comprises blood, plasma, urine, saliva, sputum, oropharyngeal and/or nasopharyngeal secretions.

[0082] The term "target", "analyte" or "target analyte" as used herein refers to any agent, including, but not limited to, a small inorganic molecule, small organic molecule, metal ion, biomolecule, toxin, biopolymer (such as a nucleic acid, carbohydrate, lipid, peptide, protein), cell, tissue, microorganism and virus, for which one would like to sense or detect. The analyte can be either isolated from a natural source or is synthetic. The analyte can be a single compound or a class of compounds, such as a class of compounds that share structural or functional features. The term analyte also includes combinations (e.g. mixtures) of compounds or agents such as, but not limited, to combinatorial libraries and samples from an organism or a natural environment.

[0083] The term "nucleic acid" as used herein refers to a polynucleotide or oligonucleotide, such as deoxyribonucleic acid (DNA), ribonucleic acid (RNA), modified nucleotides and/or nucleotide derivatives, and can be either double-stranded (ds) or single-stranded (ss). The term "strand" as used herein is understood to refer to nucleic acid unless otherwise stated. In some embodiments, modified nucleotides can contain one or more modified bases (e.g. tritiated bases and unusual bases such as inosine), modified backbones (e.g. peptide nucleic acid, PNA) and/or other chemically, enzymatically, or metabolically modified forms.

[0084] The term "severe acute respiratory syndrome coronavirus 2", "coronavirus 2", or "SARS-CoV-2" as used herein refer to a coronavirus first identified in Wuhan, China in 2019 that causes coronavirus disease (COVID-19). The virus previously had a provisional name, 2019 novel coronavirus (2019-nCoV), and has also been called the human coronavirus 2019 (HCoV-19 or hCoV-19). The term includes any variant of the SARS-CoV-2 virus with a variant and/or mutated nucleic acid sequence from the original version identified in Wuhan. Variants includes, but are not limited to, Alpha (B.1.1.7), Beta (B.1.351), Gamma (P.1), Delta (B.1617.2), and Omicron (B.1.1.529).

[0085] The term "spike protein" or "S protein" as used herein refers to a glycoprotein found on the surface of the severe acute respiratory syndrome coronavirus 2 (SARS-CoV-2), the virus responsible for COVID-19. The spike protein plays a role in the virus's ability to bind to and enter host cells. The S protein of SARS-CoV-2 consists of two functional subunits: S1 and S2. The S1 subunit contains the receptor-binding domain (RBD) that recognizes and binds to the human angiotensin-converting enzyme 2 (ACE2) receptor. This binding facilitates the virus's attachment to the surface of host cells, primarily in the respiratory tract. The S2 subunit

mediates fusion between the viral and host cell membranes, allowing the viral genome to enter the host cell and initiate infection. The spike protein is a useful marker for detecting the presence of SARS-CoV-2.

[0086] The term "influenza", "flu", or "influenza virus" as used herein refers to a group of viruses that cause acute respiratory illness in humans and various other animals. Influenza viruses are classified into four types: A, B, C, and D. Type A and B viruses cause seasonal epidemics in humans, while type C causes mild respiratory illness, and type D primarily affects cattle. Influenza A viruses are further divided into subtypes based on the hemagglutinin (H) and neuraminidase (N) proteins on their surface, such as H1N1 and H3N2. These subtypes can further evolve into various strains, including those responsible for pandemics like the H1N1 pandemic in 2009. The term includes any variant of the influenza virus with a variant and/or mutated nucleic acid sequence from the original version identified. This includes, but is not limited to, various seasonal strains that may emerge and circulate each year.

[0087] The term "hemagglutinin" or "HA" as used herein refers to a glycoprotein found on the surface of the influenza virus. It plays a role in the virus's ability to infect a host. HA is responsible for binding the virus to cells with sialic acid on the membranes, such as cells in the human respiratory tract. This binding allows the virus to be internalized by the host cell, initiating infection. There are 18 different HA subtypes in influenza A viruses, labeled H1 through H18. These subtypes can combine with various neuraminidase (NA) subtypes to create different strains of the virus. The HA subtype contributes to the naming of the strain, such as H1N1 or H3N2. HA is a useful marker for detecting the presence of influenza virus.

[0088] The term "vascular endothelial growth factor" or "VEGF" or "VEGF-A" refers to a signal protein produced by cells that stimulates the formation of blood vessels, the protein. VEGF is part of the system that restores the oxygen supply to tissues when blood circulation is inadequate. It is a key driver of angiogenesis, which is the formation of new blood vessels from pre-existing vessels. VEGF-A has several isoforms (in human: $VEGF_{121}$, $VEGF_{121b}$, $VEGF_{145}$, $VEGF_{165}$, $VEGF_{165b}$, $VEGF_{189}$, and $VEGF_{206}$), and its dysregulation has been associated with various pathological conditions, including cancer, where it may contribute to the growth of tumors by providing them with increased blood supply.

[0089] The term "electrochemical impedance spectroscopy" or "EIS" as used herein refers to an analytical technique used to characterize the behavior of electrochemical systems.

EIS is a method used to study and model the complex impedance (resistance and reactance) of an electrochemical system as a function of frequency, for example, to assess the reactions and processes occurring at the interface of an electrode and an electrolyte. In EIS, a small sinusoidal voltage or current is applied to the system, and the resultant current or voltage is measured. By sweeping through a range of frequencies, one can obtain impedance data that can be represented as a Bode plot or a Nyquist plot, which gives insights into the mechanistic details of the electrochemical process. On the other hand, running it at a single frequency provides a single impedance (analogous to a point on the Nyquist plot) value instead of a full spectrum across frequencies which helps in giving insights into the kinetic and mechanistic details of the electrochemical processes. The impedance data obtained from the EIS spectra can be, for example, fitted to a Randles circuit, which is a commonly used equivalent circuit model in impedance analysis. By fitting the Nyquist plot to the Randles circuit, the charge transfer resistance (Rct) signals can be obtained. On the other hand, at single frequency, no fitting is required as the method directly offers the impedance value for easy analysis. With respect to binding of an aptamer to a target, the skilled person appreciates that aptamer-target association increases impedance while both aptamer and target degradation decreases impedance. This gives rise to the kinetic trend which increases initially and then starts decreasing.

[0090] The term "electrochemical impedance spectroscopy module" or "EIS module" refers to a tool or component designed to facilitate or conduct EIS measurements within an electrochemical system or a broader analytical device, such as a biosensor system. The EIS module is a hardware or software component designed to carry out EIS measurements. The EIS module can include a working electrode, a reference, a counter electrode, and a circuit compatible with potentiostat. The EIS module can further incorporate a software component that can include algorithms and routines to control the hardware, collect and analyze the data, and visualize the results. Generally, the software is also capable of fitting the measured impedance data to equivalent circuit models to extract meaningful parameters related to the electrochemical system. As well, when using an EIS module at single frequency, the software can directly provide parameters which are relevant to accurate electrochemical interpretation.

[0091] In understanding the scope of the present disclosure, the term “comprising” and its derivatives, as used herein, are intended to be open ended terms that specify the presence of the stated features, elements, components, groups, integers, and/or steps, but do not exclude the presence of other unstated features, elements, components, groups, integers and/or steps. The

foregoing also applies to words having similar meanings such as the terms, "including", "having" and their derivatives. The term "consisting" and its derivatives, as used herein, are intended to be closed terms that specify the presence of the stated features, elements, components, groups, integers, and/or steps, but exclude the presence of other unstated features, elements, components, groups, integers and/or steps. The term "consisting essentially of", as used herein, is intended to specify the presence of the stated features, elements, components, groups, integers, and/or steps as well as those that do not materially affect the basic and novel characteristic(s) of features, elements, components, groups, integers, and/or steps.

[0092] Terms of degree such as "substantially", "about" and "approximately" as used herein mean a reasonable amount of deviation of the modified term such that the end result is not significantly changed. These terms of degree should be construed as including a deviation of at least ±5% of the modified term if this deviation would not negate the meaning of the word it modifies. In addition, all ranges given herein include the end of the ranges and also any intermediate range points, whether explicitly stated or not.

[0093] As used in this disclosure, the singular forms "a", "an" and "the" include plural references unless the content clearly dictates otherwise.

[0094] In embodiments comprising an "additional" or "second" component, the second component as used herein is chemically different from the other components or first component. A "third" component is different from the other, first, and second components, and further enumerated or "additional" components are similarly different.

[0095] The term "and/or" as used herein means that the listed items are present, or used, individually or in combination. In effect, this term means that "at least one of" or "one or more" of the listed items is used or present.

[0096] The abbreviation, "e.g." is derived from the Latin exempli gratia and is used herein to indicate a non-limiting example. Thus, the abbreviation "e.g." is synonymous with the term "for example." The word "or" is intended to include "and" unless the context clearly indicates otherwise.

[0097] It will be understood that any component defined herein as being included can be explicitly excluded by way of proviso or negative limitation, such as any specific compounds or method steps, whether implicitly or explicitly defined herein.

[0098] Although methods and materials similar or equivalent to those described herein can be used in the practice or testing of this disclosure, suitable methods and materials are described below.

II. Biosensor Systems, Methods and Kits of the Disclosure

[0099] The present disclosure is directed to the generation of a universal biosensor system designed to detect the presence of a target by monitoring the binding of the target to an electrode surface in real time. Utilizing single frequency electrochemical impedance spectroscopy, the biosensor system enables the real-time measurement of these interactions, employing multimeric aptamers for solution-based capture, and forming target-aptamer complexes. The biosensor system incorporates high affinity coupling chemistry, such as biotin-streptavidin chemistry, to attach the target-aptamer complexes to the electrode surface, allowing for continuous real-time monitoring. In addition, the biosensor system incorporates machine learning approach for enhanced performance. The biosensor system is versatile, suitable for a wide array of target analytes, and offers several advantages over state-of-the-art electrochemical assays.

[00100] First, the real-time analysis feature of the biosensor system allows for continuous measurement throughout the sample incubation period with an unlabeled target using electrochemical impedance. This not only captures changes induced by the target but also reveals information on binding kinetics, supporting the creation of more reliable and robust biosensor systems. Second, the use of multimeric aptamers, as opposed to their monomeric counterparts, provides enhanced binding affinity in the biosensor system. This allows for the formation of target/aptamer aggregates, resulting in a more efficient and effective binding process. Third, simplified manufacturing is another key advantage of the biosensor system, as the production process is streamlined. The diagnostic chips only require, for instance, streptavidin modification and do not depend on additional capture probe modification on the chip, thereby reducing complexity and lowering costs. The integration of these building blocks leads to an improved solution and enables the real-time electrochemical observation of target capture and aggregation. Fourth, the incorporation of machine learning approach allows the biosensor system to adapt and learn from the data it processes, thereby becoming more effective over time or under different conditions. The enhanced capabilities of the biosensor system achieved through the integration of a machine learning algorithm have led to a more robust,

versatile, and effective one-pot and label-free target detection approach. This enhancement not only streamlines the detection process but also heightens accuracy and adaptability, suiting a wide array of applications.

[00101] Accordingly, herein provided is a biosensor for detecting a target analyte in a sample comprising:

a) an electrochemical impedance spectroscopy (EIS) module comprising (i) a working electrode, operable at a single frequency for real-time monitoring of aptamer binding to target, aptamer-target dissociation, or aptamer or target degradation on the working electrode, (ii) a counter electrode, (iii) a reference electrode, and (iv) a circuit compatible with potentiostat;

b) a multimeric aptamer comprising two or more units for specific target binding and formation of an aptamer-target complex in solution, wherein the target comprises two or more binding sites, wherein the multimeric aptamer has a K_d < about 300 pM;

wherein the multimeric aptamer is configured to bind to the surface of the working electrode, and

wherein the biosensor system is configured to operate in a wash-free and single-pot format.

[00102] In some embodiments, the multimeric aptamer is biotinylated and the surface of the working electrode is coated with streptavidin. In some embodiments, the multimeric aptamer is aminated and the surface of the working electrode is coated with NHS-ester or an epoxy group. In some embodiments, the multimeric aptamer is thiolated and the surface of the working electrode is coated with a metal, a thiol, or a disulphide. In some embodiments, the multimeric aptamer is alkynylated and the surface of the working electrode is coated with an azide. In some embodiments, the multimeric aptamer is azido-modified and the surface of the working electrode is coated with an alkyne. In some embodiments, the working electrode is a gold working electrode. In some embodiments, the counter electrode is a gold counter electrode. In some embodiments, the reference electrode is a silver reference electrode. In some embodiments, the target is a viral target and K_d < about 100 pM. In some embodiments, the target is a viral target and K_d < about 25 pM. In some embodiments, the target is SARS-CoV-2 and K_d < about 23 pM. In some embodiments, the target is SARS-CoV-2 and K_d < about 8 pM.

In some embodiments, the target is SARS-CoV-2 and K_d < about 0.13 pM. In some embodiments, the target is influenza and VEGF and K_d < about 300 pM. In some embodiments, the target is influenza and VEGF and K_d < about 270 pM. In some embodiments, the target is influenza and VEGF and K_d < about 90 pM. In some embodiments, the target is influenza and K_d < about 100 pM. In some embodiments, the target is VEGF and K_d < about 300 pM. In some embodiments, the target is VEGF and K_d < about 270 pM. In some embodiments, the target is VEGF and K_d < about 90 pM.

[00103] The biosensor system described herein uses a solution comprising a readout buffer, a binding buffer, and a blocking buffer, which can be premixed or mixed prior to use. In some embodiments, the solution comprises a readout buffer comprising phosphate buffer saline, KCl, and redox reporter.

[00104] The redox reporter can be redox pair can be potassium ferricyanide and potassium ferrocyanide ($K_3[Fe(CN)_6]/K_4[Fe(CN)_6]$), ferricyanide ion and ferrocyanide ion ($[Fe(CN)_6]^{3-}/[Fe(CN)_6]^{4-}$), quinone and hydroquinone (Q/H_2Q), hexaammineruthenium(III) ion and hexaammineruthenium(II) ion ($[Ru(NH_3)_6]^{3+}/[Ru(NH_3)_6]^{2+}$), oxidized methylene blue and reduced methylene blue (MB^+/MBH_2), or methyl viologen dication and methyl viologen cation (MV^{2+}/MV^+). In some embodiments, the redox reporter comprises $K_3[Fe(CN)_6]/K_4[Fe(CN)_6]$, $[Fe(CN)_6]^{3-}/[Fe(CN)_6]^{4-}$, Q/H_2Q, $[Ru(NH_3)_6]^{3+}/[Ru(NH_3)_6]^{2+}$, MB^+/MBH_2, or MV^{2+}/MV^+ redox reporter. In some embodiments, the solution comprises redox reporter at about 2 mM $K_3[Fe(CN)_6]$ and about 2 mM $K_4[Fe(CN)_6]$.

[00105] In some embodiments, the solution comprises a blocking buffer comprising biotin-BSA and BSA. In some embodiments, the solution comprises about 0.01 μM biotin-BSA and about 0.1% BSA. In some embodiments, the solution comprises a binding buffer comprising HEPES, NaCl, KCl, $MgCl_2$, and $CaCl_2$. In some embodiments, the solution comprises about 5 mM HEPES, pH about 7.4, about 15 mM NaCl, about 0.6 mM KCl, about 0.25 mM $MgCl_2$, and about 0.25 mM $CaCl_2$.

[00106] The biosensor system described herein can be used for detecting a target in different types of samples. In some embodiments, the sample is a clinical sample. In some embodiments, the sample comprises blood, plasma, urine, saliva, sputum, oropharyngeal and/or nasopharyngeal secretions. In some embodiments, the sample comprises saliva. In some

embodiments, the sample is saliva. In some embodiments, the sample is a heat-treated sample. In some embodiments, the saliva is heat-treated saliva.

[00107] The biosensor system described herein can be used for detecting different types of targets. In some embodiments, the target is a small inorganic molecule, a small organic molecule, a metal ion, a biomolecule, a toxin, a biopolymer, a cell, a tissue, a microorganism, or a virus. In some embodiments, the target is a component from a cell, a tissue, a microorganism, or a virus. In some embodiments, the biopolymer is a nucleic acid, a carbohydrate, a lipid, peptide, or a protein. In some embodiments, the target is a protein target, a viral target, or a bacterial target. In some embodiments, the target is a protein target. In some embodiments, the target is a viral target. In some embodiments, the target is a bacterial target. In some embodiments, the viral target is SARS-CoV-2, influenza, or HIV. In some embodiments, the viral target is SARS-CoV-2. In some embodiments, the SARS-CoV-2 is SARS-CoV-2 B.1.1.529 omicron variant. In some embodiments, the protein target is SARS-CoV-2 B.1.1.529 omicron variant spike protein. In some embodiments, the aptamer is a SARS-CoV-2 specific aptamer and it does not cross-react with human coronavirus 229E, human coronavirus OC43, influenza A, adenovirus, or other respiratory viruses. In some embodiments, the aptamer is a SARS-CoV-2 specific aptamer having the nucleic acid sequence of SEQ ID NO: 6, 7, or 11. In some embodiments, the aptamer is a SARS-CoV-2 specific aptamer having the nucleic acid sequence of SEQ ID NO: 6. In some embodiments, the aptamer is a SARS-CoV-2 specific aptamer having the nucleic acid sequence of SEQ ID NO: 7. In some embodiments, the aptamer is a SARS-CoV-2 specific aptamer having the nucleic acid sequence of SEQ ID NO: 11. In some embodiments, the aptamer is a monomeric SARS-CoV-2 specific aptamer having the nucleic acid sequence of SEQ ID NO: 6. In some embodiments, the aptamer is a trimeric SARS-CoV-2 specific aptamer having the nucleic acid sequence of SEQ ID NO: 6. In some embodiments, the aptamer is a trimeric SARS-CoV-2 specific aptamer having the nucleic acid sequence of SEQ ID NO: 7. In some embodiments, the aptamer is a monomeric SARS-CoV-2 specific aptamer having the nucleic acid sequence of SEQ ID NO: 11. In some embodiments, the aptamer is a trimeric SARS-CoV-2 specific aptamer having the nucleic acid sequence of SEQ ID NO: 11. In some embodiments, the biosensor system is configured to detect SARS-CoV-2 B.1.1.529 omicron variant with a limit-of-detection of about 138 copies/mL in the solution comprising the redox buffer, the blocking buffer, and the binding buffer. In some embodiments, the biosensor system is configured to detect SARS-CoV-2 with

a limit-of-detection of about 584 copies/mL in heat-treated saliva diluted to about 25% (v/v) in the solution comprising the redox buffer, the blocking buffer, and the binding buffer. In some embodiments, the viral target is influenza. In some embodiments, the target is influenza hemagglutinin (HA). In some embodiments, the target is H3N2. In some embodiments, the aptamer is an influenza specific aptamer having the nucleic acid sequence of SEQ ID NO: 1, 2, or 9. In some embodiments, the aptamer is an influenza specific aptamer having the nucleic acid sequence of SEQ ID NO: 1. In some embodiments, the aptamer is an influenza specific aptamer having the nucleic acid sequence of SEQ ID NO: 2. In some embodiments, the aptamer is an influenza specific aptamer having the nucleic acid sequence of SEQ ID NO: 9. In some embodiments, the aptamer is a monomeric influenza specific aptamer having the nucleic acid sequence of SEQ ID NO: 1. In some embodiments, the aptamer is a trimeric influenza specific aptamer having the nucleic acid sequence of SEQ ID NO: 1. In some embodiments, the aptamer is a trimeric influenza specific aptamer having the nucleic acid sequence of SEQ ID NO: 2. In some embodiments, the aptamer is a monomeric influenza specific aptamer having the nucleic acid sequence of SEQ ID NO: 9. In some embodiments, the aptamer is a trimeric influenza specific aptamer having the nucleic acid sequence of SEQ ID NO: 9. In some embodiments, the biosensor system is configured to detect H3N2 with a limit-of-detection of about 408 copies/mL in heat-treated saliva diluted to about 25% (v/v) in the solution comprising the redox buffer, the blocking buffer, and the binding buffer. In some embodiments, the viral target is HIV. In some embodiments, the protein target is vascular endothelial growth factor (VEGF). In some embodiments, the VEGF is isoform $VEGF_{165}$. In some embodiments, the aptamer is a VEGF specific aptamer having the nucleic acid sequence of SEQ ID NO: 4 or 5. In some embodiments, the aptamer is a VEGF specific aptamer having the nucleic acid sequence of SEQ ID NO: 4. In some embodiments, the aptamer is a VEGF specific aptamer having the nucleic acid sequence of SEQ ID NO: 5. In some embodiments, the aptamer is a VEGF specific aptamer having the nucleic acid sequence of SEQ ID NO: 10. In some embodiments, the aptamer is a monomeric VEGF specific aptamer having the nucleic acid sequence of SEQ ID NO: 4. In some embodiments, the aptamer is a trimeric VEGF specific aptamer having the nucleic acid sequence of SEQ ID NO: 4. In some embodiments, the aptamer is a trimeric VEGF specific aptamer having the nucleic acid sequence of SEQ ID NO: 5. In some embodiments, the aptamer is a monomeric VEGF specific aptamer having the nucleic acid sequence of SEQ ID NO: 10. In some embodiments, the aptamer is a trimeric VEGF specific aptamer having the

nucleic acid sequence of SEQ ID NO: 10. In some embodiments, the aptamer described herein comprises or further comprises a linker (T)n at the carboxy terminus, where n = 4 to 15. In some embodiments, the aptamer described herein comprises or further comprises a functional group. In some embodiments, the aptamer described herein comprises or further comprises trebler-(T)n-functional group, where n = 4 to 9. In some embodiments, the functional group is biotin, an amine, a thiol, an alkyne, or an azide. In some embodiments, the aptamer described herein comprises or further comprises trebler-(T)n-biotin, where n = 4 to 9. In some embodiments, the aptamer described herein comprises or further comprises trebler-(T)n-biotin, where n = 5. In some embodiments, the trebler is 3,3'-((2-(oxidomethyl)-2-((3-oxidopropoxy)methyl)propane-1,3-diyl)bis(oxy))bis(propan-1-olate). In some embodiments, the trebler is Formula (I):

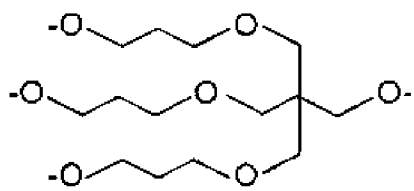

(I)

[00108] In some embodiments, the biosensor system is configured to detect $VEGF_{165}$ with a limit-of-detection of about 0.96 pM $VEGF_{165}$ in the solution comprising the redox buffer, the blocking buffer, and the binding buffer. In some embodiments, the biosensor system provides at least 80% sensitivity and at least 99% specificity. In some embodiments, the biosensor system provides at least 93% sensitivity. In some embodiments, the biosensor system provides at least 98% sensitivity. In some embodiments, the biosensor system provides 100% specificity.

[00109] Also provided is a method for detecting a label-free target real-time in a sample, comprising:

a) mixing the sample with a solution comprising a redox readout buffer, a binding buffer, a blocking buffer, and the multimeric aptamer of the biosensor system described herein to provide a mixture,

b) applying the mixture onto the working electrode of the biosensor system described herein,

c) measuring total impedance at a single frequency at real-time for about 30 minutes, and

d) calculating fold change of the total impedance (ΔZt/Zt),

wherein ΔZt/Zt >= about 1.2 at any time from 1 minute to 30 minutes indicates the presence of the target in the sample.

[00110] In some embodiments, the single frequency is between about 1 and about 20 kHz. In some embodiments, the single frequency is between about 12.6 and about 80 Hz. In some embodiments, the single frequency is about 10, 10.1, 10.2, 10.3, 10.4, 10.5, 10.6, 10.7, 10.8, 10.9, 11, 11.1, 11.2, 11.3, 11.4, 11.5, 11.6, 11.7, 11.8, 11.9, 12, 12.1, 12.2, 12.3, 12.4, 12.5, 12.6, 12.7, 12.8, 12.9, 13, 13.1, 13.2, 13.3, 13.4, 13.5, 13.6, 13.7, 13.8, 13.9, 14, 14.1, 14.2, 14.3, 14.4, 14.5, 14.6, 14.7, 14.8, 14.9, 15, 15.1, 15.2, 15.3, 15.4, 15.5, 15.6, 15.7, 15.8, 15.9, 16, 16.1, 16.2, 16.3, 16.4, 16.5, 16.6, 16.7, 16.8, 16.9, 17, 17.1, 17.2, 17.3, 17.4, 17.5, 17.6, 17.7, 17.8, 17.9, or 18 Hz. In some embodiments, the single frequency is about 12.6 Hz. In some embodiments, the total impedance is measured at intervals of every 2 minutes. In some embodiments, the total impedance is measured continuously.

[00111] Also provided is a kit for detecting a label-free target in a sample, comprising the biosensor system described herein, further comprising at least one of a dropper, a collection tube, a container holding the redox readout buffer, a container holding the binding buffer, a container holding the block buffer, and instruction for use.

EXAMPLE

[00112] The following non-limiting example is illustrative of the present disclosure:

Materials and Methods

[00113] DNA oligonucleotides for aptamer synthesis were obtained from Integrated DNA Technologies (IDT). Before use, the oligonucleotides were purified using standard 10% denaturing polyacrylamide gel electrophoresis (dPAGE) with 8 M urea. The trebler phosphoramidite (Tris-2,2,2-[3-(4,4'-dimethoxytrityloxy)propyloxymethyl]ethyl-[(2-cyanoethyl)-(N,Ndiisopropyl)]-phosphoramidite, Cat. No. 10-1922-90) for the synthesis of trimeric aptamer was ordered from Glen Research (Virginia, United States). Synthetic DNA oligonucleotides used in this research are provided in the **Table 1**. The B.1.1.529 omicron

variant of the SARS-CoV-2 spike pseudotyped lentivirus (OMPV) was sourced from BPS Bioscience (catalog number: 78349-1). For the dot blot assay, nitrocellulose blotting membranes (catalog No. 10600125) from GE Healthcare Inc. were used and nylon hybridization transfer membranes (NEF994001PK) were purchased from PerkinElmer Inc. (Woodbridge, ON, Canada). Thermo Scientific (Ottawa, ON, Canada) provided T4 DNA ligase, T4 polynucleotide kinase (PNK), adenosine triphosphate (ATP), and deoxyribonucleoside 5'-triphosphates (dNTPs) for biotinylation of the aptamers. γ-[32P]-ATP, acquired from PerkinElmer, was used for radio-tagging the aptamers to visualize and analyze the dot-blot assay. All other chemicals and reagents, including 4-(2-hydroxyethyl)-1-piperazineethanesulfonic acid (HEPES), sodium chloride, magnesium chloride, Tween-20, Bovine serum albumin, Biotinylated Bovine Serum albumin, $K_3[Fe(CN)_6]$, and $K_4[Fe(CN)_6]$, were purchased from Sigma-Aldrich (Oakville, Canada) and used without further purification. All electrochemical tests were conducted using screen printed gold electrodes with silver reference and gold auxiliary electrodes purchased from Palmsens. Autoclaved DI water was used for all experiments. The SARS-Related Coronavirus 2 Pseudotyped Lentiviral Kit (BEI catalog number NR-52948) was obtained from BEI resources, National Institute of Allergy and Infectious Diseases, National Institutes of Health.

Table 1: Synthetic DNA oligonucleotides (aptamers) used in this work. All sequences are written in a 5′ to 3′ direction. Italics in SEQ ID NO: 2, 3, 5, 7, and 8 are linkers.

SEQ ID NO.	Name	Target	Final Size (nt)	Sequence (5'-3') italic nucleotides act as linkers (monomeric sequence shown)
1	RHA06	Influenza HA	48	GGGTTTGGGTTGGGTTGGGTTTTTGGGTTTG GGTTGGGTTGGGAAAAA
2	TRHA06	Influenza HA	185	GGGTTTGGGTTGGGTTGGGTTTTTGGGTTTG GGTTGGGTTGGGAAAAA *TTTTTCTCTCGC*-Trebler-*TTTTT*-Biotin
3	M-TRHA06	(K_d> 300 nM for Influenza HA)	185	GTTTGGTTATGGGAGTGTGGGGGGAGGTTGG TGGTGTGTGGTTATTAT *TTTTTCTCTCGC*--Trebler-*TTTTT*-Biotin
4	H1A	$VEGF_{165}$	28	GCCCGTCTTCCAGACAAGAGTGCAGGGC

5	TH1A	$VEGF_{165}$	125	GCCCGTCTTCCAGACAAGAGTGCAGGGC*TTT TTCTCTCGC*-Trebler-*TTTTT*-Biotin
6	MSA52	SARS-Cov-2 spike protein	79	TTACGTCAAG GTGTCACTCC GTAGGGTTTG GCTCCGGGCC TGGCGTCGGT CGTCTCTCGC GAAGCATCTC TTTGGCGTG
7	TMSA52	SARS-Cov-2 spike protein	282	TTACGTCAAG GTGTCACTCC GTAGGGTTTG GCTCCGGGCC TGGCGTCGGT CGTCTCTCGC GAAGCATCTC TTTGGCGTG *TTTTTTTTTT*-Trebler-*TTTTT*-Biotin
8	M-TMSA52	(K_d> 150 nM for SARS-Cov-2 spike protein)	198	CGAAGCATCTCGTGTCACTCGAGCTGGTTTG GCGGCCTGCCTGGCGTCG TTTTTCTCTCGC-Trebler-*TTTTT*-Biotin
9	TRHA06-pre-trebler-sequence	Influenza HA		GGGTTTGGGTTGGGTTGGGTTTTTGGGTTTG GGTTGGGTTGGGAAAAA TTTTTCTCTCGC
10	TH1A-pre-trebler-sequence	$VEGF_{165}$		GCCCGTCTTCCAGACAAGAGTGCAGGGCTTT TTCTCTCGC
11	TMSA52-pre-trebler-sequence	SARS-Cov-2 spike protein		TTACGTCAAG GTGTCACTCC GTAGGGTTTG GCTCCGGGCC TGGCGTCGGT CGTCTCTCGC GAAGCATCTC TTTGGCGTG TTTTTTTTTT

e-CoV chip functionalization and reagent information

[00114] The e-CoV sensor chip used screen printed electrodes with gold working and counter electrodes, as well as silver reference electrodes, obtained from Palmsens.[39] To prepare the chip, it was initially cleaned by washing it with isopropanol (IPA) and DI water. The working electrode was then electroactivated through 15 cyclic voltammetry scans in 0.5 M H_2SO_4.[40] The scans ranged from 0 V to 1.5 V, with a scan rate of 10 mV/s. Afterward, the chip was washed with water. Then, two bare cyclic voltammetry scans were performed in a 1X

readout buffer which consisted of 1X phosphate buffer saline, 50 mM KCl, 2 mM ferrocyanide ($K_3[Fe(CN)_6]$), and 2 mM ferricyanide ($K_4[Fe(CN)_6]$). These scans were conducted immediately after cleaning the chip, and the second scan was considered for analysis. Chips showing less than 40 µA of redox current were discarded. To prepare the DSP (dithiobis[succinimidylpropionate]), 2 mg of DSP was mixed with 500 µl of dimethyl sulfoxide (DMSO) by vortexing. For DSP reduction, 50 µl of DSP-DMSO was added to 450 µl of tris(2-carboxyethyl)phosphine (TCEP) dissolved in DMSO and thoroughly mixed. The mixture was then incubated for at least 1 hour. Then, 3.5 µl of TCEP-reduced DSP was deposited onto the working electrode and incubated for 2 hours. The chip was subsequently washed with DMSO and then with water. Then, 5 µl of streptavidin, diluted to a concentration of 0.5 µM in 1X PBS, was deposited onto the working electrode and left to incubate overnight (at least 6 hours) at 4°C. Finally, the chips were washed and stored in 1X PBS. In this way, streptavidin modified electrodes were prepared and then treated using three different strategies to determine the most effective approach for assay development.

[00115] The first strategy involved the sequential deposition of aptamer and target on the streptavidin modified electrodes. First, 5 µl of a selected concentration of aptamer diluted in 1X ***binding buffer*** (50 mM HEPES, pH 7.4, 150 mM NaCl, 6 mM KCl, 2.5 mM $MgCl_2$, 2.5 mM $CaCl_2$) was incubated on the streptavidin modified electrodes for 30 minutes. Subsequently, the electrodes were washed and incubated with 5 µl of the target solution diluted in 1X binding buffer or a blank binding buffer solution for 10-minute. Finally, the electrodes were washed again by dipping them in 1X binding buffer and taken for reading charge transfer resistance change using multi-frequency EIS. This strategy was carried out only in a control buffer (1X binding buffer).

[00116] The second strategy involved depositing a monolayer of aptamer on the streptavidin modified electrodes and then monitoring the kinetics of target binding to the deposited aptamers in real-time. Similar to the first strategy, 5 µl of a selected concentration of aptamer diluted in 1X binding buffer was incubated on the streptavidin modified electrodes for 30 minutes. Subsequently, 50 µl of the target solution diluted in BR Buffer which contains 1X binding buffer and 1X readout buffer was dropped onto the aptamer modified electrodes. Single frequency electrochemical impedance spectroscopy (EIS) was then performed continuously for 30 minutes at a selected frequency of 12.6 Hz to monitor the signal change as the target binds

to the aptamer and dissociates. This strategy was also carried out only in the control buffer (1X binding buffer).

[00117] The third strategy, which was selected as the best-performing strategy for the study, involved mixing the aptamer and target in a "one-pot" fashion with BBR Buffer which contains 1X binding buffer, blocking buffer and 1X redox readout solution. A 50 µl mixture was prepared, consisting of 25 µl of 2X redox readout buffer (comprising 2X phosphate buffer saline, 100 mM KCl, 4 mM ferrocyanide, and 4 mM ferricyanide), 2.5 µl of a 10 µM aptamer, 5 µl of a 10X target (diluted in binding buffer, specifically when working with spike samples), 2.5 µl of blocking buffer (0.2 µM biotin-BSA + 2% BSA) prepared in 1X binding buffer, 2.5 µl of 1X binding buffer without tween, and 12.5 µl of saliva (only for spiked clinical saliva samples). The entire mixture was drop-deposited onto the streptavidin-modified chips, and single frequency EIS was performed continuously for 30 minutes at a selected frequency of 12.6 Hz to monitor the signal change as the aptamer and target formed multilayered stacked aggregates and bound to the streptavidin modified electrodes.

[00118] All three strategies were tested using monomeric and trimeric aptamers, and the system-strategy combination that demonstrated the best target to blank signal resolution was selected for the remainder of the study. For the second and third strategies, the total impedance was analyzed.

Electrochemical sensing and data analysis

[00119] In the first strategy, multifrequency electrochemical impedance spectroscopy (EIS) spectra were recorded before and after the deposition of either the blank or the target. For this analysis, 25 µl of 1X redox readout solution was used. The impedance data obtained from the EIS spectra were fitted to a Randles circuit, which is a commonly used equivalent circuit model in impedance analysis.[14] By fitting the Nyquist plot to the Randles circuit, the charge transfer resistance (Rct) signals were obtained for both the blank and the target. The R_{ct} values reflect the resistance to charge transfer at the electrode-electrolyte interface and can provide information about the binding events occurring on the electrode surface.[14] The R_{ct} values before and after deposition of the blank or target were compared as fold change to determine the presence or absence of target.

The R_{ct} fold change was calculated as:

$$\frac{\Delta R_{ct}}{R_{ct}} = \frac{R_{ct_{target\ or\ blank}} - R_{ct_{pre\ target\ or\ blank}}}{R_{ct_{pre\ target\ or\ blank}}}$$

[00120] To perform the EIS measurements for the second and third strategies, a script was created that automated the process. The script executed 175 repeats of single-frequency EIS measurements at a frequency of 12.6 Hz. 175 repeats are performed to ensure a total run time of 30 minutes. Additionally, to maintain redox stability and prevent chip drying, a dark and humid environment was maintained around the chip. This precaution helps to minimize any degradation of the redox species and ensures the stability of the system throughout the experiment. These strategies enabled observation of the binding kinetics of the aptamer and target in BR Buffer (second strategy) and in BBR Buffer (third strategy) in real-time to streptavidin modified electrodes. The transient fold change of the total impedance for both target and blank were calculated as follows:

$$\frac{\Delta Z_t}{Z_t} = \frac{Z_{time=t} - Z_{time=0}}{Z_{time=t}}$$

[00121] The fold change at every 2 min was then considered for further analysis, calibration, specificity assessment and clinical validation.

Machine learning algorithm and model

[00122] To enhance the efficiency of the biosensor, disclosed herein, for evaluating unknown samples and determining their positive/negative attributes, a machine learning algorithm was integrated (**FIG. 9A**). The algorithm generated a model which incorporates viral and aptamer association and dissociation, molecular degradation, non-specific adsorption and time lag to signal generation.

[00123] In one embodiment, the algorithm generated a segmented model based on its analysis of various parameters derived from the recorded graph of impedance kinetics data. The kinetics data revealed two distinct patterns: one characterized by a relatively steady or gradual increase in signal, and another marked by an initial signal increase followed by a rapid decline.

[00124] Accordingly, the resulting segmented model combined an association-dissociation binding kinetic model with an extra initial transient lag phase. The lag phase consisted of two components: the first simulated a decay function (Weibull decay) that appeared to commence from the outset. This component could represent either adsorbed Bovine serum albumin (BSA) or the time-sensitive protein streptavidin, both subject to degradation over time. The second component of the lag was attributed to non-specific adsorption resulting from salivary proteins.

[00125] The consideration of the lag term and associative component were limited to the interval where the signal exhibited an increase. The association component was formulated as follows:

$$Z_{assoc} = \frac{Z_{max} \times C_{ligand}}{C_{ligand} + \left({}^{k_A}/_{k_D}\right)} \times 1 - e^{-(k_A \times C_{lig} + k_D) \times t}$$

[00126] Where, Z_{assoc} denotes the signal (impedance fold change) corresponding to ligand association, Z_{max} represents the maximum attainable signal, k_A and k_D are the association and dissociation constants, k_D is the dissociation constant, t is the time and C_{ligand} is the resultant ligand concentration (aptamer and virus for target and aptamer only for blank) in micromolar (μM). The aptamer concentration was kept constant at 0.5 μM which is the concentration used for assay. The viral concentration was considerable as a variable to the model.

[00127] The lag term was modeled as:

$$Z_{lag} = k_{ads} \times t \times e^{-\tau/t} + Z_{NS}$$

[00128] Where, Z_{lag} represents the signal during the initial lag phase, k_{ads} is the adsorption rate constant, τ is the lag residence time, Z_{NS} is the non-specific signal contribution.

[00129] The dissociation component was considered after the time point at which the maximum signal was obtained following which signal decreased. The dissociation component was incorporated into the model to generate the resultant signal as:

$$Z_{result} = (Z_{assoc} + Z_{lag}) \times e^{-\frac{k_D}{k_A} \times (t - t_{max})}$$

[00130] Where, Z_{result} is the resultant signal considering all functions, t_{max} is the time corresponding to maximum signal Z_{max}.

[00131] As shown in Fig. 9A, the model was applied to the calibration data 905 to validate the model at 910. In the illustrated embodiment, the calibration data 905 was obtained from spiked saliva samples.

[00132] Next, training data 915 was used for model fitting and training at 920. In the illustrated embodiment, training data 915 included a randomly selected subset of clinical samples. Fig. 9B illustrates an example of curve fitting with the validated model for impedance kinetics data derived from select clinical samples used as training data.

[00133] Next, at 925, a two-dimensional principal component analysis (PCA) was performed on the training data 915 to reduce the dimensionality of the data while retaining as much of its variation as possible. In the illustrated embodiment, the training data 915 contained values for various parameters such as, for example, k_A, k_D, k_{ads}, τ, t_{max}, Z_{max}, area under the recorded curve (AUC) and R-squared (goodness of fit), where k_A and k_D are the association and dissociation constants, k_{ads} is the adsorption rate constant, τ is the lag residence time, Z_{max} represents the maximum attainable signal and t_{max} is the time corresponding to maximum signal Z_{max}.

[00134] The PCA of the training data resulted in two new variables: a first principal component (PC1) and a second principal component (PC2), where PC1 represents the direction in the data where there is the most variance and PC2 represents the second most variance. The first and second principal components were created as linear combinations of the original variables with specific weights assigned to the original variables. Fig. 9C illustrates an example of weights for the first and second principal components (PC1 and PC2) generated from PCA or dimensionality reduction of curve fitting features.

[00135] Next, at 930, the variables generated at 925 were used for binary classification of the remaining clinical samples to categorize them into one of the two classes (a 'positive' class or a 'negative' class). Fig. 9D illustrates an example of binary classification of clinical samples through support vector machine analysis. As shown in Fig. 9D, the two principal components, PC1 and PC2, are plotted on x- and y- axis, respectively. The clinical samples are visualized as a scatterplot with their first two principal components, overlaid with the decision map from support vector machine analysis. The decision map shows the boundaries between

the positive and negative samples. Also shown in Fig. 9D is a confusion matrix 935 of the support vector machine model on the test set of clinical samples. The binary classification of the clinical samples shown in Fig. 9D resulted in a 100% accuracy.

[00136] The established model and the insights gained from the comprehensive analysis and the machine learning algorithm provide the advantage of accurately performing assessment procedures in clinical and at-home settings, allowing for informed decisions about the nature and status of the samples without prior knowledge.

RESULTS AND DISCUSSION

[00137] First, it was investigated whether it would be possible to perform real-time electrochemical monitoring of target binding using single frequency impedance measurement. For this purpose, gold electrodes were modified with streptavidin and biotinylated monomeric aptamers specific to the spike protein of SARS-CoV-2 and introduced a one-pot solution containing the SARS-CoV-2 Omicron pseudotyped lentivirus (OPV) mixed with a solution of $K_3[Fe(CN)_6]/K_4[Fe(CN)_6]$ redox reporter. Conventional electrochemical impedance spectroscopy was run to determine the frequency at which point the target-to-blank ratio was maximized (**FIG. 1A, FIG. 5A-5C**). This value (12.6 Hz) was used for single frequency impedance measurements. During the real-time measurement, it was observed that as the viral target binds to the aptamers on the electrode, the charge transfer from the redox solution to the electrode is impeded, causing an increase in charge transfer resistance (0.71 kΩ for blank and 1.79 kΩ for target) and a decrease in the double layer capacitance (236 nF for blanks and 182 nF for target), resulting in a corresponding increase in the magnitude of electrochemical impedance (0.82 kΩ for blank and 2.432 kΩ for target) with increasing time (**FIG. 1B**). The blank signal showed a similar trend with a lower increase in impedance. This minor increase is attributed to the adsorption of HEPES in the binding buffer (control buffer in blank) onto the gold electrodes.[17] This showed the necessity of including a surface blocker (also see below for further testing). By monitoring the impedance, binding of the target to the aptamer-modified electrodes could be tracked in real-time in a single pot and without any wash steps. Furthermore, it was found that by examining the total impedance at a single frequency, which includes information from the entire electrical circuit, a stronger signal can be obtained compared to monitoring only the charge transfer resistance or double layer capacitance.

[00138] In order to enhance the target-to-blank ratio of the real-time assay, surface-based target capture using monomeric aptamers was replaced with solution-based biorecognition using trimeric aptamers, developing the Real-Time Multimeric Aptamer Assay (RT-MAP Assay). The benefit of using trimeric aptamers is two-fold. Trimeric aptamers have a higher binding affinity to multimeric targets[10] compared to monomeric aptamers. For example, the trimeric aptamer, TMSA52, has a 2 orders of magnitude improvement in binding affinity compared to its monomeric counterpart toward the trimeric spike protein of SARS-CoV-2 Omicron variant.[10] Additionally, similar to antibodies, multimeric aptamers possessing multiple binding regions can extract, concentrate, and aggregate targets in solution for more effective delivery of targets to the surface[12,18] and improved surface blocking and signal transduction.

[00139] To create the RT-MAP Assay, electrodes were modified with streptavidin and introduced biotinylated trimeric aptamers (or monomeric as control, **FIG. 1C**), viral targets (10^4 copies/mL of OPV and nothing in case of blank), binding buffer, and a readout buffer in a single pot and performed real-time measurements using single frequency impedance monitoring (**FIG. 1D**). Using this method, impedance was monitored every 2 minutes, starting at the instance the one-pot solution was deposited on the chip (T=0 minutes). For the solution containing the monomeric aptamer and the target, it was observed that the impedance monotonically increases until 22 minutes; however, the signal from the blank solution only increased until 12-14 minutes and decreased following that time point. The target-to-blank ratio calculated from the ratio of the peak target current, and the peak blank current is 2.1, which, as expected, is higher than the value (1.98) obtained using surface-based monomeric aptamers. Interestingly, for the trimeric aptamers in solution, the real-time target and blank signals demonstrated a similar trend, with blank increasing till 14-16 minutes and target reaching peak values monotonically till 22 minutes, with a target-to-blank ratio of only 3.5. This clearly highlights the importance of using trimeric aptamers for the RT-MAP Assay. The enhanced target-to-blank ratio observed with the trimeric aptamer is likely caused by the increased binding affinity of trimeric *versus* monomeric aptamers, increased number of negatively charged nucleotides bound to each viral target, and the steric hindrance produced by virus/aptamer cluster formation as opposed to monolayer surface binding of individual targets.[19,20]

[00140] Following the demonstration that real-time monitoring of target binding was possible using a wash-free and single pot aptamer assay, the experimentation aimed at determining the limit-of-detection of the assay both in buffer and saliva. To enable measurement in saliva, a blocking buffer was added and a selected concentration of the surface blocker (bovine serum albumin) used for reducing non-specific binding (**FIG. 6A-6C**). It was observed that the direct detection of 10^4 copies/mL OPV in saliva led to a reduced signal-to-blank ratio and unpredictable trends compared to the measurements made in buffer (**FIG. 7A**). It is expected that this is caused by enzymes that degrade DNA or streptavidin on the electrode surface.[21] To overcome this problem and generate higher target-to-blank ratios, a pre-heating step was introduced for the saliva samples at 60° C for 10 min before testing. With pre-heating, the signals were recovered, and the trends were consistent with that in buffer (**FIG. 7B**), indicating that pre-heating prevents the interference of saliva enzymes but does not affect target binding. The use of a heat step for viral testing in saliva has been used in previous works[9,22] and can be achieved using compact flexible heaters that are powered using portable electrochemical potentiostats.[23–25]

[00141] Following the abovementioned selections, the limit-of-detection of the RT-MAP Assay was measured in analyzing OPV (0-10^5 copies/mL) spiked in both buffer and pre-heated saliva (**FIG. 2A**). In buffer, three distinct trends were observed when comparing the target and blank time series. A custom-built Python code was utilized (**FIG. 9A-9D**) to analyze and extract three important metrics, namely maximum signal, time taken to achieve the maximum signal, and the rate of ligand association, from the acquired transient signals. When the target concentrations were at least 10^3 copies/mL or higher, two key trends were observed: 1) the peak target current was at least 1.6 times higher than the peak blank current, and 2) the rate of increase in the target signals (aptamer and aptamer-target complex association) was about 6 times higher than that of the blank signals (aptamer-only association rate). However, no clear trend was observed with increasing target concentration for the time it took to reach the maximum signal. This variability can be attributed to the differing onset of surface degradation, which is influenced by the variable streptavidin deposition on the functionalized electrodes. In saliva, starting from a target concentration of 10^3 copies/mL, a similar trend in the three metrics was noticed. However, the peak signals were increased by 1.2-fold for the target, and the rate of signal increase was 3.3-fold higher compared to the values observed in the buffer medium.

[00142] Overall, the limit-of-detection was very good in saliva (584 copies/mL) and excellent in buffer (138 copies/mL), which can be attributed to the reduced target-to-blank ratio at lower target concentrations caused by the interference of salivary proteins.[26,27] Next, clinical assessment of the assay design was undertaken (**FIG. 3A**).

[00143] Four specific time points were isolated (2 min, 10 min, 18 min and 26 min) from real-time kinetics which showed most signal transitions due to binding including improvement in sensitivity and specificity (**FIG. 3B-3C**). To establish a threshold for clinical decision making, 16 patient samples were analyzed, symptomatic or close contacts, that were confirmed as negative by polymerase chain reaction (PCR) (**FIG. 10A-10C**). Using these known negative samples, diagnostic thresholds were established starting at 2 min till 30 min (**Table 2**) using Youden's index.[28] Following the establishment of the diagnostic threshold, 20 single-blinded saliva samples were examined (**FIG. 11A-11C**), also obtained from symptomatic or close contact patients. The Receiver Operating Characteristic (ROC) curve was employed to assess the sensitivity, specificity, and concordance values of the test compared to PCR at every 2 minutes interval (**FIG. 12A-12C**). The sensitivity showed a substantial improvement, increasing from 78% at 10 minutes to 89% at 18 minutes. After 18 minutes, the sensitivity remained relatively constant, hovering around 89%. Meanwhile, the specificity showed a continuous improvement, starting from 10% at 2 minutes, reaching 33% at 18 minutes, and finally achieving 100% at 26 minutes. The enhanced sensitivity and specificity over time can be attributed to the optimal binding of the aptamer, which is essential for discernible viral association. However, beyond 26 minutes, there was a slight deterioration in specificity, likely due to increased non-specific fouling of the sensor surface caused by saliva samples.

Table 2: Diagnostic Thresholds

Time	Threshold
2 min	0.3
4 min	0.55
6 min	0.7
8 min	0.9
10 min	1.3

12 min	1.5
14 min	1.8
16 min	1.4
18 min	1.9
20 min	2.0
22 min	2.0
24 min	2.0
26 min	1.3
28 min	2.0
30 min	2.0

[00144] Data obtained at the 26-minute time point was considered because it provided the best sensitivity and specificity compared to other time points. Considering a threshold of $\Delta Z/Z = 1.3$ for a binding time of 26 min (**FIG. 4H-4J**), the Area Under Curve (AUC)[29] was obtained as 0.9889 with a sensitivity of 93% (**FIG. 10A-10C**), specificity of 100%, and concordance values of 89.5%. These results successfully meet the FDA requirement of minimum 80% sensitivity and 99% specificity for validation of at-home antigen tests.[29–31]

[00145] To assess the versatility of this assay, the testing aimed to implement the RT-MAp strategy for detecting the flu virus. For this purpose, a trimeric aptamer TRHA06 targeting the Influenza virus which exhibited a 93-fold higher affinity (best $K_d = 0.09 \pm 0.02$ nM for subtype H3N2 according to **FIG. 13A-13B and FIG. 14A-14B**) when compared to the developed monomeric aptamer TRHA06 (best $K_d = 8.4 \pm 0.5$ nM for subtype H3N2 according to **FIG. 13A-13B and FIG. 14A-14B**) was selected. To facilitate the application of this assay for Influenza detection, the concentration of the TRHA06 was selected at 500 nM (**FIG. 15**). The assay was then used by using spiked H3N2 (which displayed the best affinity towards TRHA06) in 25% saliva mixed with BBR Buffer. The obtained limit of detection in saliva was 408 copies/mL of H3N2 (**FIG. 4A-4B**). The limitation of detection for Influenza A (H3N2) was similar in comparison to COVID (OPV), and the resolution of the signal was different with

OPV having a better resolution of the signal with increasing target concentration. This difference can be attributed to the lower affinity of the TRHA06 (**FIG. 13A-13B**).[10] Interestingly, generation of the maximum signal took longer for the Influenza A assay (24 minutes to 30 minutes) compared to COVID (14 minutes to 26 minutes).

[00146] In addition, the application of the assay was extended to detect $VEGF_{165}$ (vascular endothelial growth factor) in BBR Buffer. Likewise, the trimeric configuration of its aptamer H1A demonstrated 78-fold higher affinity (K_d = 21.3±5.3 nM as shown in **FIG. 16A-16B and FIG. 17A-17B**) compared to the monomeric counterpart TH1A (K_d = 0.27±0.04 nM as shown in **FIG. 16A-16B and FIG. 17A-17B**). This enhanced affinity trend allowed the present inventors to use the trimeric aptamer for VEGF detection as well. By selection, the aptamer concentration to 250 nM (as illustrated in **FIG. 18A-18D**), a limit of detection of 0.96 pM $VEGF_{165}$ in buffer solution was achieved (**FIG. 4C-4D**). This accomplishment allowed the present inventors to translate this assay into plasma or serum samples.

[00147] Such an extension of the assay provides for expanding the scope of research and contributing to more comprehensive diagnostic applications.

[00148] Next, the COVID assay's specificity was examined by evaluating its performance against other respiratory viruses, Human coronavirus 229E, Human coronavirus OC43, Influenza A, and Adenovirus spiked in BBR Buffer. Minimal cross-reactivity was observed when comparing the three-assay metrics between OPV and other respiratory viruses (**FIG. 19A**). Considering an upper control threshold of $\Delta Z/Z = 1.4$, calculated as OPV (Specific target) $\Delta Z/Z$ - 3* standard deviation [13,32]), only the samples containing OPV yielded positive results. Additionally, the efficiency of both the COVID and Influenza A assay in recognizing specific targets from a mixture of specific and non-specific target were tested (**FIG. 19B**). Considering upper thresholds of 1.4 for OPV and 0.8 for InfA, no cross-reactivity was observed for TMSA52 (OPV aptamer) towards Influenza A or for TInfA towards OPV. The signals for detecting both OPV and InfA are found to be suppressed when both viruses coexisted. This can be due to weak cross-species (OPV and InfA) interactions to each other and specific aptamers which can impact the specific binding affinity.[33]

CONCLUSION

[00149] Point-of-care tests (POCTs) play a crucial role in disease monitoring by providing rapid diagnostic information at the point of patient care, enabling early intervention

and treatment.[34,35] They are particularly valuable for infectious diseases like influenza, HIV, and COVID-19, aiding in disease prevention and management. POCTs are used for rapid disease screening in various healthcare settings and facilitate immediate decision-making for patient care.[36,37] Additionally, they are employed for real-time monitoring of health parameters, allowing for timely adjustments to treatment and lifestyle. Electrochemical biosensors, including electrochemical impedance spectroscopy (EIS), offer sensitive, portable, and versatile options for real-time POCTs, providing dynamic information on biomolecular interactions and enabling continuous monitoring without the need for frequent sampling.[38] EIS multifrequency spectra can capture comprehensive electrical properties of the system across a range of frequencies, while single frequency EIS simplifies experimental setup and analysis for specific biomolecular interactions.[16]

[00150] This disclosure showed a sensor for real-time monitoring of infections. The sensor utilizes single frequency Electrochemical Impedance Spectroscopy (EIS) and aptamers to detect the viral targets and monitor the progress of the infection in real-time. Initially, monomeric aptamers were used, but trimeric aptamers were found to have higher binding affinity. A one-pot strategy was adopted, where the aptamers and viral targets were introduced together with the readout buffer. This approach improved the signal by forming large aptamer-virus aggregates and demonstrated a sensor with superior sensitivity. The sensor could detect as low as 138 copies/mL of the COVID viral target in buffer and 584 copies/mL in 25% diluted heat-treated saliva. The specificity of the assay was evaluated, and minimal cross-reactivity was observed in both buffer and saliva samples. Assessment of known and unknown clinical samples demonstrated an optimal clinical sensitivity of 93%.

[00151] Overall, the experimentations presented a sensor design and assay strategy for real-time monitoring of infections, with primary focus on COVID-19 and extended for Influenza A. The use of aptamers and single frequency EIS provided a sensitive, rapid and versatile real-time detection method without the requirement for multiple sampling and wash. The assay showed useful results in terms of specificity and detection sensitivity, highlighting its usefulness for clinical applications.

[00152] While the present disclosure has been described with reference to examples, it is to be understood that the scope of the claims should not be limited by the embodiments set

forth in the examples, but should be given the broadest interpretation consistent with the description as a whole.

[00153] All publications, patents and patent applications are herein incorporated by reference in their entirety to the same extent as if each individual publication, patent or patent application was specifically and individually indicated to be incorporated by reference in its entirety. Where a term in the present disclosure is found to be defined differently in a document incorporated herein by reference, the definition provided herein is to serve as the definition for the term.

REFERENCES

1. Koczula, K. M. & Gallotta, A. Lateral flow assays. *Essays in Biochemistry* **60**, 111–120 (2016).

2. Sena-Torralba, A., Álvarez-Diduk, R., Parolo, C., Piper, A. & Merkoçi, A. Toward Next Generation Lateral Flow Assays: Integration of Nanomaterials. *Chem. Rev.* **122**, 14881–14910 (2022).

3. Leonardi, A. A. *et al.* SARS-CoV-2 and omicron variant detection with a high selectivity, sensitivity, and low-cost silicon bio-nanosensor. *Nano Select* **4**, 160–169 (2023).

4. Iravani, S. Nano- and biosensors for the detection of SARS-CoV-2: challenges and opportunities. *Mater. Adv.* **1**, 3092–3103 (2020).

5. Li, J. & Li, Y. One-pot high-yield synthesis of Pd nanocubes for Pd-Ir nanocube-based immunoassay of nucleocapsid protein from SARS-CoV-2. *Anal Bioanal Chem* **413**, 4635–4644 (2021).

6. Kim, C. *et al.* Nanoelectrokinetic-assisted lateral flow assay for COVID-19 antibody test. *Biosensors and Bioelectronics* **212**, 114385 (2022).

7. Cardoso, A. G. *et al.* Electrochemical sensing of analytes in saliva: Challenges, progress, and perspectives. *TrAC Trends in Analytical Chemistry* **160**, 116965 (2023).

8. Schoukroun-Barnes, L. R. *et al.* Reagentless, Structure-Switching, Electrochemical Aptamer-Based Sensors. *Annual Rev. Anal. Chem.* **9**, 163–181 (2016).

9. Zhang, Z. *et al.* High-Affinity Dimeric Aptamers Enable the Rapid Electrochemical Detection of Wild-Type and B.1.1.7 SARS-CoV-2 in Unprocessed Saliva. *Angewandte Chemie Intl Edit* **60**, 24266–24274 (2021).

10. Li, J. *et al.* Three on Three: Universal and High-Affinity Molecular Recognition of the Symmetric Homotrimeric Spike Protein of SARS-CoV-2 with a Symmetric Homotrimeric Aptamer. *J. Am. Chem. Soc.* **144**, 23465–23473 (2022).

11. Zhang, Z. *et al.* A Universal DNA Aptamer that Recognizes Spike Proteins of Diverse SARS-CoV-2 Variants of Concern. *Chemistry A European J* **28**, (2022).

12. Wang, J. *et al.* Highly efficient and multidimensional extraction of targets from complex matrices using aptamer-driven recognition. *Nano Res.* **10**, 145–156 (2017).

13. Sen, P. *et al.* Integrating Water Purification with Electrochemical Aptamer Sensing for Detecting SARS-CoV-2 in Wastewater. *ACS Sens.* **8**, 1558–1567 (2023).

14. Lazanas, A. Ch. & Prodromidis, M. I. Electrochemical Impedance Spectroscopy—A Tutorial. *ACS Meas. Sci. Au* acsmeasuresciau.2c00070 (2023) doi:10.1021/acsmeasuresciau.2c00070.

15. Van Duuren, J. B. J. H. *et al.* Use of Single-Frequency Impedance Spectroscopy to Characterize the Growth Dynamics of Biofilm Formation in Pseudomonas aeruginosa. *Sci Rep* **7**, 5223 (2017).

16. Sopčić, S., Antonić, D., Mandić, Z., Kvastek, K. & Horvat-Radošević, V. Single and multi-frequency impedance characterization of symmetric activated carbon single capacitor cells. *J. Electrochem. Sci. Eng.* **8**, 183–195 (2018).

17. Xi, W. & Haes, A. J. Elucidation of HEPES Affinity to and Structure on Gold Nanostars. *J. Am. Chem. Soc.* **141**, 4034–4042 (2019).

18. Lew, T. T. S. *et al.* Epitope-Functionalized Gold Nanoparticles for Rapid and Selective Detection of SARS-CoV-2 IgG Antibodies. *ACS Nano* **15**, 12286–12297 (2021).

19. Vogiazi, V., De La Cruz, A., Heineman, W. R., White, R. J. & Dionysiou, D. D. Effects of Experimental Conditions on the Signaling Fidelity of Impedance-Based Nucleic Acid Sensors. *Anal. Chem.* **93**, 812–819 (2021).

20. Dai, Y., Xu, W. & Liu, C. C. Immunoglobulin G-Based Steric Hindrance Assay for Protein Detection. *ACS Sens.* **5**, 140–146 (2020).

21. Chiappin, S., Antonelli, G., Gatti, R. & De Palo, E. F. Saliva specimen: A new laboratory tool for diagnostic and basic investigation. *Clinica Chimica Acta* **383**, 30–40 (2007).

22. Yousefi, H. *et al.* Detection of SARS-CoV-2 Viral Particles Using Direct, Reagent-Free Electrochemical Sensing. *J. Am. Chem. Soc.* **143**, 1722–1727 (2021).

23. Vogels, C. B. F. *et al.* SalivaDirect: A simplified and flexible platform to enhance SARS-CoV-2 testing capacity. *Med* **2**, 263-280.e6 (2021).

24. Lamy, E. *et al.* Effect of thermal and chemical treatments used for SARS-COV-2 inactivation in the measurement of saliva analytes. *Sci Rep* **12**, 9434 (2022).

25. Vaghasiya, J. V., Mayorga-Martinez, C. C. & Pumera, M. Wearable sensors for telehealth based on emerging materials and nanoarchitectonics. *npj Flex Electron* **7**, 26 (2023).

26. Dong, T., Matos Pires, N. M., Yang, Z. & Jiang, Z. Advances in Electrochemical Biosensors Based on Nanomaterials for Protein Biomarker Detection in Saliva. *Advanced Science* **10**, 2205429 (2023).

27. Malon, R. S. P., Sadir, S., Balakrishnan, M. & Córcoles, E. P. Saliva-Based Biosensors: Noninvasive Monitoring Tool for Clinical Diagnostics. *BioMed Research International* **2014**, 1–20 (2014).

28. Ruopp, M. D., Perkins, N. J., Whitcomb, B. W. & Schisterman, E. F. Youden Index and Optimal Cut-Point Estimated from Observations Affected by a Lower Limit of Detection. *Biom. J.* **50**, 419–430 (2008).

29. Nahm, F. S. Receiver operating characteristic curve: overview and practical use for clinicians. *Korean J Anesthesiol* **75**, 25–36 (2022).

30. Emergency Use Authorization of Medical Products and Related Authorities. Guidance for Industry and Other Stakeholders. U.S. Department of Health and Human Services Food and Drug Administration Office of the Commissioner Office of the Chief Scientist Office of Counterterrorism and Emerging Threats. January 2017.

31. Policy for Coronavirus Disease-2019 Tests (Revised). Guidance for Developers and Food and Drug Administration Staff. U.S. Department of Health and Human Services Food and Drug Administration, Center for Devices and Radiological Health January 12, 2023.

32. Kenton, W. Three Sigma Limits Statistical Calculation, With an Example. May 31, 2022.

33. Breitkopf, S. B. *et al.* A Cross-Species Study of PI3K Protein-Protein Interactions Reveals the Direct Interaction of P85 and SHP2. *Sci Rep* **6**, 20471 (2016).

34. Chen, H., Liu, K., Li, Z. & Wang, P. Point of care testing for infectious diseases. *Clinica Chimica Acta* **493**, 138–147 (2019).

35. Choi, J. R. Development of Point-of-Care Biosensors for COVID-19. *Front. Chem.* **8**, 517 (2020).

36. Batra, R. *et al.* A comparative evaluation between the Abbott Panbio™ COVID-19 IgG/IgM rapid test device and Abbott Architect™ SARS CoV-2 IgG assay. *Journal of Clinical Virology* **132**, 104645 (2020).

37. Gremmels, H. *et al.* Real-life validation of the Panbio™ COVID-19 antigen rapid test (Abbott) in community-dwelling subjects with symptoms of potential SARS-CoV-2 infection. *EClinicalMedicine* **31**, 100677 (2021).

38. Downs, A. M. & Plaxco, K. W. Real-Time, *In Vivo* Molecular Monitoring Using Electrochemical Aptamer Based Sensors: Opportunities and Challenges. *ACS Sens.* **7**, 2823–2832 (2022).

39. PalmSens4 Brochure. Jan 2, 2023.

40. Fischer, L. M. *et al.* Gold cleaning methods for electrochemical detection applications. *Microelectronic Engineering* **86**, 1282–1285 (2009).

CLAIMS

1. A biosensor system for detecting a label-free target in a sample, comprising:
   a) an electrochemical impedance spectroscopy (EIS) module comprising (i) a working electrode, operable at a single frequency for real-time monitoring of aptamer binding to target, aptamer-target dissociation, or aptamer or target degradation on the working electrode, (ii) a counter electrode, (iii) a reference electrode, and (iv) a circuit compatible with potentiostat;
   b) a multimeric aptamer comprising two or more units for specific target binding and formation of an aptamer-target complex in solution, wherein the target comprises two or more binding sites, wherein the multimeric aptamer has a K_d < about 300 pM;
   wherein the multimeric aptamer is configured to bind to the surface of the working electrode, and
   wherein the biosensor system is configured to operate in a wash-free and single-pot format.

2. The biosensor system of claim 1, wherein the multimeric aptamer is biotinylated and the surface of the working electrode is coated with streptavidin.

3. The biosensor system of claim 1 or 2, wherein the working electrode is a gold working electrode.

4. The biosensor system of claim 3, wherein the counter electrode is a gold counter electrode.

5. The biosensor system of claim 3 or 4, wherein the reference electrode is a silver reference electrode.

6. The biosensor system of any one of claims 1-5, wherein the solution comprises a readout buffer comprising phosphate buffer saline, KCl, and redox reporter.

7. The biosensor system of claim 6, wherein the redox reporter comprises $K_3[Fe(CN)_6]/K_4[Fe(CN)_6]$, $[Fe(CN)_6]^{3-}/[Fe(CN)_6]^{4-}$, Q/H_2Q, $[Ru(NH_3)_6]^{3+}/[Ru(NH_3)_6]^{2+}$, MB^+/MBH_2, or MV^{2+}/MV^+ redox reporter.

8. The biosensor system claim 7, wherein the solution comprises redox reporter at about 2 mM $K_3[Fe(CN)_6]$ and about 2 mM $K_4[Fe(CN)_6]$.

9. The biosensor system of any one of claims 1-8, wherein the solution comprises a blocking buffer comprising biotin-BSA and BSA.

10. The biosensor system of claim 9, wherein the solution comprises about 0.01 μM biotin-BSA and about 0.1% BSA.

11. The biosensor system of any one of claims 1-10, wherein the solution comprises a binding buffer comprising HEPES, NaCl, KCl, $MgCl_2$, and $CaCl_2$.

12. The biosensor system of claim 11, wherein the solution comprises about 5 mM HEPES, pH about 7.4, about 15 mM NaCl, about 0.6 mM KCl, about 0.25 mM $MgCl_2$, and about 0.25 mM $CaCl_2$.

13. The biosensor system of any one of claims 1-12, wherein the sample is a clinical sample.

14. The biosensor system of any one of claims 1-13, wherein the sample is saliva.

15. The biosensor system of claim 14, wherein the saliva is heat-treated saliva.

16. The biosensor system of any one of claims 1-15, wherein the target is a protein target, a viral target, or a bacterial target.

17. The biosensor system of claim 16, wherein the viral target is SARS-CoV-2 or influenza.

18. The biosensor system of claim 17, wherein the viral target is SARS-CoV-2.

19. The biosensor system of claim 18, wherein the SARS-CoV-2 is SARS-CoV-2 B.1.1.529 omicron variant.

20. The biosensor system of claim 16, wherein the protein target is SARS-CoV-2 B.1.1.529 omicron variant spike protein.

21. The biosensor system of any one of claims 17-20, wherein the aptamer is a SARS-CoV-2 specific aptamer having the nucleic acid sequence of SEQ ID NO: 6, 7, or 11.

22. The biosensor system of any one of claims 17-21, wherein the biosensor system is configured to detect SARS-CoV-2 B.1.1.529 omicron variant with a limit-of-detection of about 138 copies/mL in the solution comprising the redox buffer, the blocking buffer, and the binding buffer.

23. The biosensor system of any one of claims 17-21, wherein the biosensor system is configured to detect SARS-CoV-2 with a limit-of-detection of about 584 copies/mL in heat-treated saliva diluted to about 25% (v/v) in the solution comprising the redox buffer, the blocking buffer, and the binding buffer.

24. The biosensor system of claim 17, wherein the viral target is influenza, and/or wherein the aptamer is an influenza specific aptamer having the nucleic acid sequence of SEQ ID NO: 1, 2, or 9.

25. The biosensor system of claim 16, wherein the protein target is vascular endothelial growth factor (VEGF).

26. The biosensor system of claim 25, wherein the aptamer is a VEGF specific aptamer having the nucleic acid sequence of SEQ ID NO: 4, 5, or 10.

27. The biosensor system of any one of claims 1-26, wherein the biosensor system provides at least 80% sensitivity and at least 99% specificity.

28. The biosensor system of claim 27, wherein the biosensor system provides at least 93% sensitivity.

29. The biosensor system of claim 27 or 28, wherein the biosensor system provides at least 98% sensitivity.

30. The biosensor system of any one of claims 27-29, wherein the biosensor system provides 100% specificity.

31. A method for detecting a label-free target real-time in a sample, comprising:

a) mixing the sample with a solution comprising a redox readout buffer, a binding buffer, a blocking buffer, and the multimeric aptamer of the biosensor system of any one of claims 1-30 to provide a mixture,

b) applying the mixture onto the working electrode of the biosensor system of any one of claims 1-30,

c) measuring total impedance at a single frequency at real-time for about 30 minutes, and

d) calculating fold change of the total impedance ($\Delta Z_t/Z_t$),

wherein $\Delta Z_t/Z_t$ >= about 1.2 at any time from 1 minute to 30 minutes indicates the presence of the target in the sample.

32. The method of claim 31, wherein the single frequency is between about 1 and about 20 kHz.

33. The method of claim 32, wherein the single frequency is between about 12.6 and about 80 Hz.

34. The method of claim 33, wherein the single frequency is about 12.6 Hz.

35. The method of any one of claims 31-34, wherein the total impedance is measured at intervals of every 2 minutes.

36. A kit for detecting a label-free target in a sample, comprising the biosensor system of any one of claims 1-30, further comprising at least one of a dropper, a collection tube, a container holding the redox readout buffer, a container holding the binding buffer, a container holding the block buffer, and instruction for use.

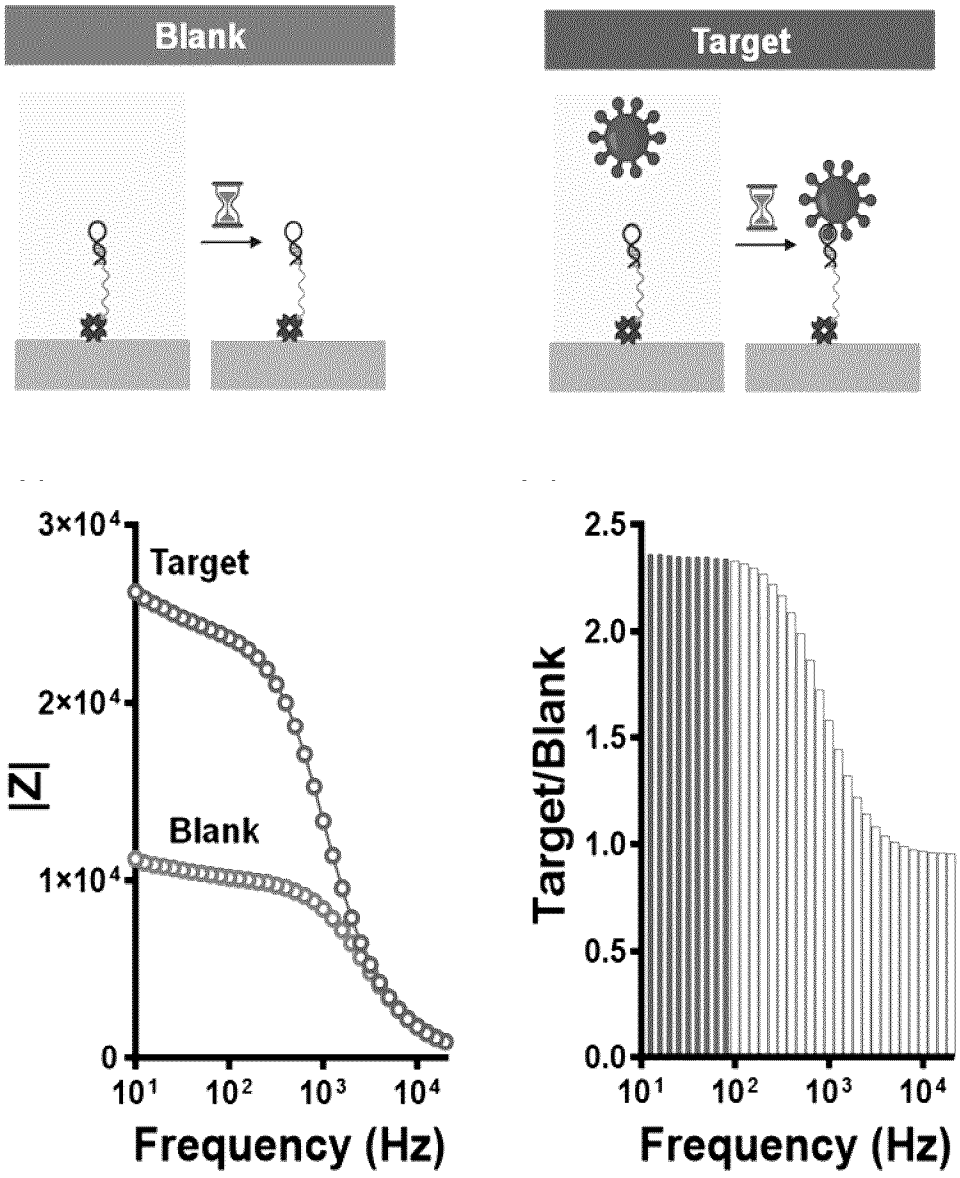
Blank
Target
3×10⁴
2×10⁴
1×10⁴
0
|Z|
Target
Blank
10¹
10²
10³
10⁴
Frequency (Hz)
2.5
2.0
1.5
1.0
0.5
0.0
Target/Blank
10¹
10²
10³
10⁴
Frequency (Hz)

FIG. 1A

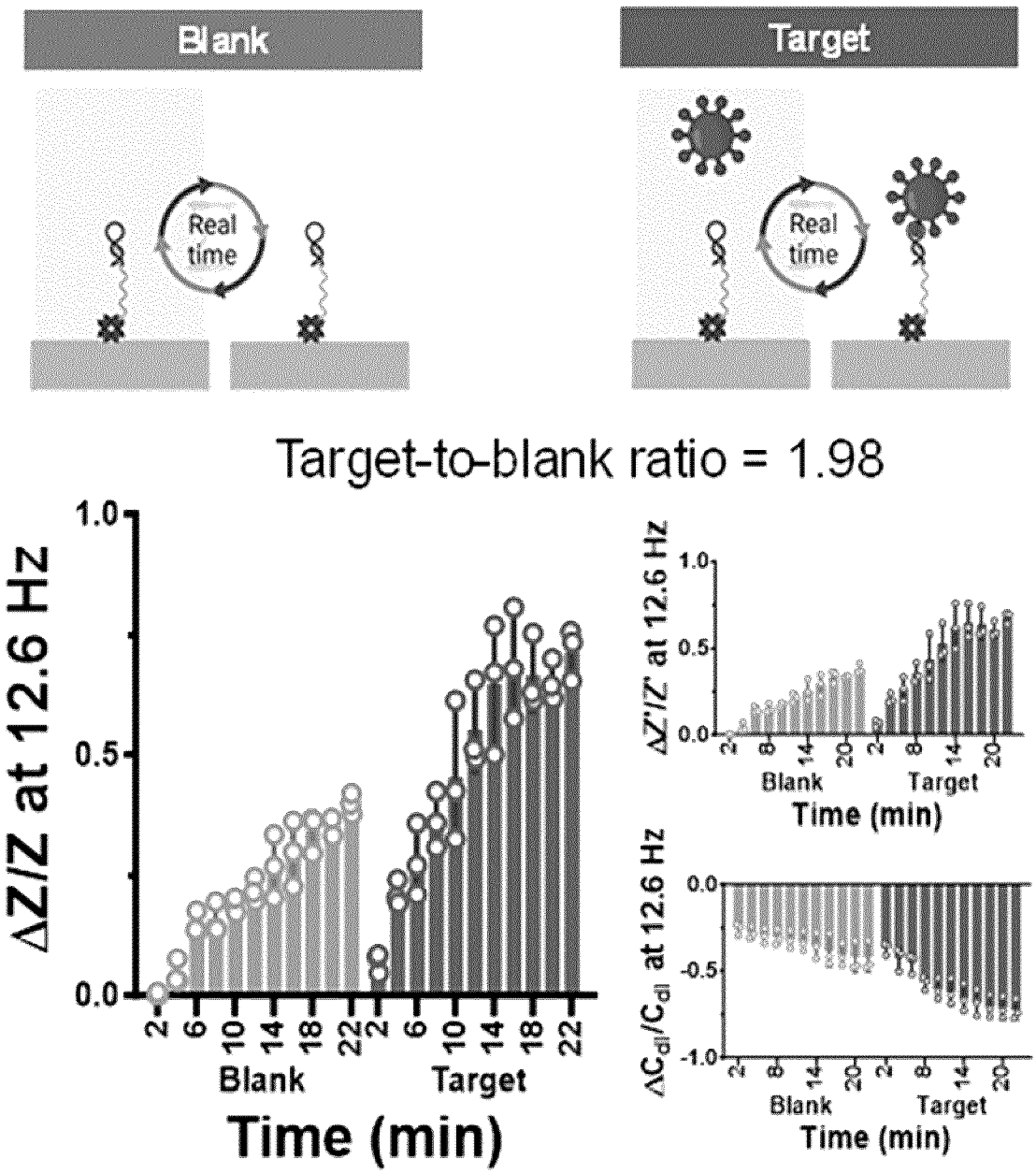
Blank
Target
Real time
Real time
Target-to-blank ratio = 1.98
ΔZ/Z at 12.6 Hz
1.0
0.5
0.0
2 6 10 14 18 22 2 6 10 14 18 22
Blank
Target
Time (min)
ΔZ'/Z' at 12.6 Hz
1.0
0.5
0.0
2 8 14 20 2 8 14 20
Blank
Target
Time (min)
ΔCdl/Cdl at 12.6 Hz
0.0
-0.5
-1.0
2 8 14 20 2 8 14 20
Blank
Target
Time (min)

FIG. 1B

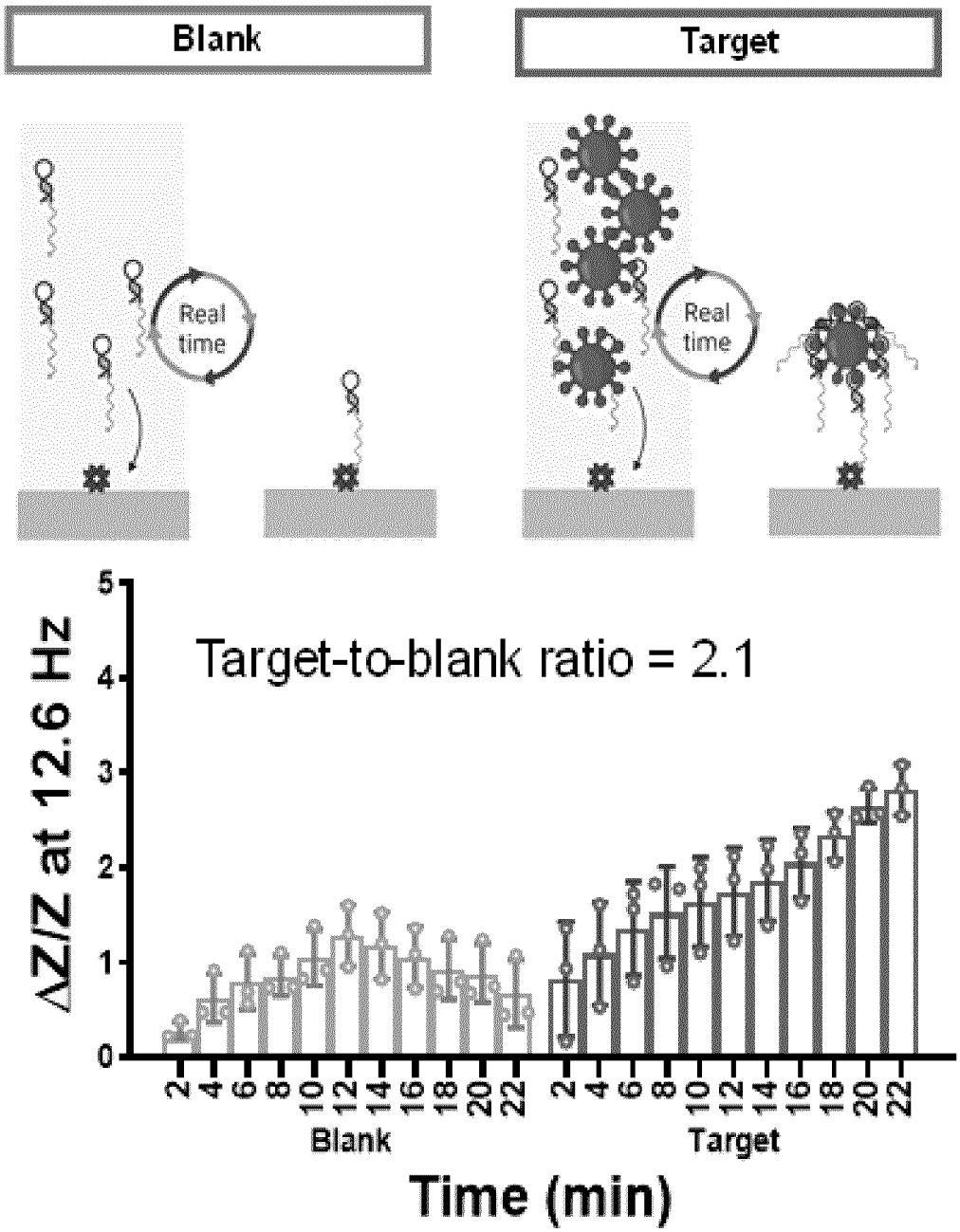
Blank
Target
Real time
Real time
Target-to-blank ratio = 2.1
ΔZ/Z at 12.6 Hz
0
1
2
3
4
5
2 4 6 8 10 12 14 16 18 20 22
2 4 6 8 10 12 14 16 18 20 22
Blank
Target
Time (min)

FIG. 1C

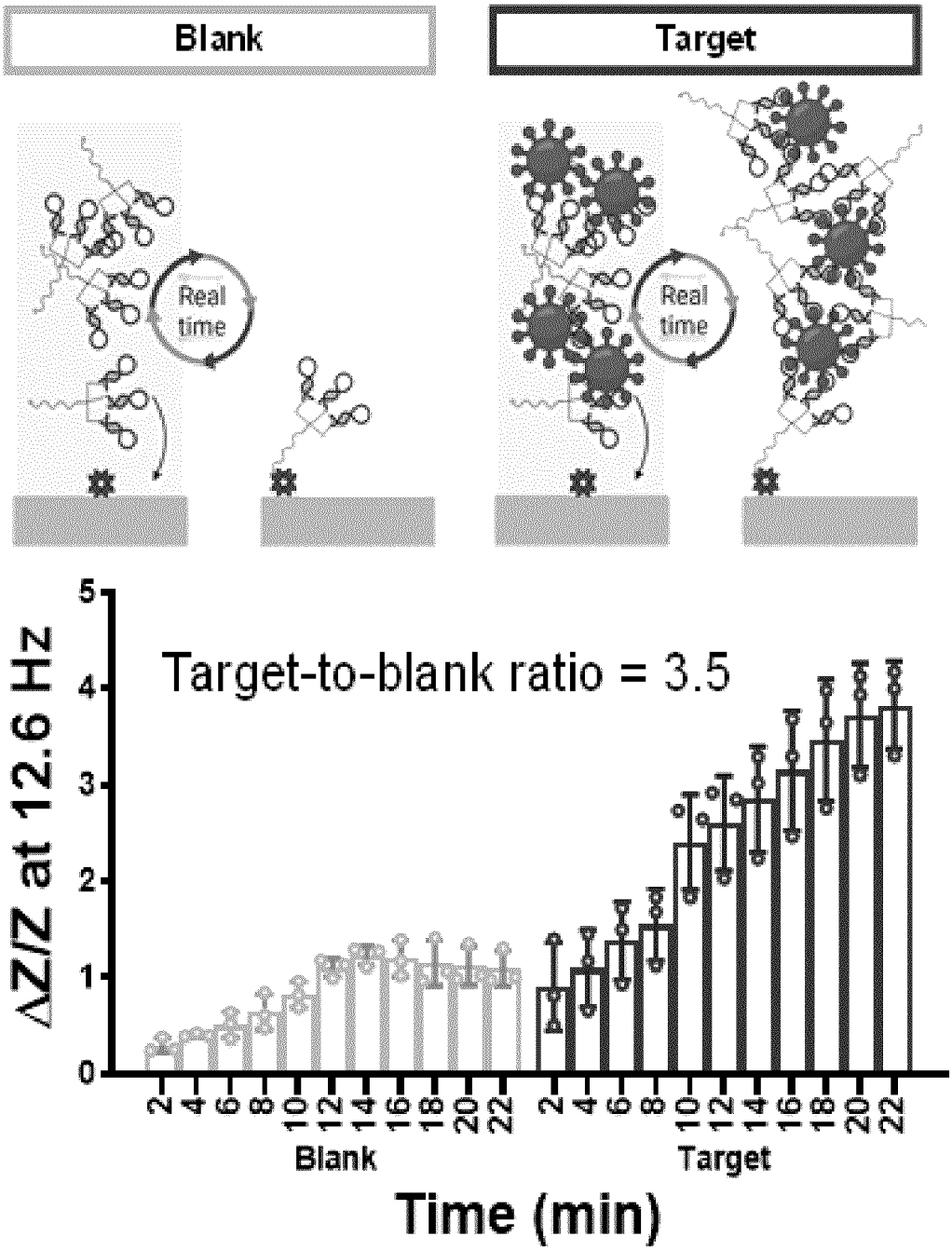
Blank
Target
Real time
Real time
Target-to-blank ratio = 3.5
ΔZ/Z at 12.6 Hz
0
1
2
3
4
5
2 4 6 8 10 12 14 16 18 20 22
2 4 6 8 10 12 14 16 18 20 22
Blank
Target
Time (min)

FIG. 1D

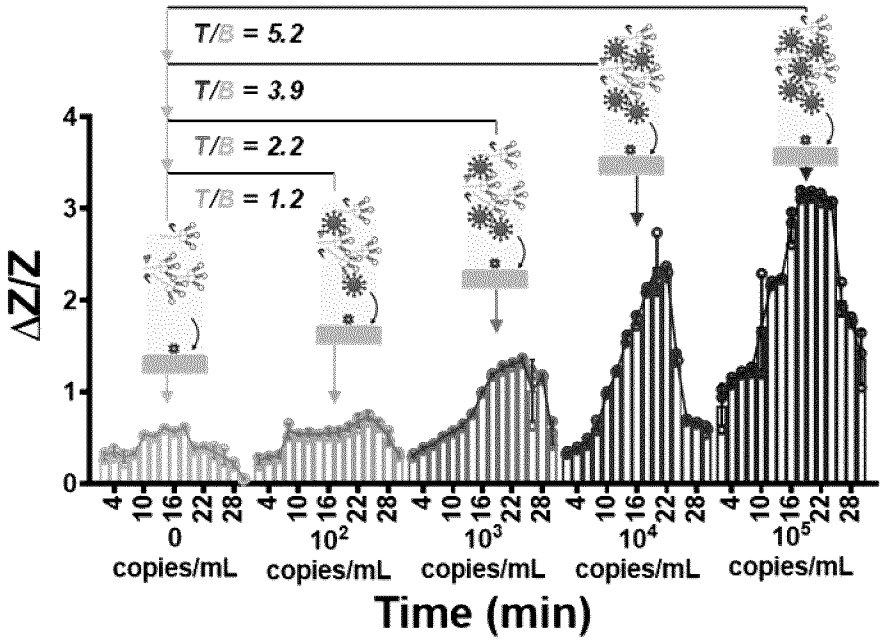
T/B = 5.2
T/B = 3.9
T/B = 2.2
T/B = 1.2
ΔZ/Z
0
1
2
3
4
4 10 16 22 28
0 copies/mL
10² copies/mL
10³ copies/mL
10⁴ copies/mL
10⁵ copies/mL
Time (min)

FIG. 2A

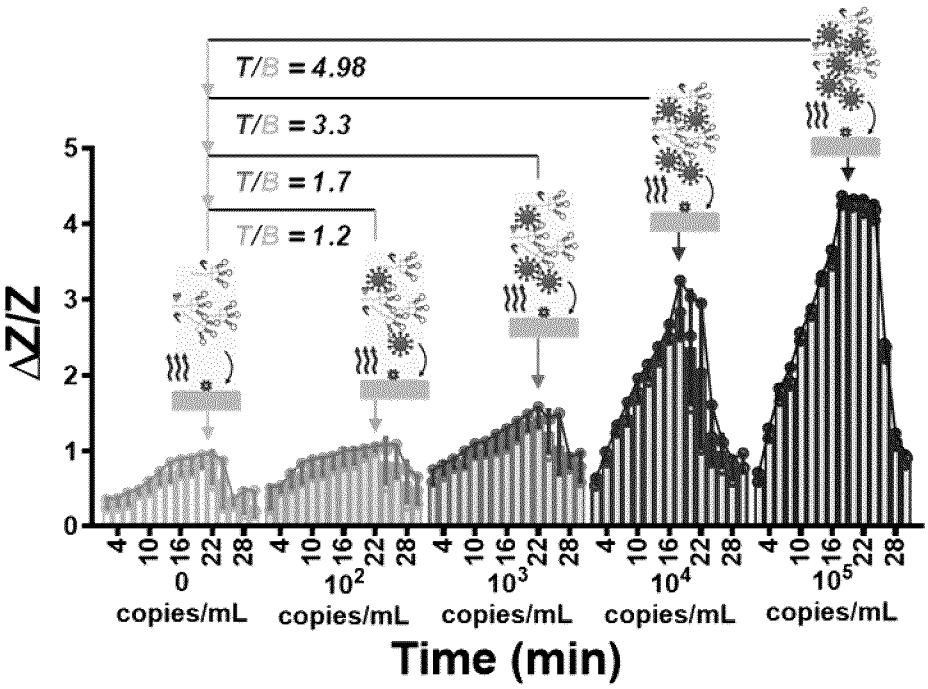
T/B = 4.98
T/B = 3.3
T/B = 1.7
T/B = 1.2
ΔZ/Z
0
1
2
3
4
5
4 10 16 22 28
0 copies/mL
10² copies/mL
10³ copies/mL
10⁴ copies/mL
10⁵ copies/mL
Time (min)

FIG. 2B

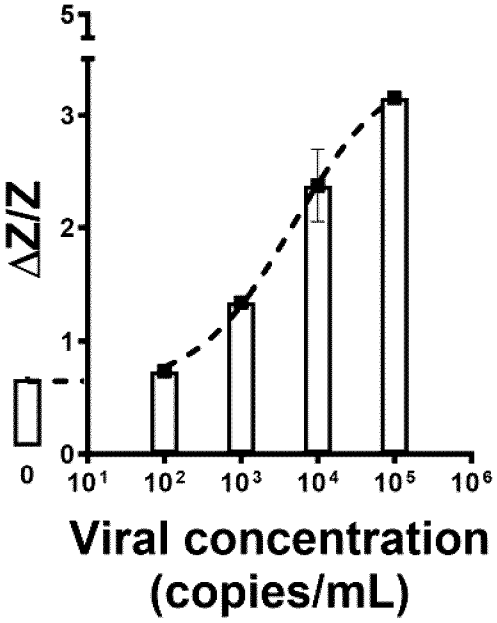
5
3
2
1
0
ΔZ/Z
0
10^1
10^2
10^3
10^4
10^5
10^6
Viral concentration
(copies/mL)

FIG. 2C

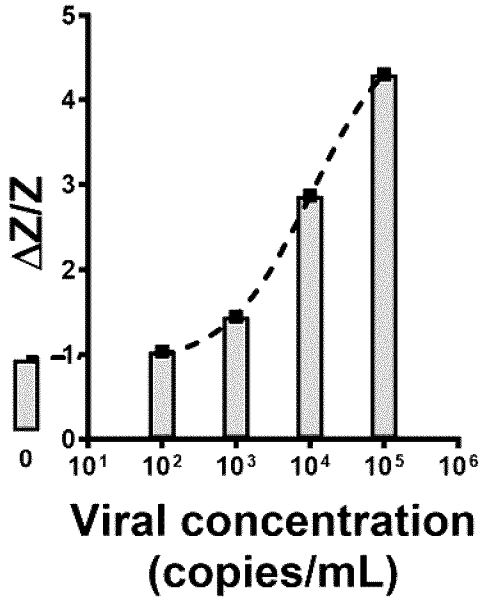
5
4
3
2
1
0
ΔZ/Z
0
10^1
10^2
10^3
10^4
10^5
10^6
Viral concentration
(copies/mL)

FIG. 2D

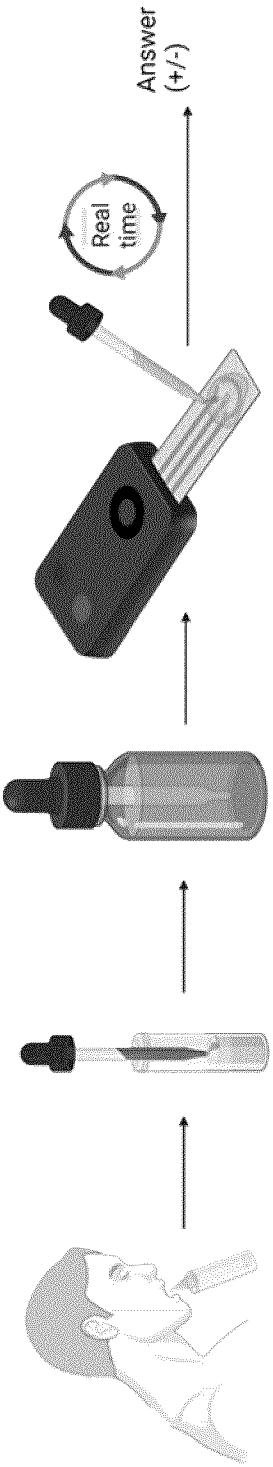

FIG. 3A

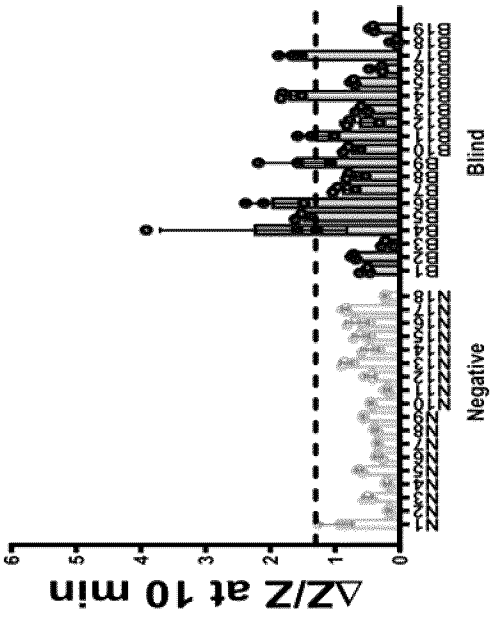

FIG. 3C

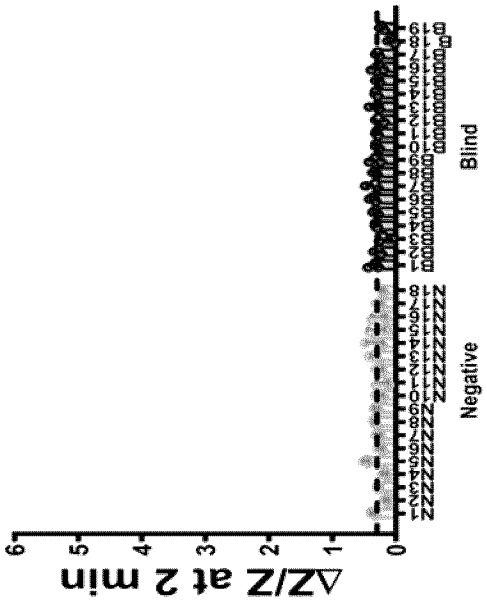

FIG. 3B

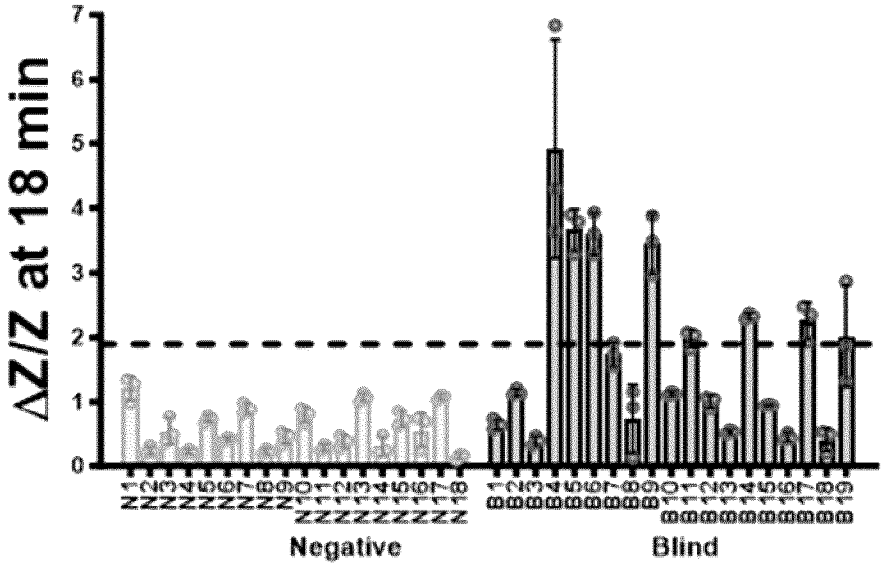
ΔZ/Z at 18 min
0
1
2
3
4
5
6
7
Negative
Blind

FIG. 3D

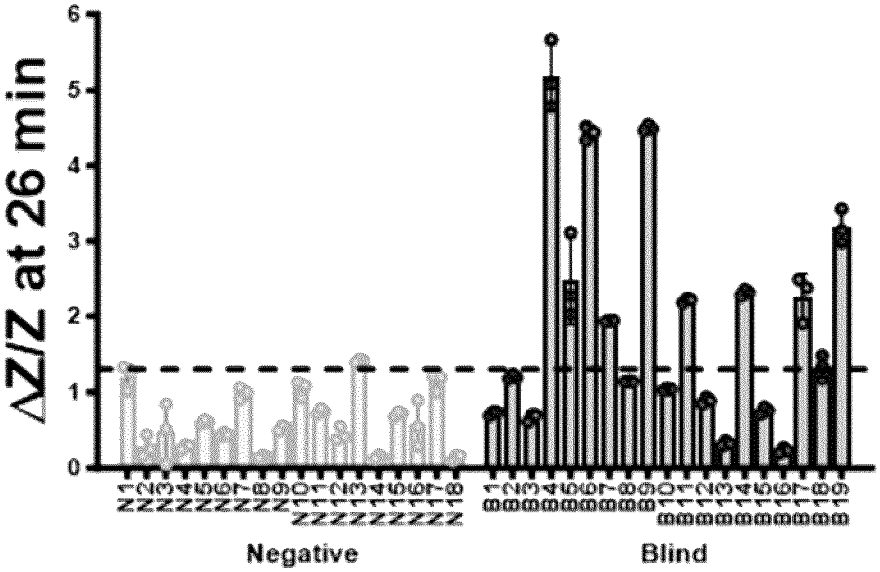
ΔZ/Z at 26 min
0
1
2
3
4
5
6
Negative
Blind

FIG. 3E

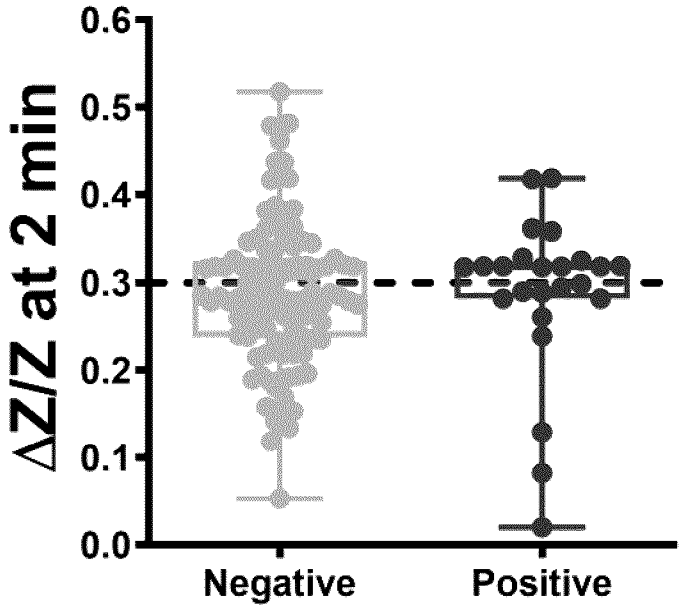
ΔZ/Z at 2 min
0.6
0.5
0.4
0.3
0.2
0.1
0.0
Negative
Positive

FIG. 3F

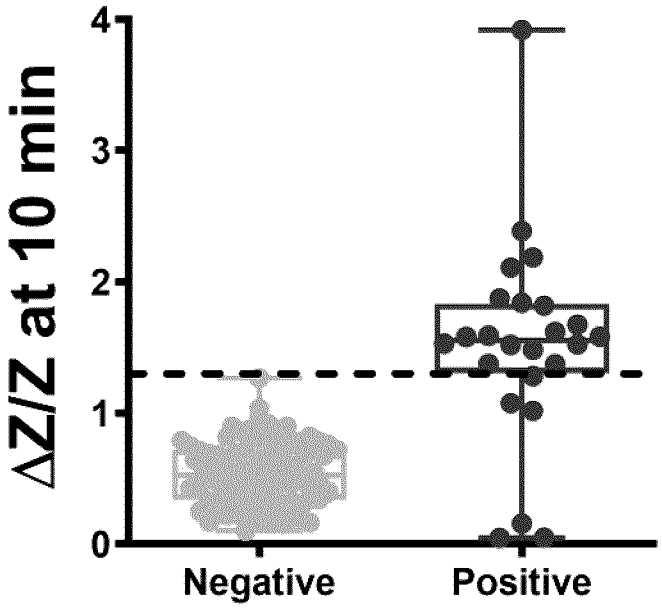
ΔZ/Z at 10 min
4
3
2
1
0
Negative
Positive

FIG. 3G

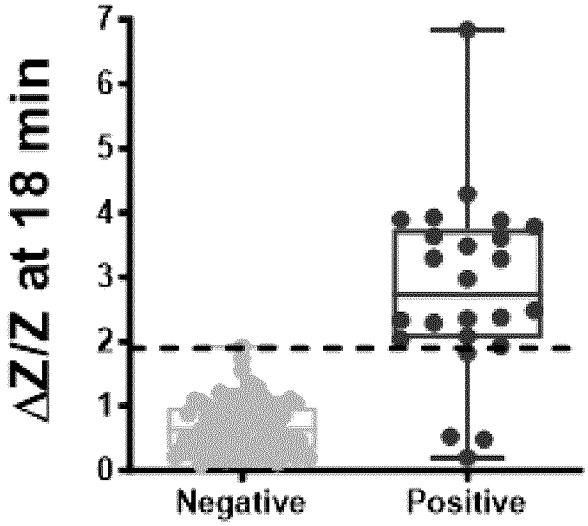
ΔZ/Z at 18 min
7
6
5
4
3
2
1
0
Negative
Positive

FIG. 3H

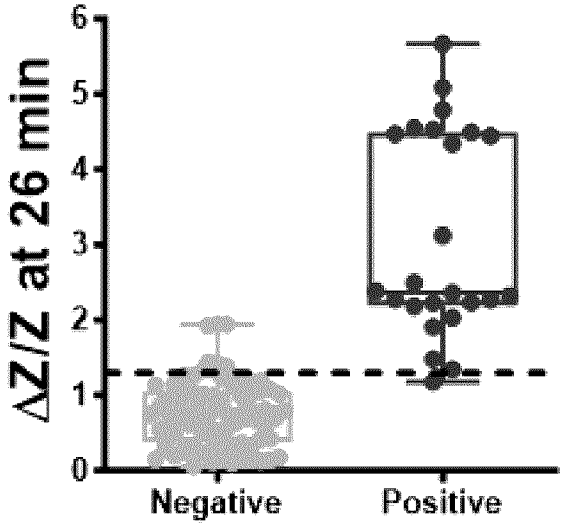
ΔZ/Z at 26 min
6
5
4
3
2
1
0
Negative
Positive

FIG. 3I

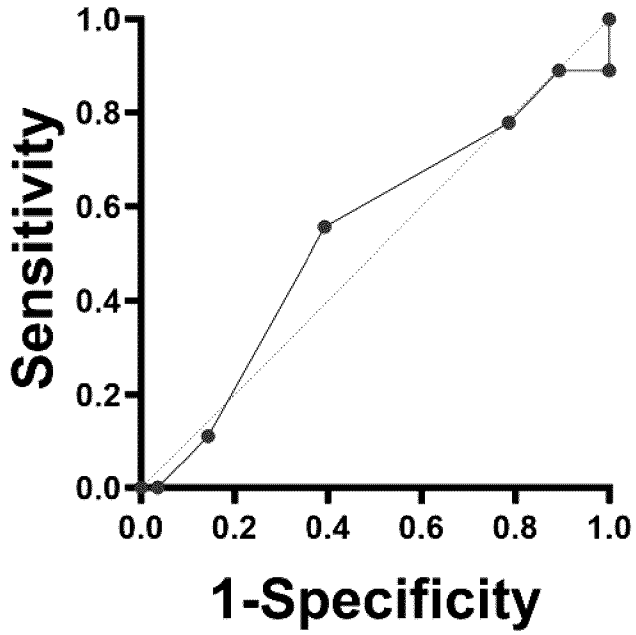
Sensitivity
1.0
0.8
0.6
0.4
0.2
0.0
0.0
0.2
0.4
0.6
0.8
1.0
1-Specificity

FIG. 3J

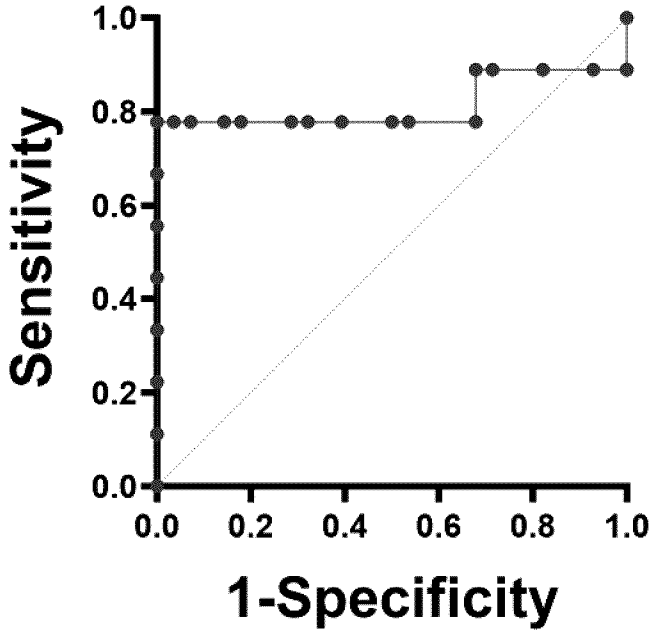
Sensitivity
1.0
0.8
0.6
0.4
0.2
0.0
0.0
0.2
0.4
0.6
0.8
1.0
1-Specificity

FIG. 3K

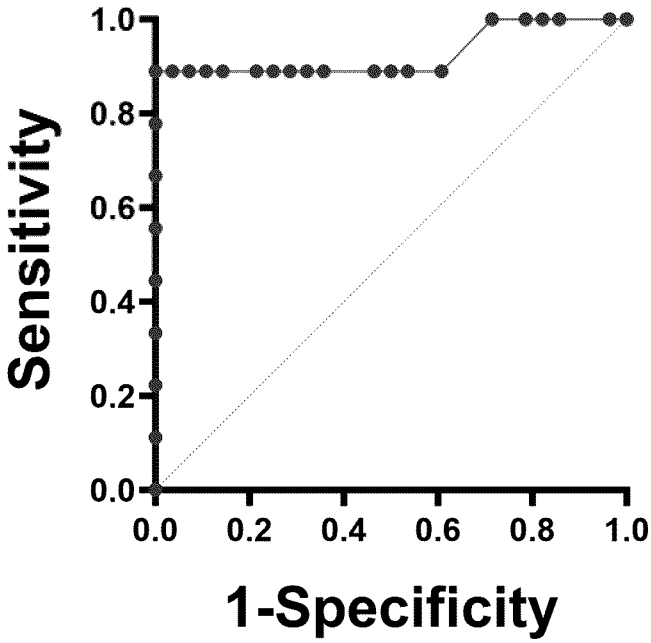
Sensitivity
1.0
0.8
0.6
0.4
0.2
0.0
0.0
0.2
0.4
0.6
0.8
1.0
1-Specificity

FIG. 3L

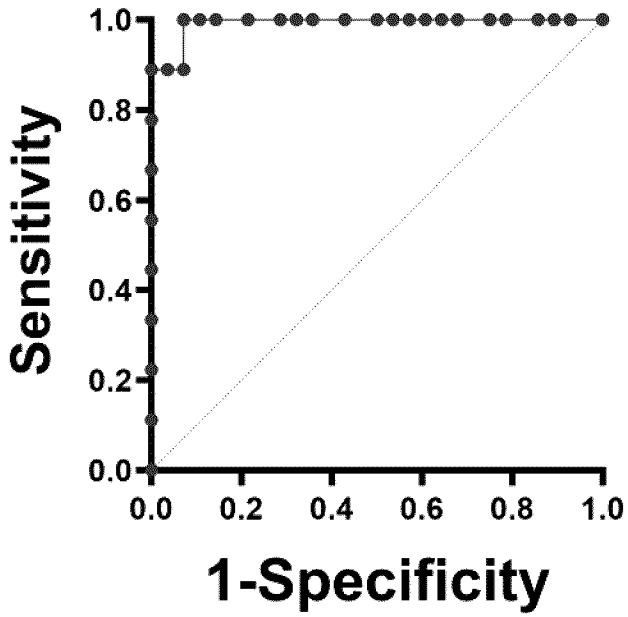
Sensitivity
1.0
0.8
0.6
0.4
0.2
0.0
0.0
0.2
0.4
0.6
0.8
1.0
1-Specificity

FIG. 3M

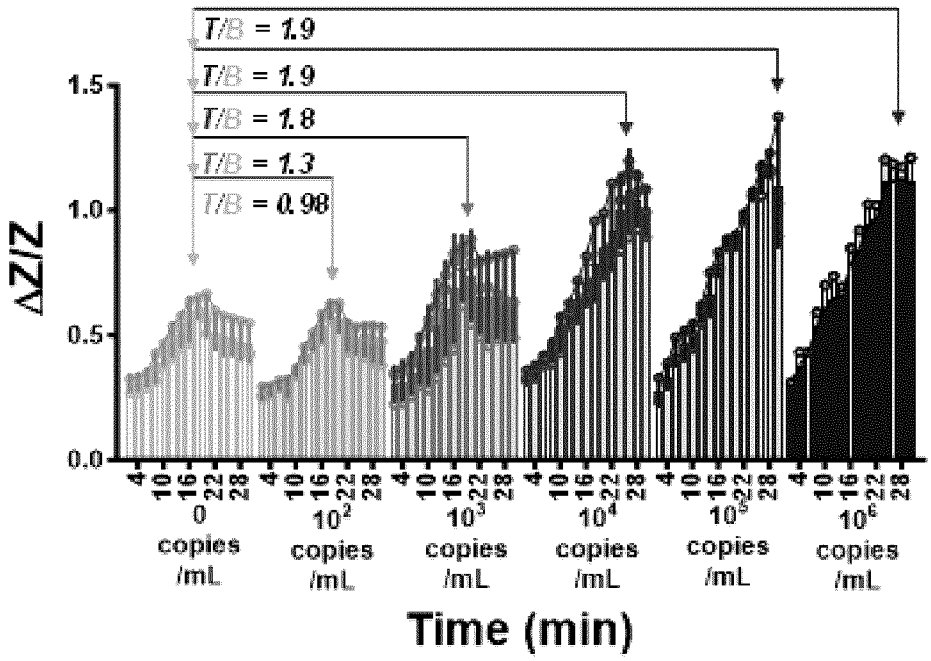
T/B = 1.9
T/B = 1.9
T/B = 1.8
T/B = 1.3
T/B = 0.98
ΔZ/Z
1.5
1.0
0.5
0.0
4 10 16 22 28
0 copies /mL
10² copies /mL
10³ copies /mL
10⁴ copies /mL
10⁵ copies /mL
10⁶ copies /mL
Time (min)

FIG. 4A

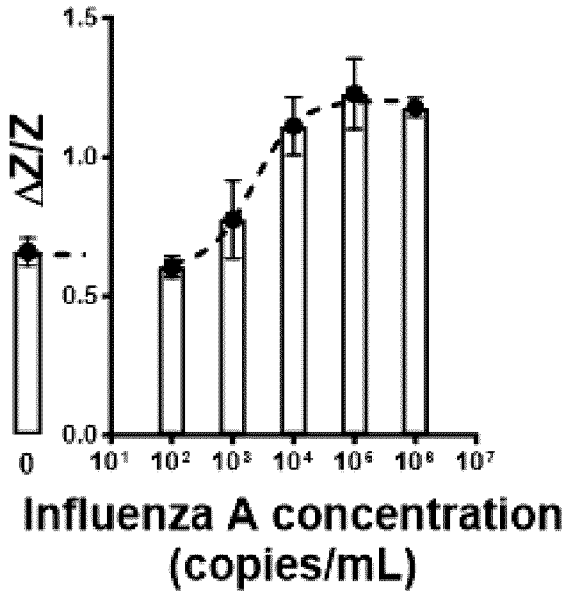
ΔZ/Z
1.5
1.0
0.5
0.0
0
10¹ 10² 10³ 10⁴ 10⁵ 10⁶ 10⁷
Influenza A concentration (copies/mL)

FIG. 4B

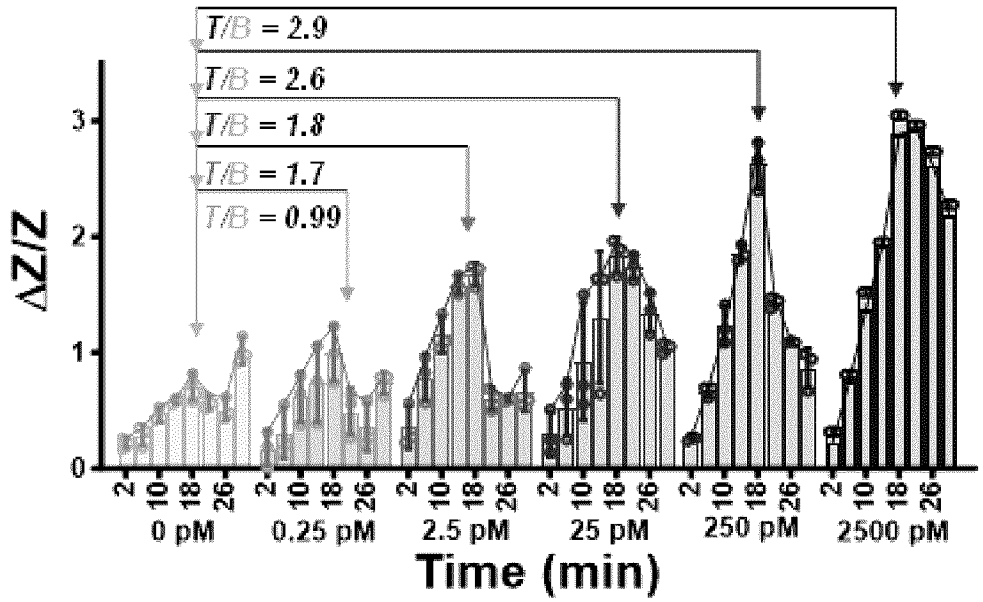
T/B = 2.9
T/B = 2.6
T/B = 1.8
T/B = 1.7
T/B = 0.99
ΔZ/Z
0
1
2
3
2 10 18 26
0 pM
0.25 pM
2.5 pM
25 pM
250 pM
2500 pM
Time (min)

FIG. 4C

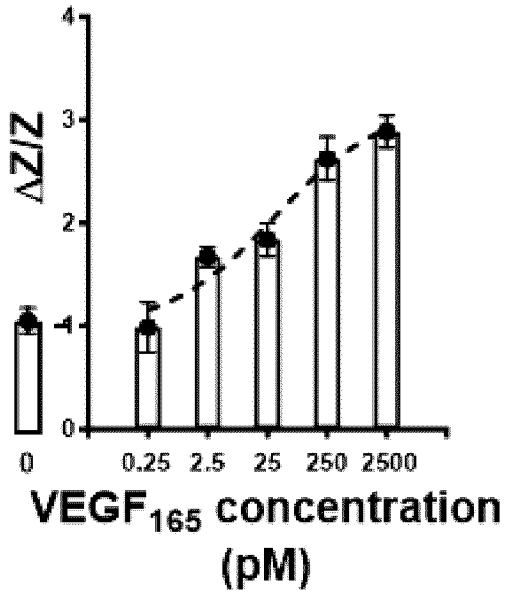
ΔZ/Z
0
1
2
3
4
0
0.25
2.5
25
250
2500
VEGF165 concentration (pM)

FIG. 4D

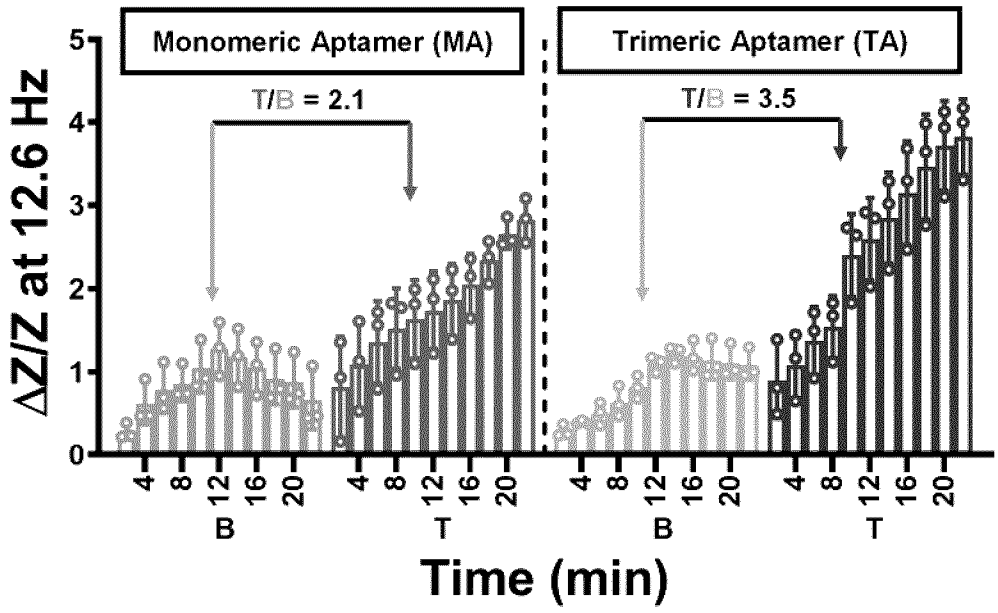
Monomeric Aptamer (MA)
Trimeric Aptamer (TA)
T/B = 2.1
T/B = 3.5
ΔZ/Z at 12.6 Hz
0
1
2
3
4
5
4
8
12
16
20
B
T
Time (min)

FIG. 5A

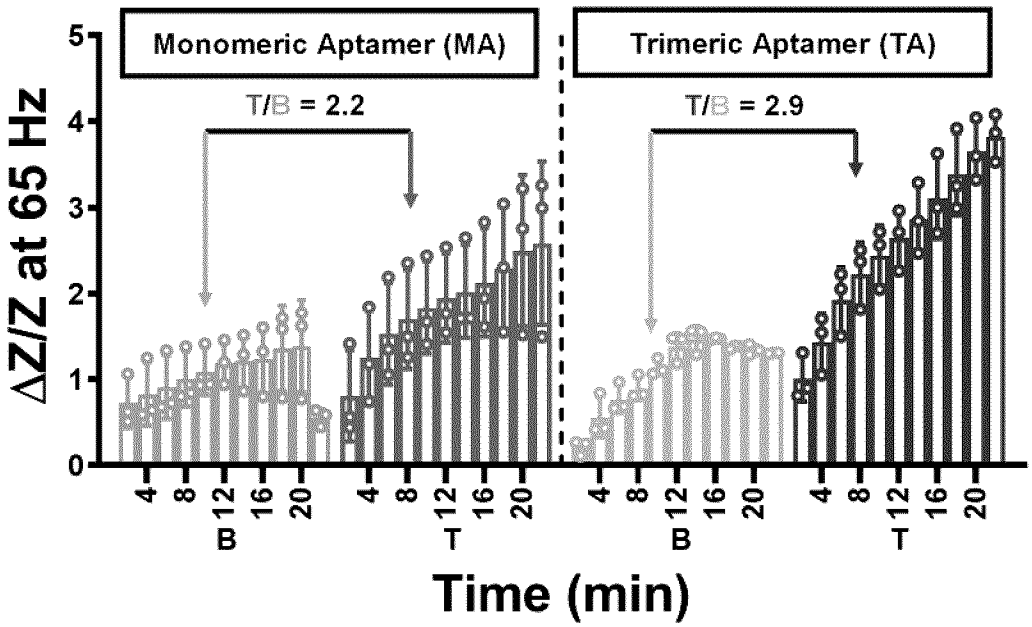
Monomeric Aptamer (MA)
Trimeric Aptamer (TA)
T/B = 2.2
T/B = 2.9
ΔZ/Z at 65 Hz
0
1
2
3
4
5
4
8
12
16
20
B
T
Time (min)

FIG. 5B

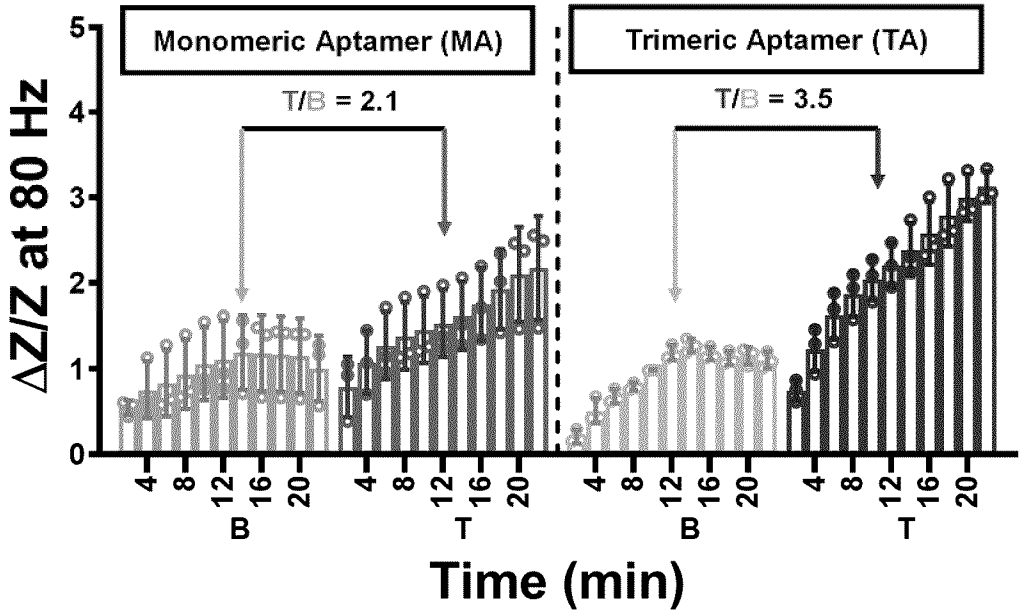
Monomeric Aptamer (MA)
Trimeric Aptamer (TA)
T/B = 2.1
T/B = 3.5
ΔZ/Z at 80 Hz
0
1
2
3
4
5
4 8 12 16 20 4 8 12 16 20 4 8 12 16 20 4 8 12 16 20
B T B T
Time (min)

FIG. 5C

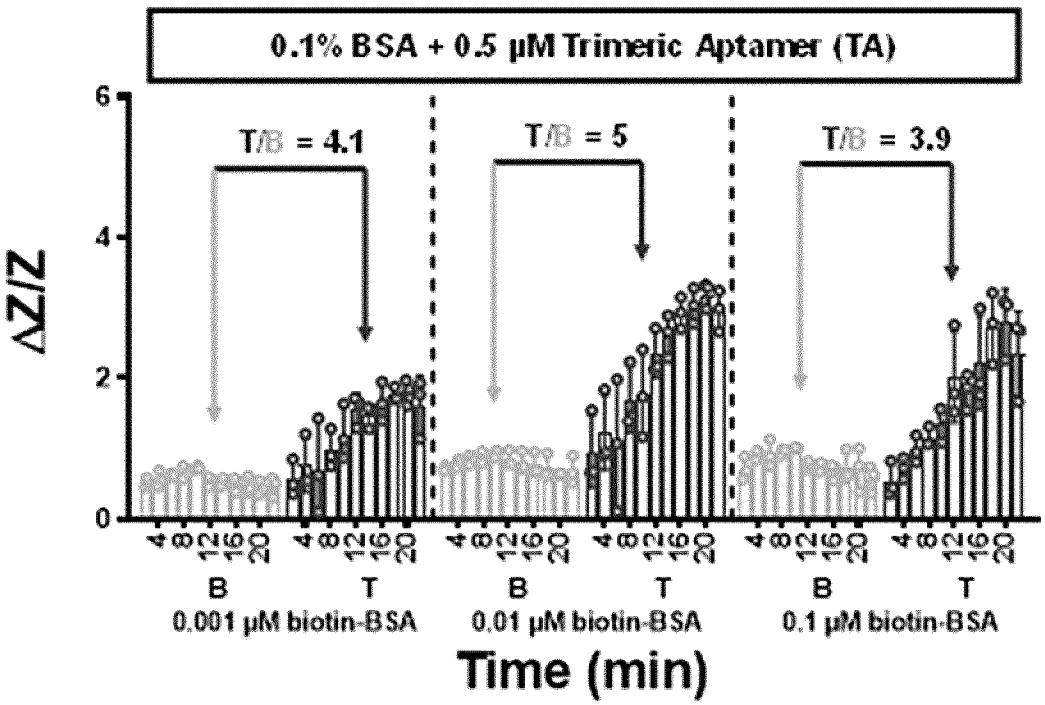
0.1% BSA + 0.5 μM Trimeric Aptamer (TA)
T/B = 4.1
T/B = 5
T/B = 3.9
ΔZ/Z
0
2
4
6
B T B T B T
0.001 μM biotin-BSA
0.01 μM biotin-BSA
0.1 μM biotin-BSA
Time (min)

FIG. 6A

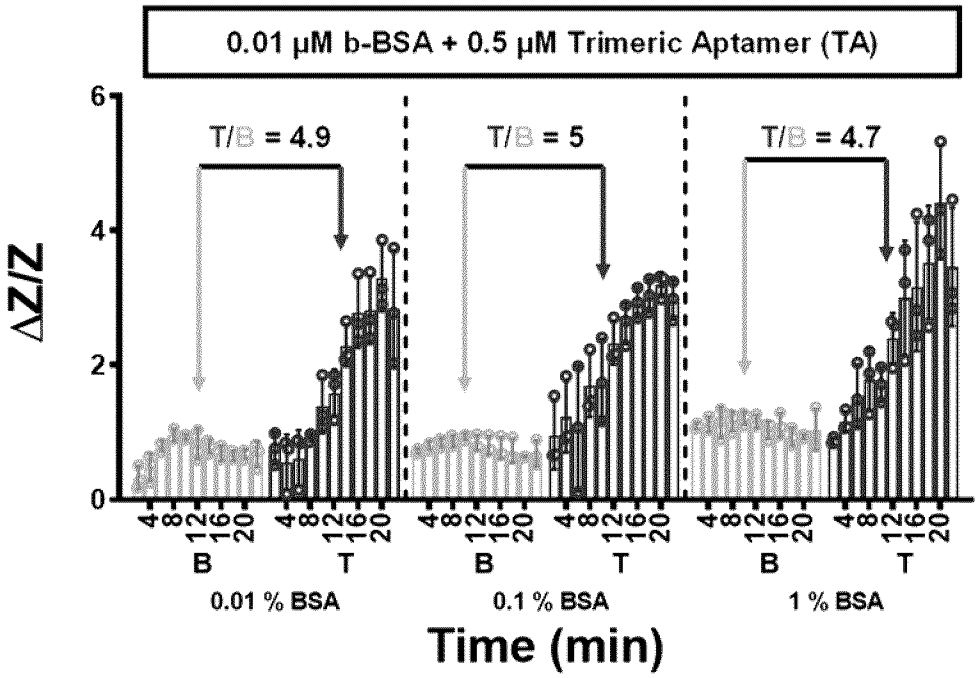
0.01 µM b-BSA + 0.5 µM Trimeric Aptamer (TA)
T/B = 4.9
T/B = 5
T/B = 4.7
ΔZ/Z
0
2
4
6
4 8 12 16 20
B
T
0.01 % BSA
0.1 % BSA
1 % BSA
Time (min)

FIG. 6B

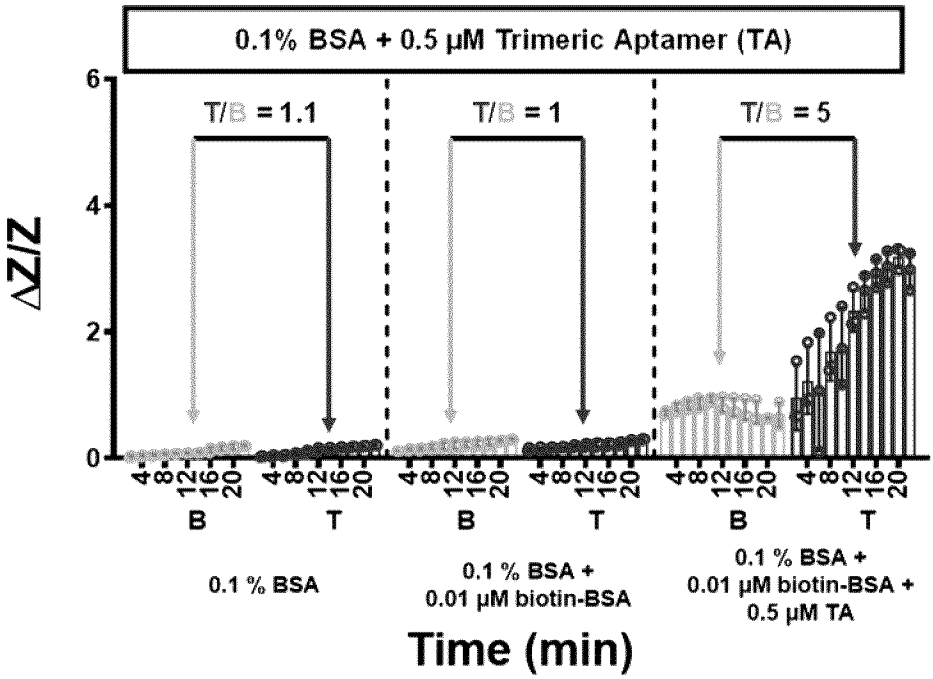
0.1% BSA + 0.5 µM Trimeric Aptamer (TA)
T/B = 1.1
T/B = 1
T/B = 5
ΔZ/Z
0
2
4
6
4 8 12 16 20
B
T
0.1 % BSA
0.1 % BSA +
0.01 µM biotin-BSA
0.1 % BSA +
0.01 µM biotin-BSA +
0.5 µM TA
Time (min)

FIG. 6C

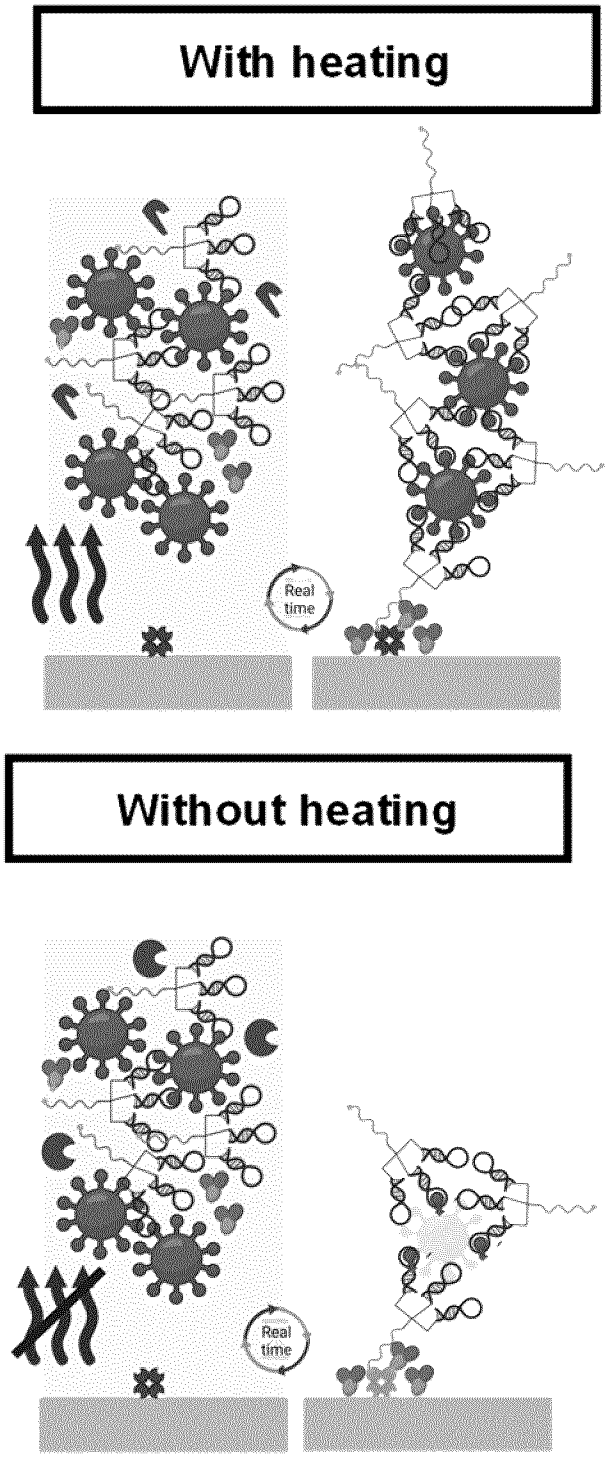

FIG. 7A

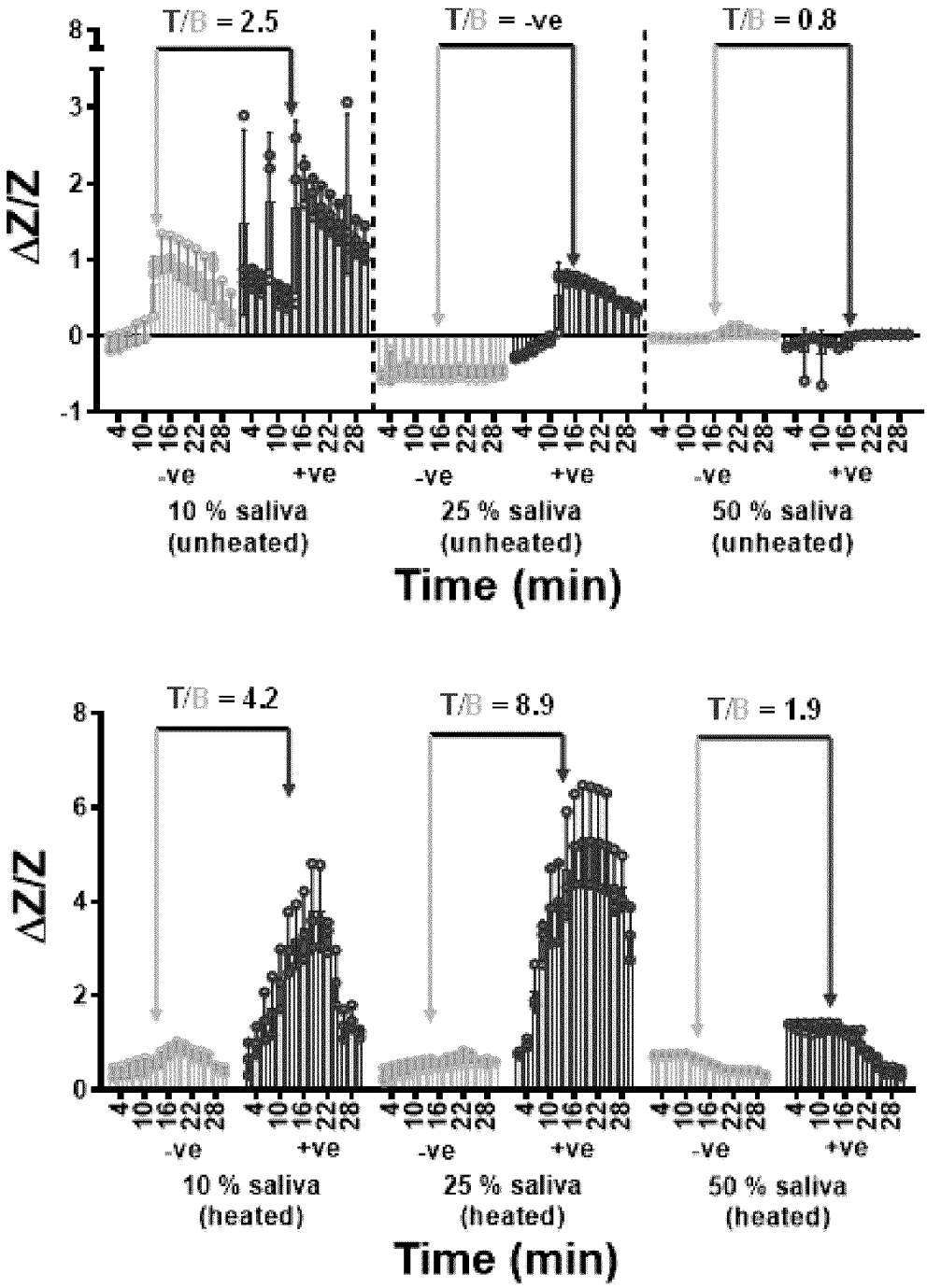
T/B = 2.5
T/B = -ve
T/B = 0.8
ΔZ/Z
-ve
+ve
10 % saliva (unheated)
25 % saliva (unheated)
50 % saliva (unheated)
Time (min)
T/B = 4.2
T/B = 8.9
T/B = 1.9
10 % saliva (heated)
25 % saliva (heated)
50 % saliva (heated)
Time (min)

FIG. 7B

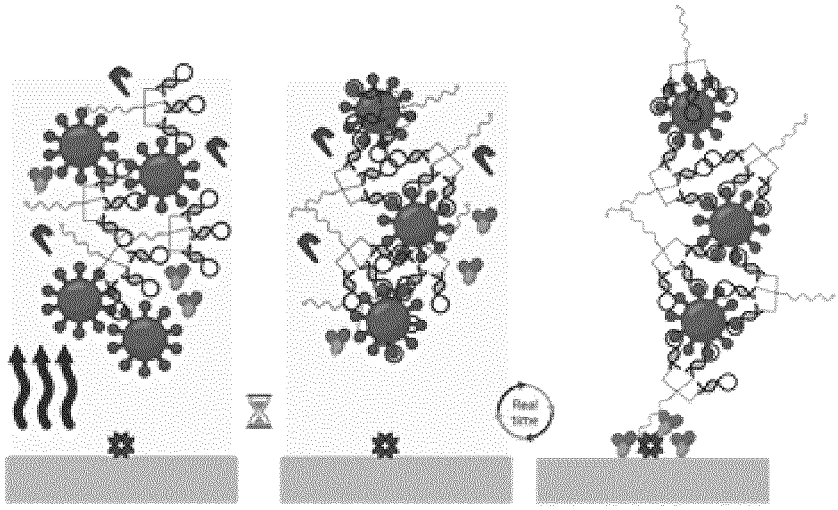

FIG. 8A

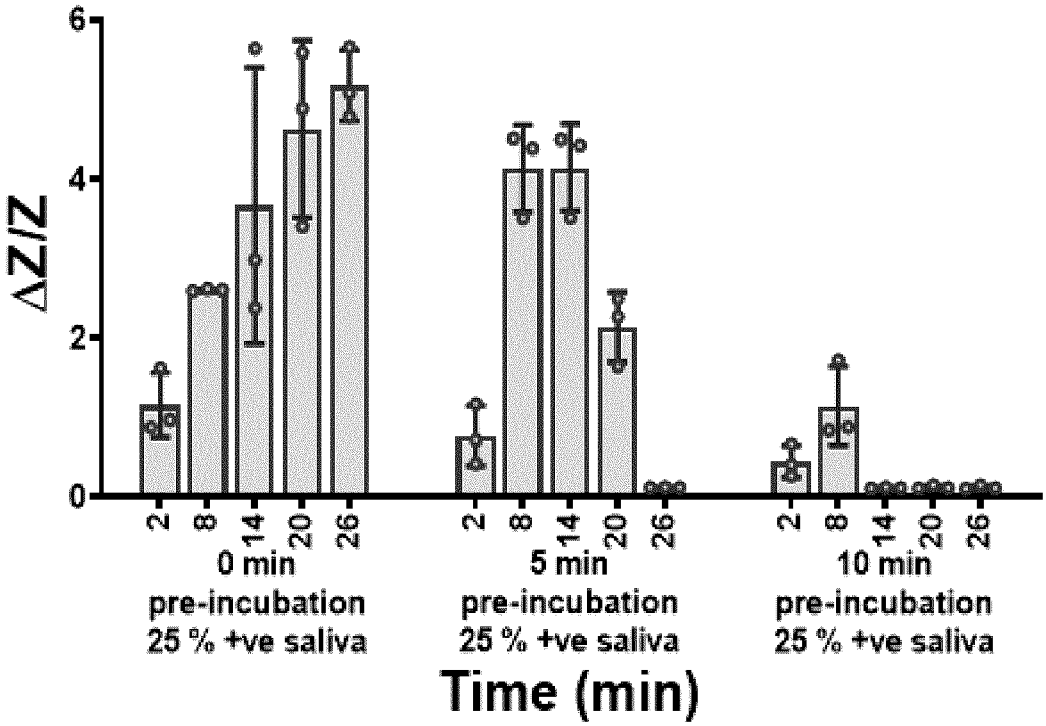
ΔZ/Z
6
4
2
0
2
8
14
20
26
0 min
pre-incubation
25 % +ve saliva
5 min
pre-incubation
25 % +ve saliva
10 min
pre-incubation
25 % +ve saliva
Time (min)

FIG. 8B

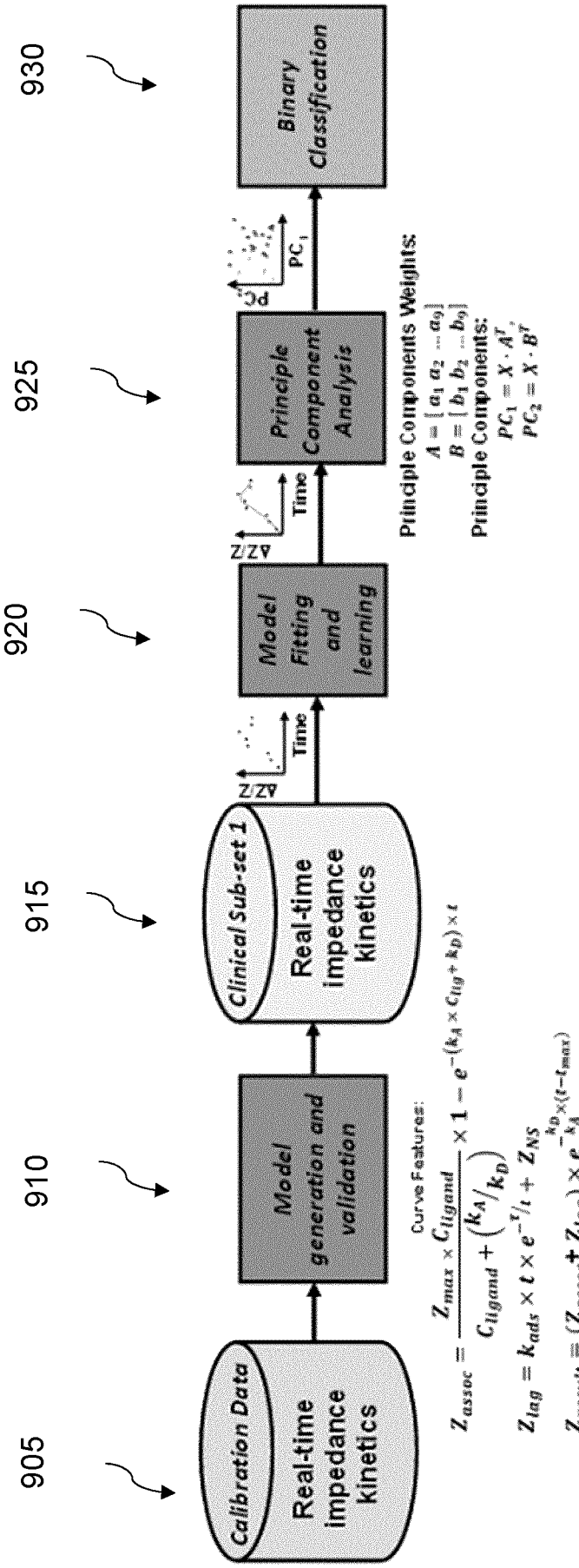
905
Calibration Data
Real-time impedance kinetics
910
Model generation and validation
915
Clinical Sub-set 1
Real-time impedance kinetics
920
Model Fitting and learning
925
Principle Component Analysis
930
Binary Classification
Time
Z/ΔZ
PC1
PC2
Curve Features:
$Z_{assoc} = \frac{Z_{max} \times C_{ligand}}{C_{ligand} + \left(k_A/k_D\right)} \times 1 - e^{-(k_A \times C_{lig} + k_D) \times t}$
$Z_{lag} = k_{ads} \times t \times e^{-t/t} + Z_{NS}$
$Z_{result} = (Z_{assoc} + Z_{lag}) \times e^{-k_D \times (t - t_{max})}$
Principle Components Weights:
$A = [a_1\ a_2 \ldots a_9]$
$B = [b_1\ b_2 \ldots b_9]$
Principle Components:
$PC_1 = X \cdot A^T$,
$PC_2 = X \cdot B^T$

FIG. 9A

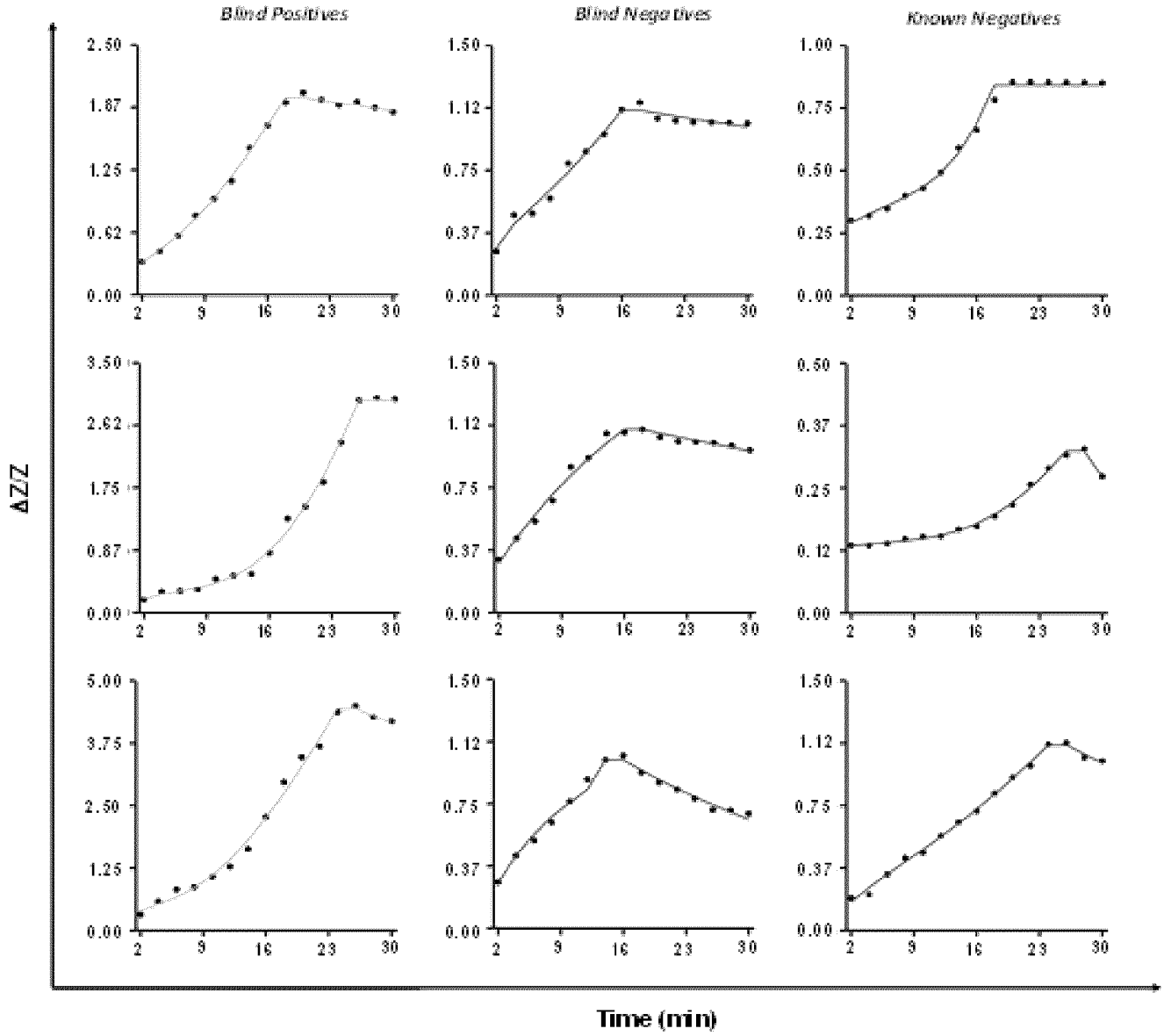
Blind Positives
Blind Negatives
Known Negatives
ΔZ/Z
Time (min)

FIG. 9B

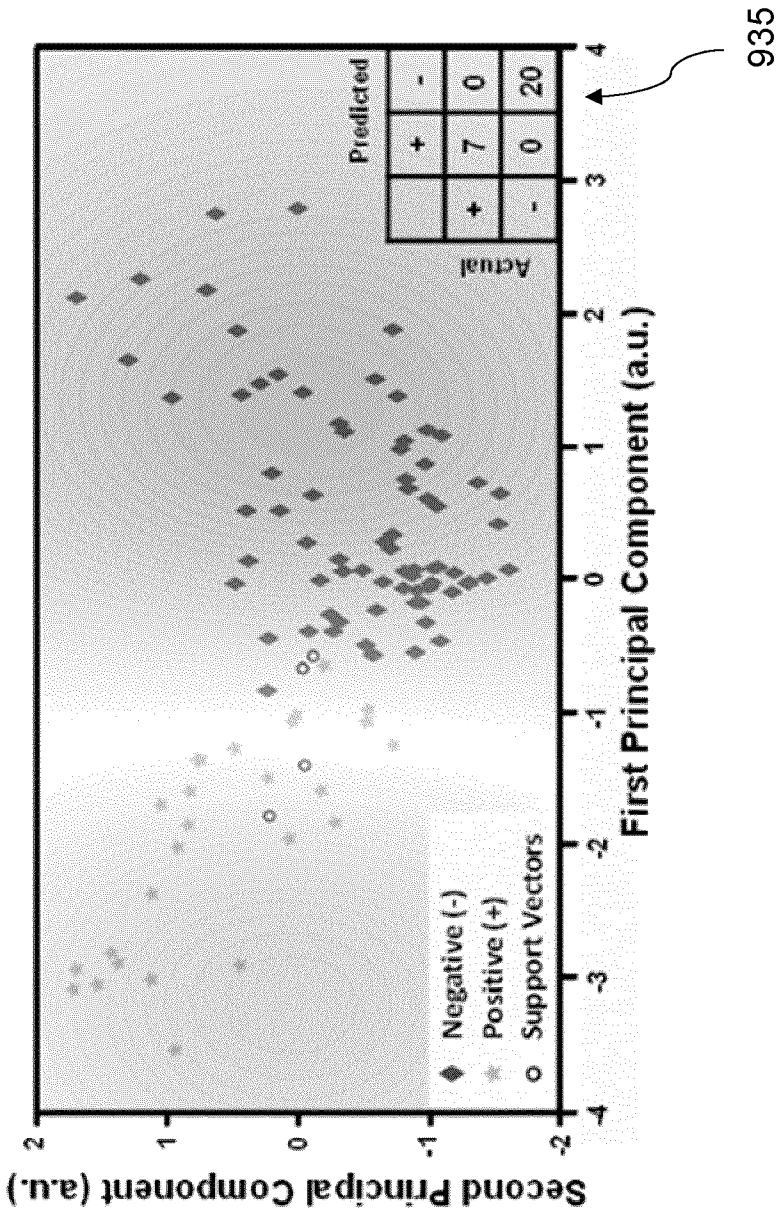

FIG. 9D

	PC_1	PC_2
I_{NS}	-0.12	-0.42
k_A	0.06	0.38
k_0	0.07	0.36
A	0.21	-0.07
τ	0.43	0.23
t_0	-0.18	0.30
B_{max}	-0.53	0.31
AUC	-0.53	0.28
R^2	-0.40	-0.47

FIG. 9C

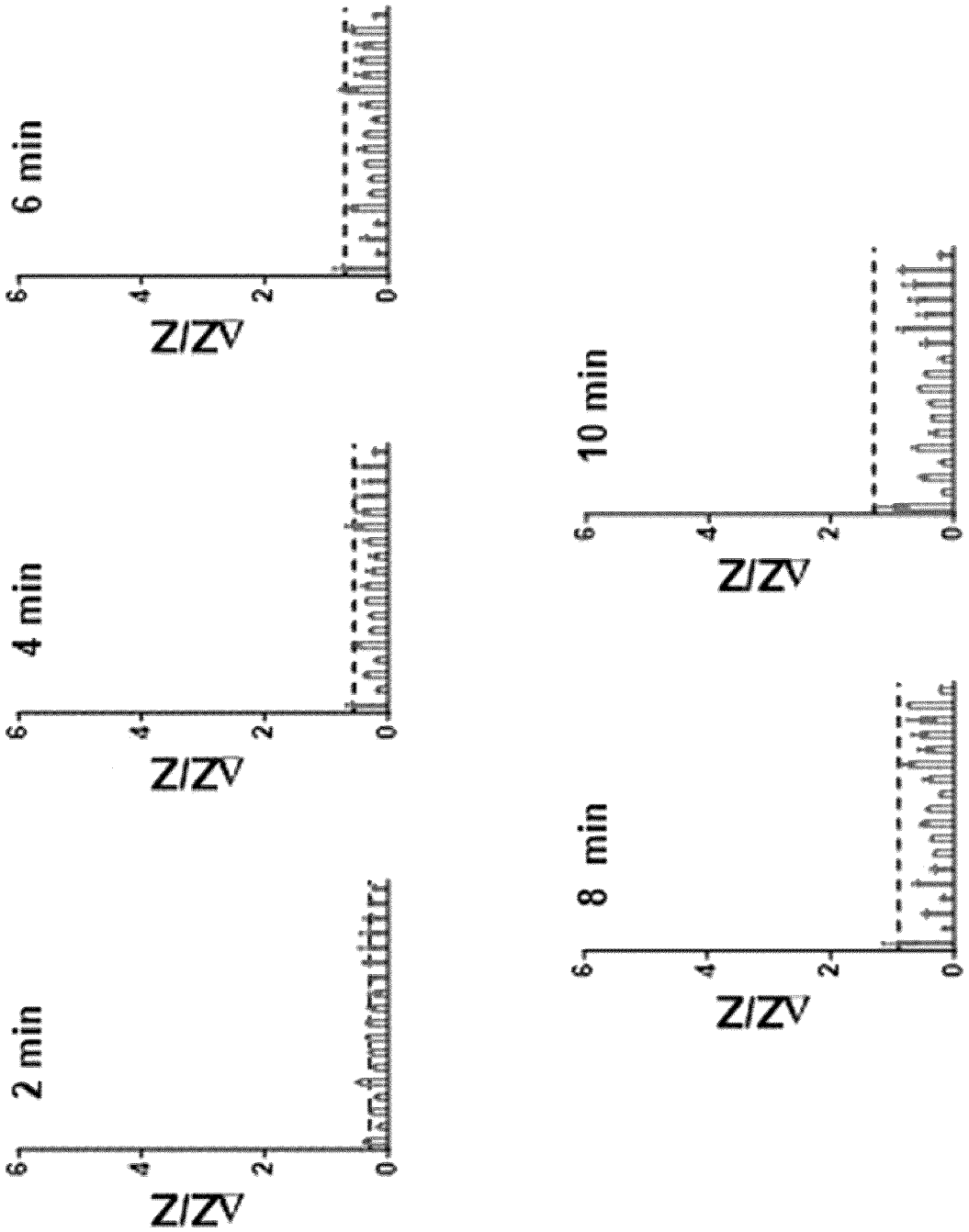

FIG. 10A

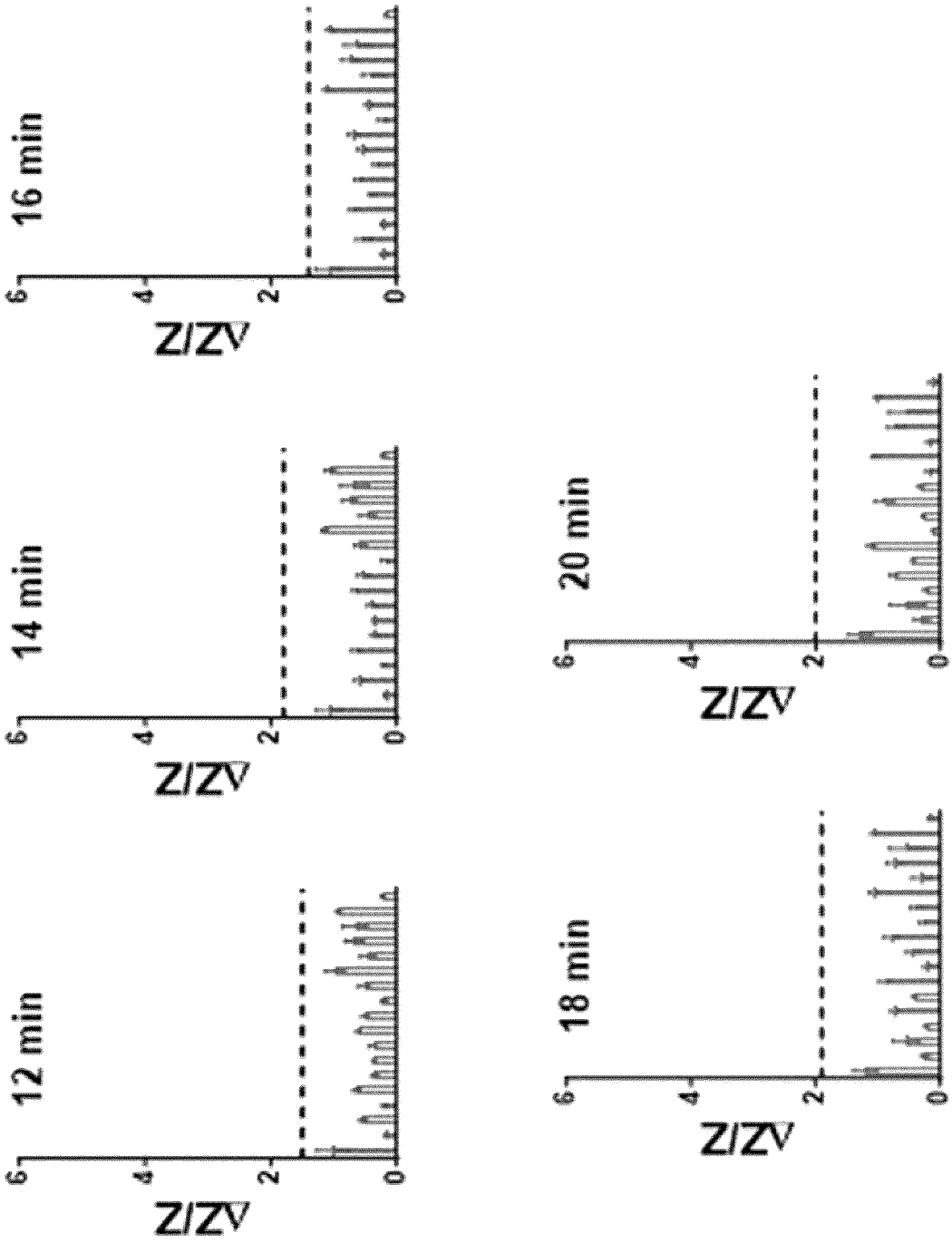

FIG. 10B

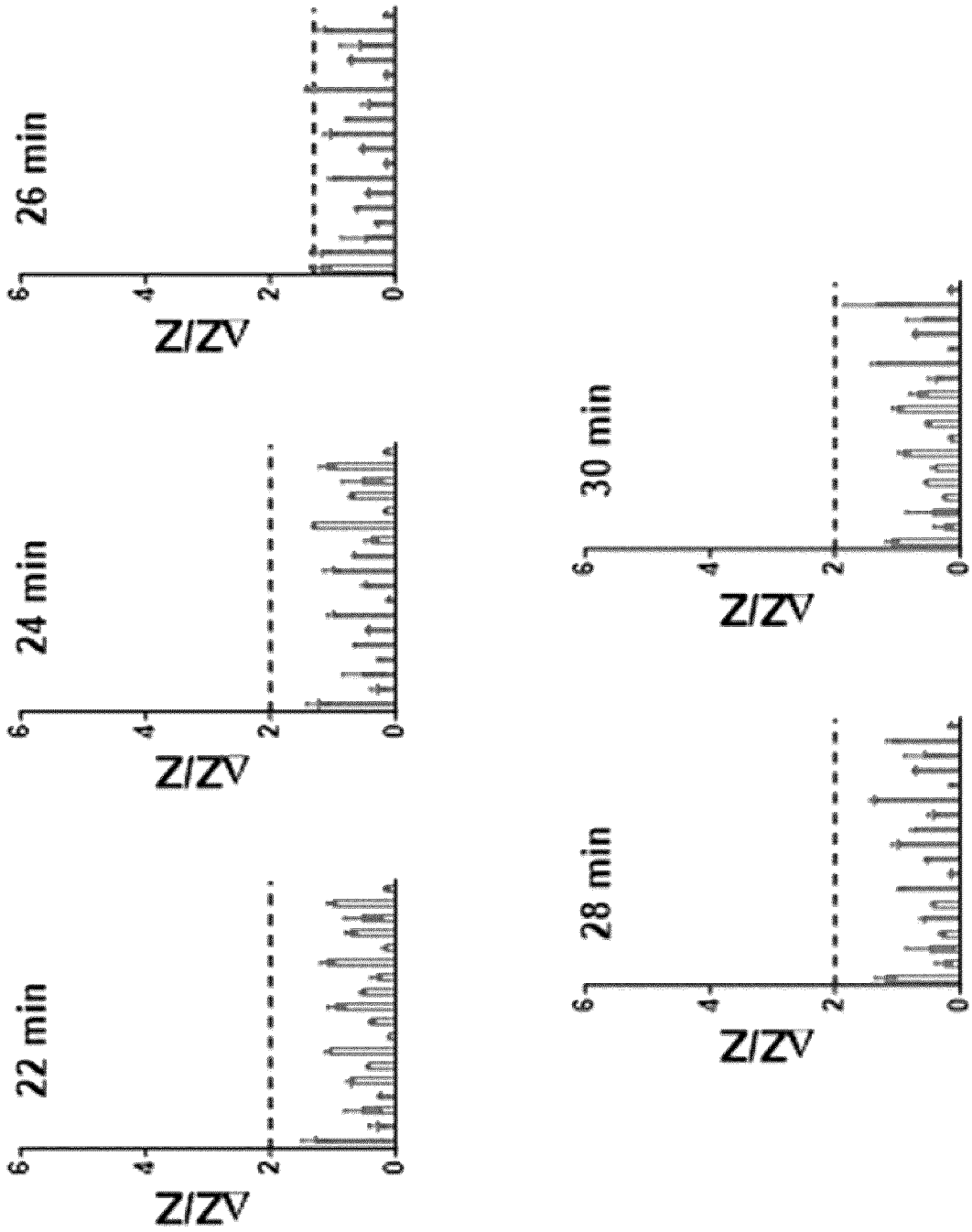

FIG. 10C

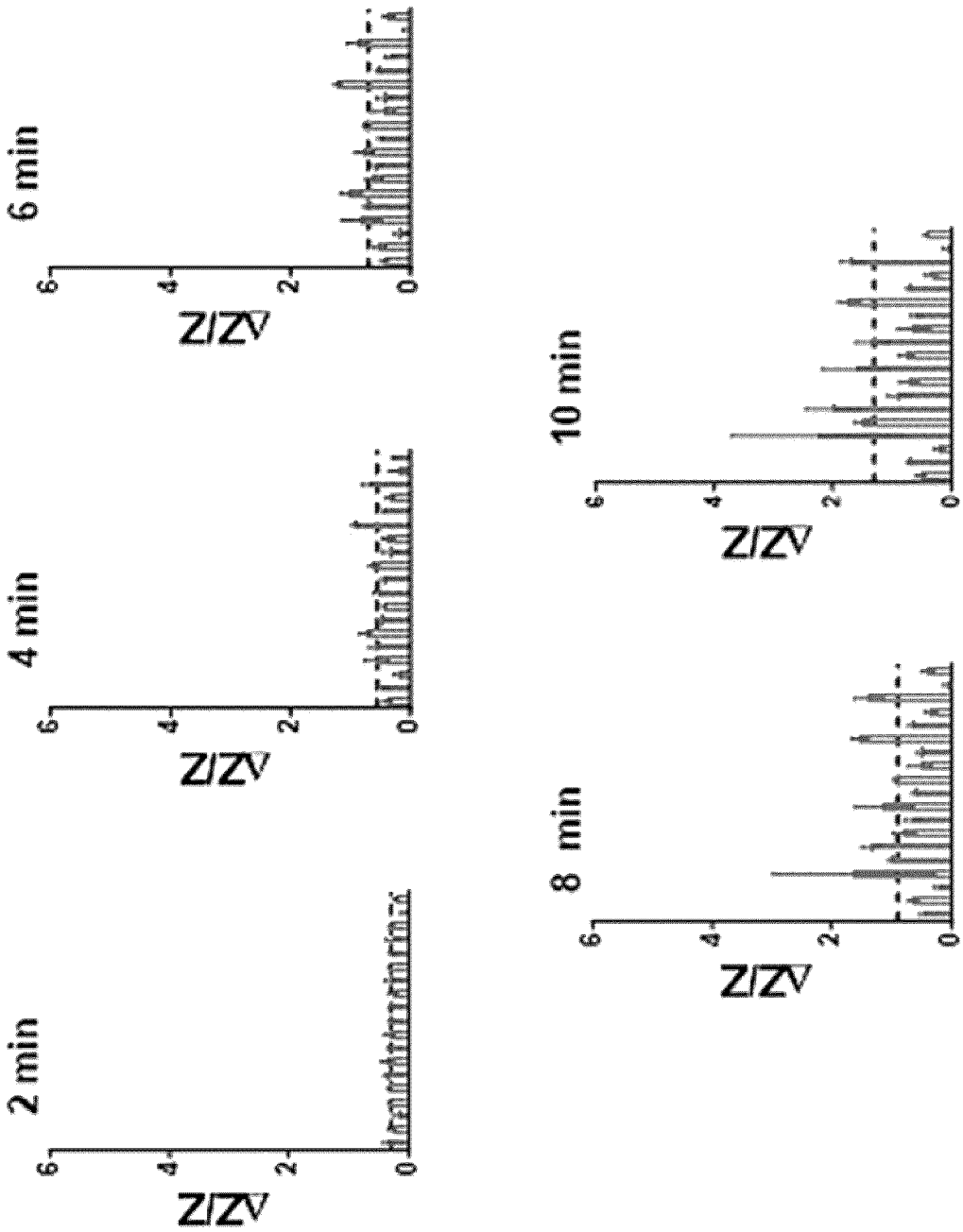

FIG. 11A

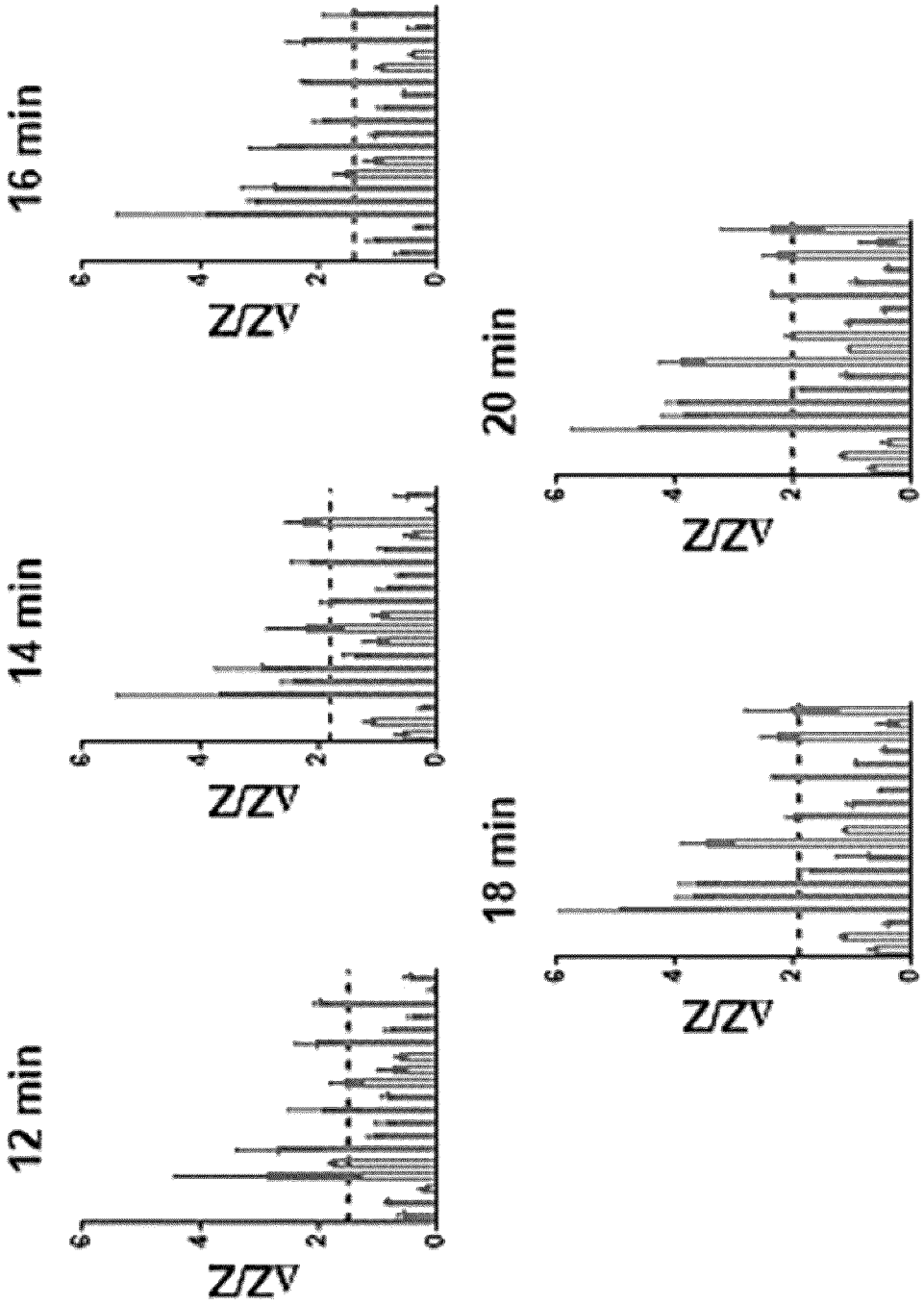

FIG. 11B

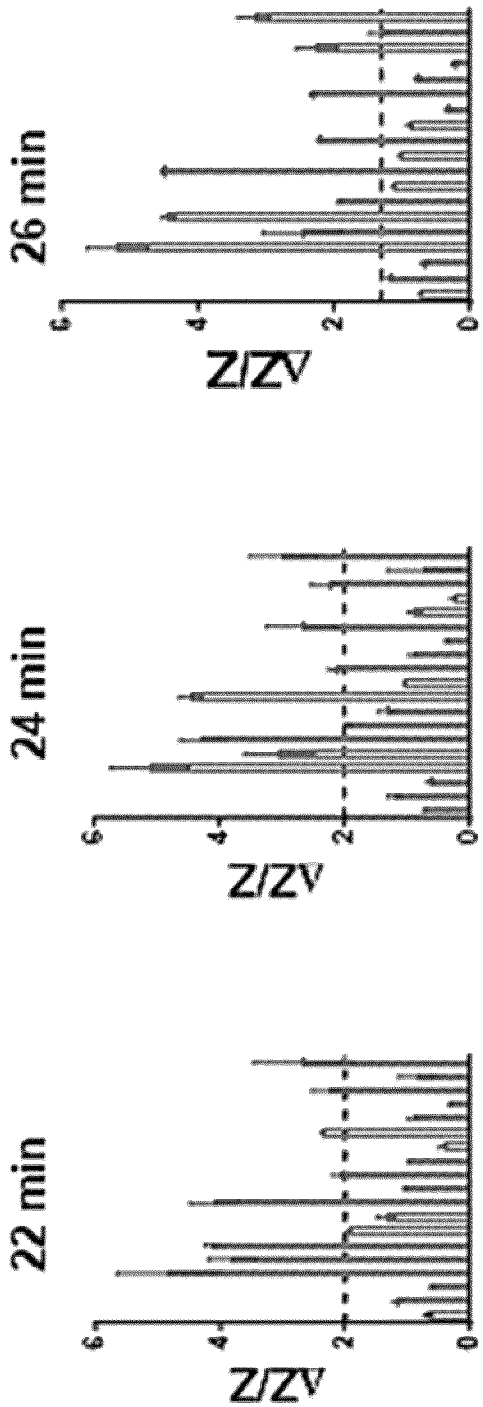

FIG. 11C

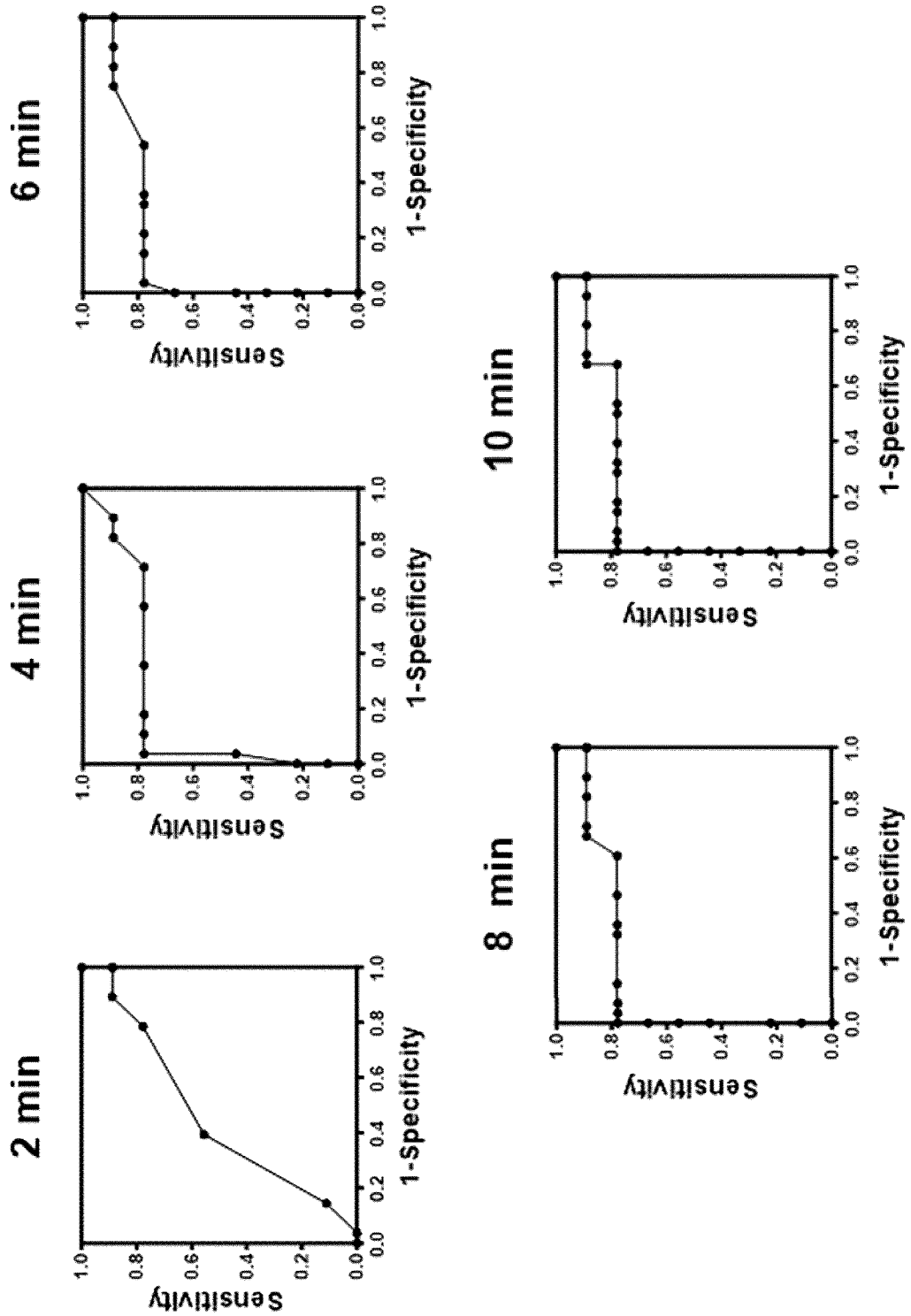
2 min
4 min
6 min
8 min
10 min
Sensitivity
1-Specificity
0.0
0.2
0.4
0.6
0.8
1.0

FIG. 12A

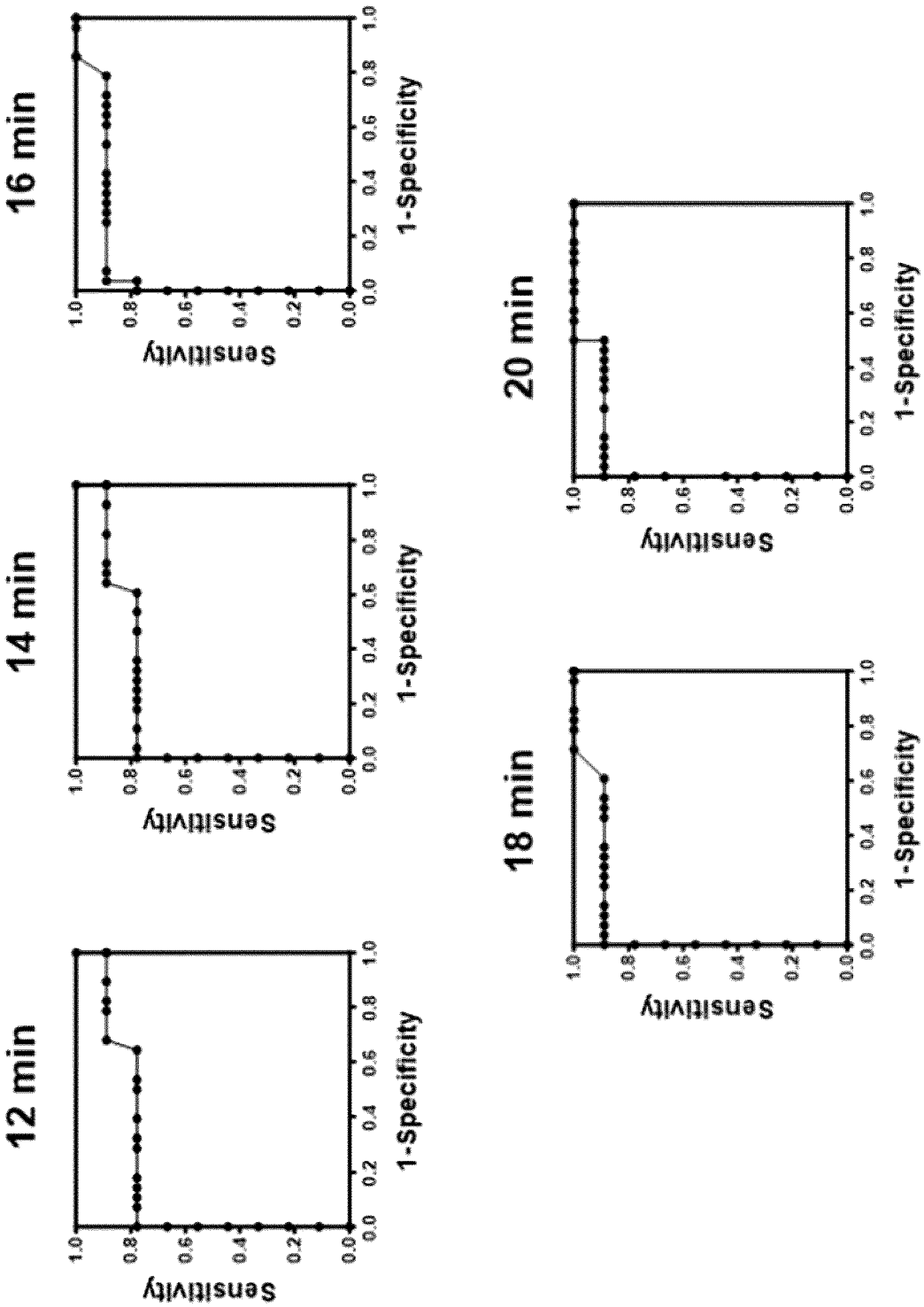
16 min
14 min
12 min
20 min
18 min
Sensitivity
1-Specificity
0.0
0.2
0.4
0.6
0.8
1.0

FIG. 12B

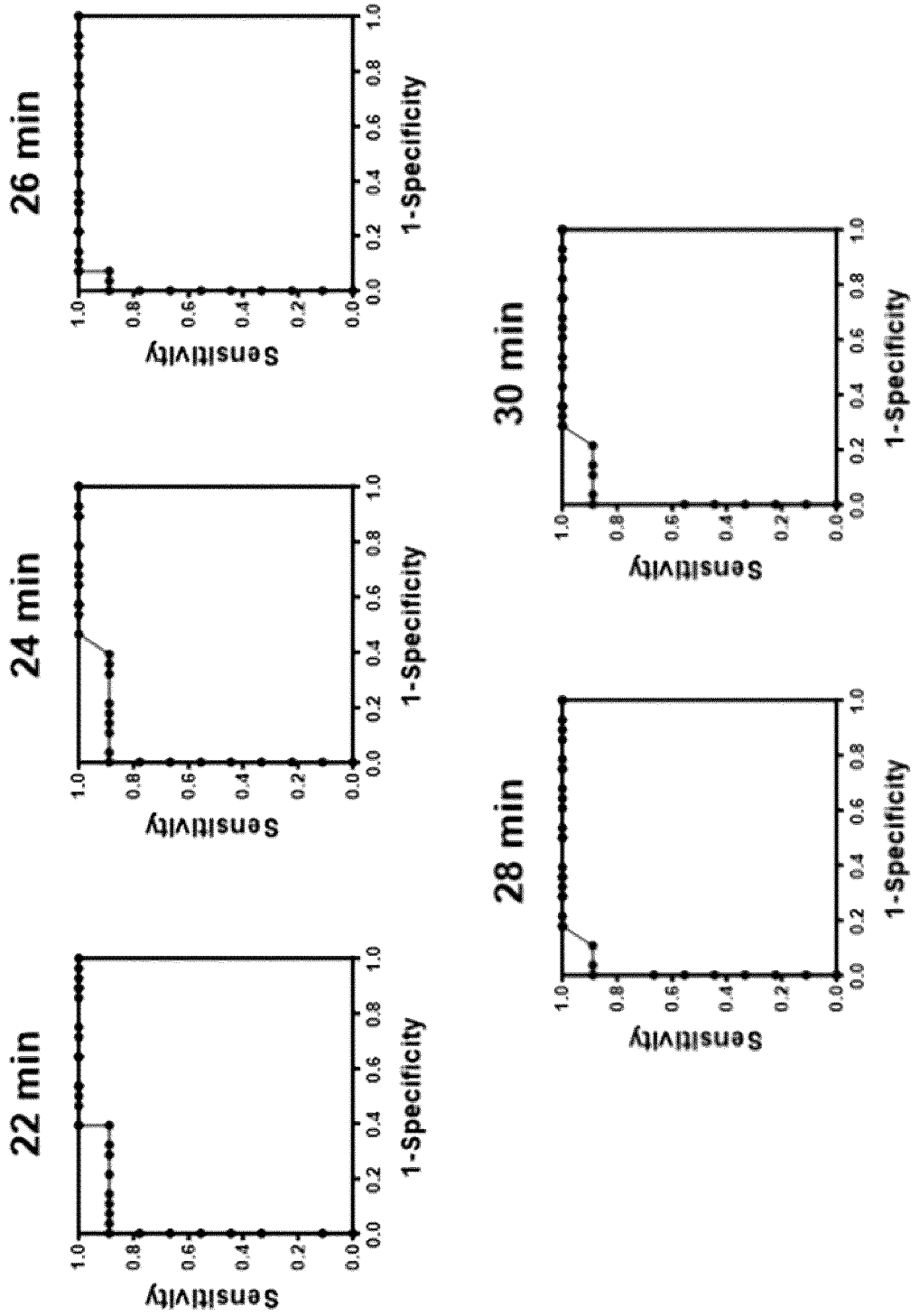
22 min
24 min
26 min
28 min
30 min
Sensitivity
1-Specificity
0.0
0.2
0.4
0.6
0.8
1.0

FIG. 12C

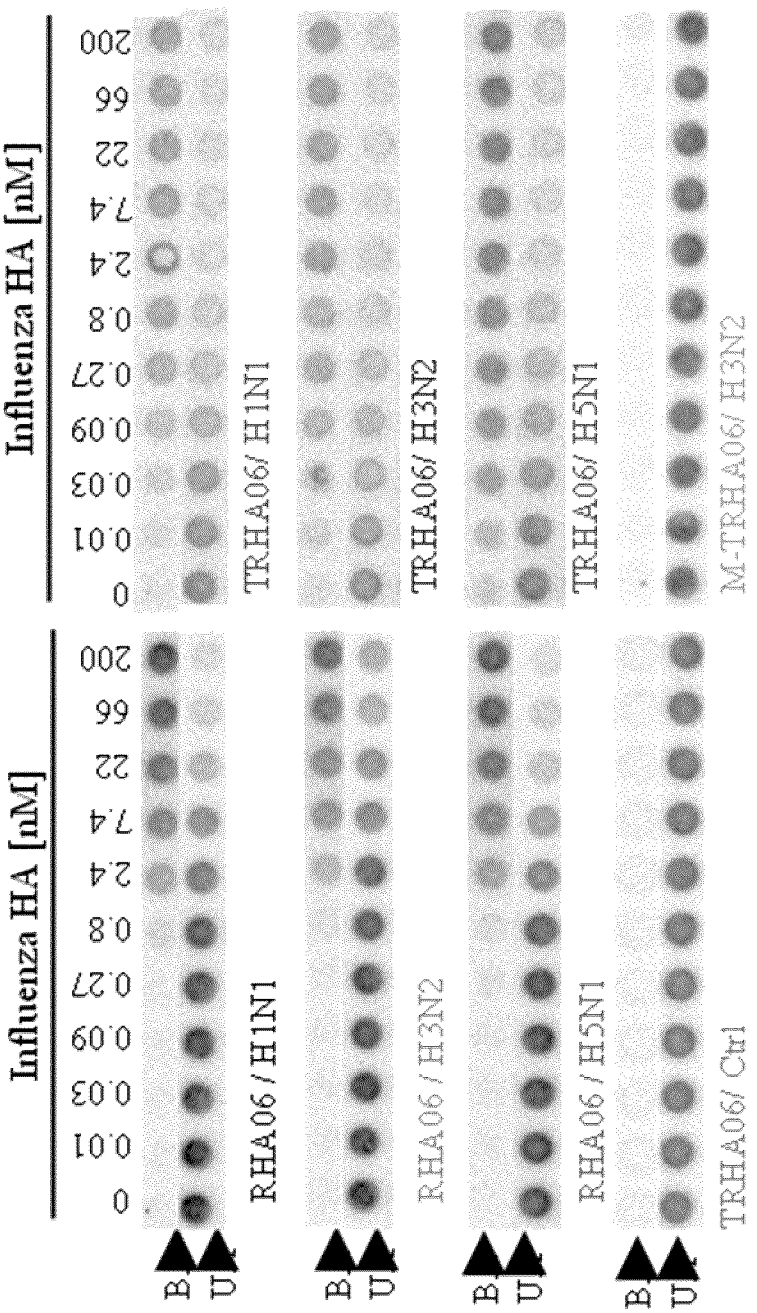
Influenza HA [nM]
0
0.01
0.03
0.09
0.27
0.8
2.4
7.4
22
66
200
B
U
RHA06 / H1N1
RHA06 / H3N2
RHA06 / H5N1
TRHA06/ Ctrl
TRHA06/ H1N1
TRHA06/ H3N2
TRHA06/ H5N1
M-TRHA06/ H3N2

FIG. 13A

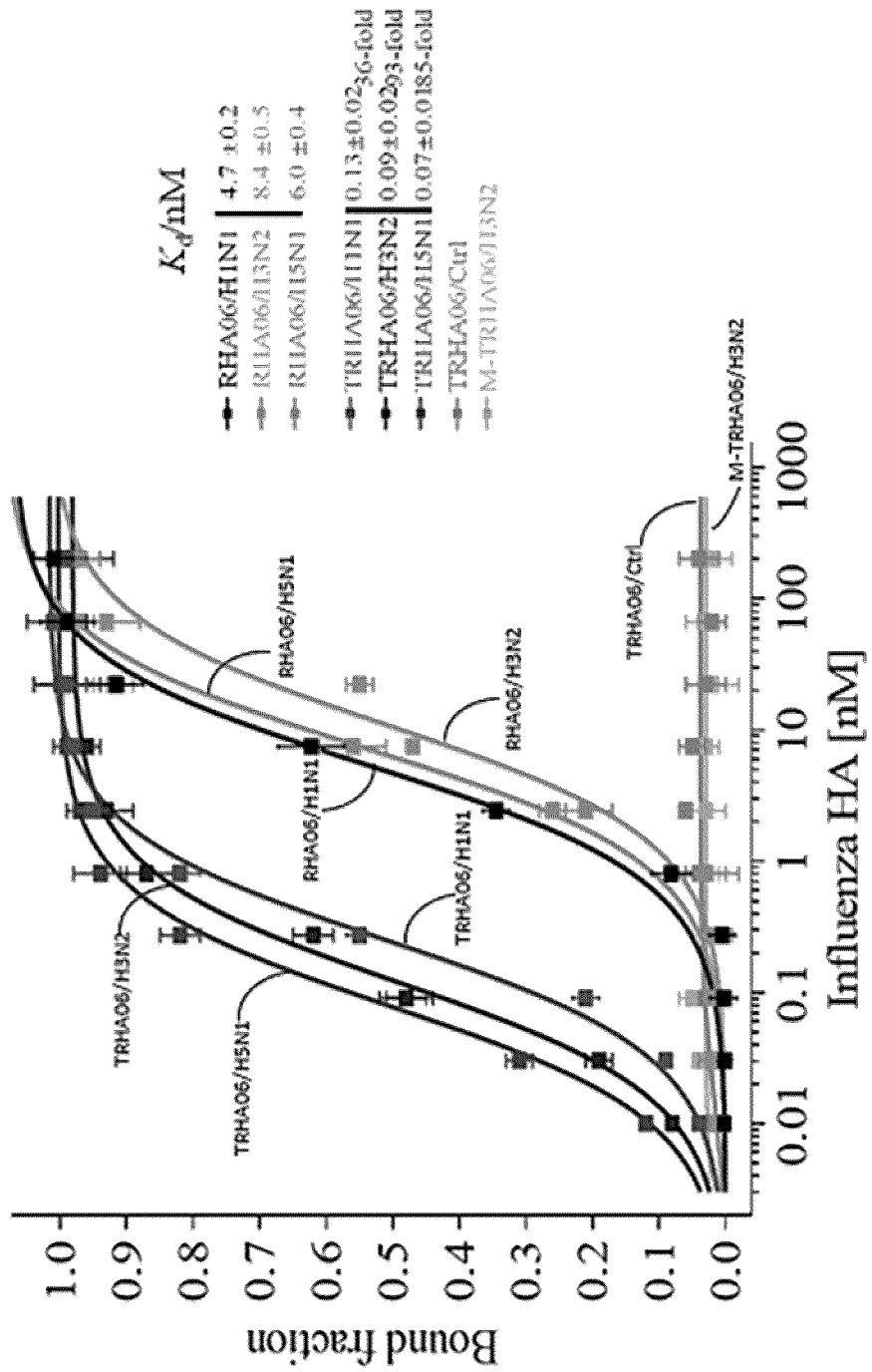
K_d/nM
RHA06/H1N1 | 4.7 ±0.2
RHA06/H3N2 | 8.4 ±0.5
RHA06/H5N1 | 6.0 ±0.4
TRHA06/H1N1 | 0.13±0.02 36-fold
TRHA06/H3N2 | 0.09±0.02 93-fold
TRHA06/H5N1 | 0.07±0.0185-fold
TRHA06/Ctrl
M-TRHA06/H3N2
Bound fraction
Influenza HA [nM]
0.01
0.1
1
10
100
1000
0.0
0.1
0.2
0.3
0.4
0.5
0.6
0.7
0.8
0.9
1.0
TRHA06/H3N2
TRHA06/H5N1
RHA06/H1N1
RHA06/H5N1
TRHA06/H1N1
RHA06/H3N2
TRHA06/Ctrl
M-TRHA06/H3N2

FIG. 13B

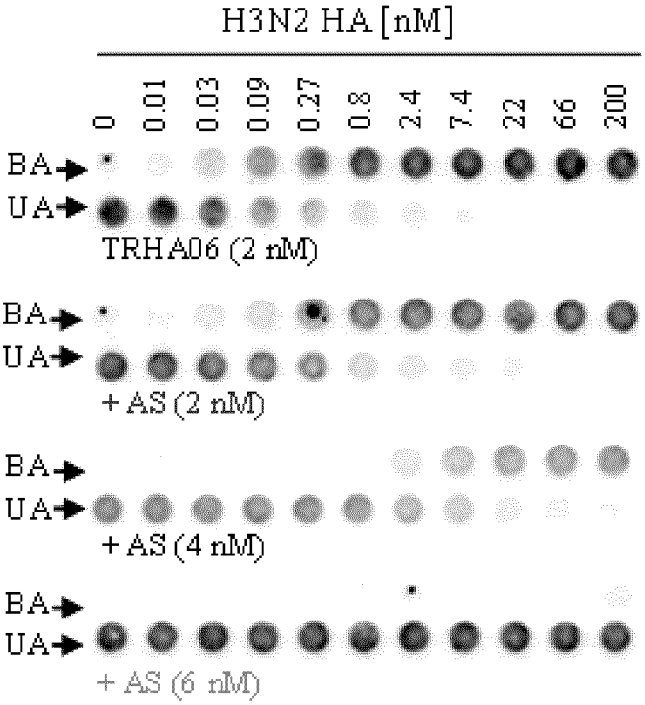

FIG. 14A

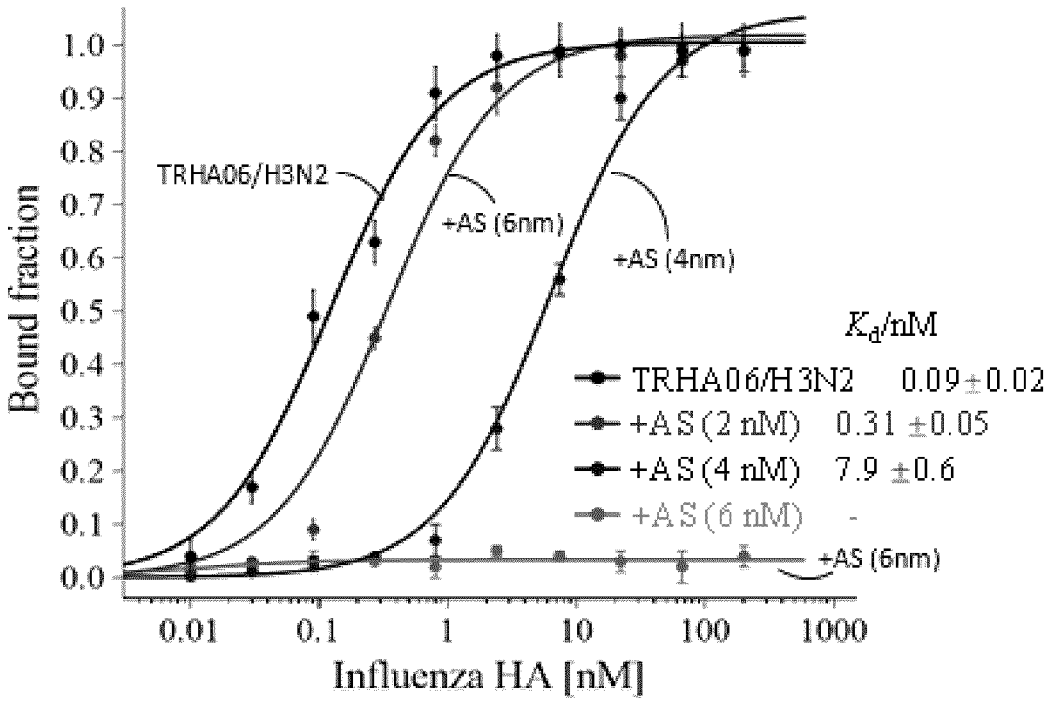

FIG. 14B

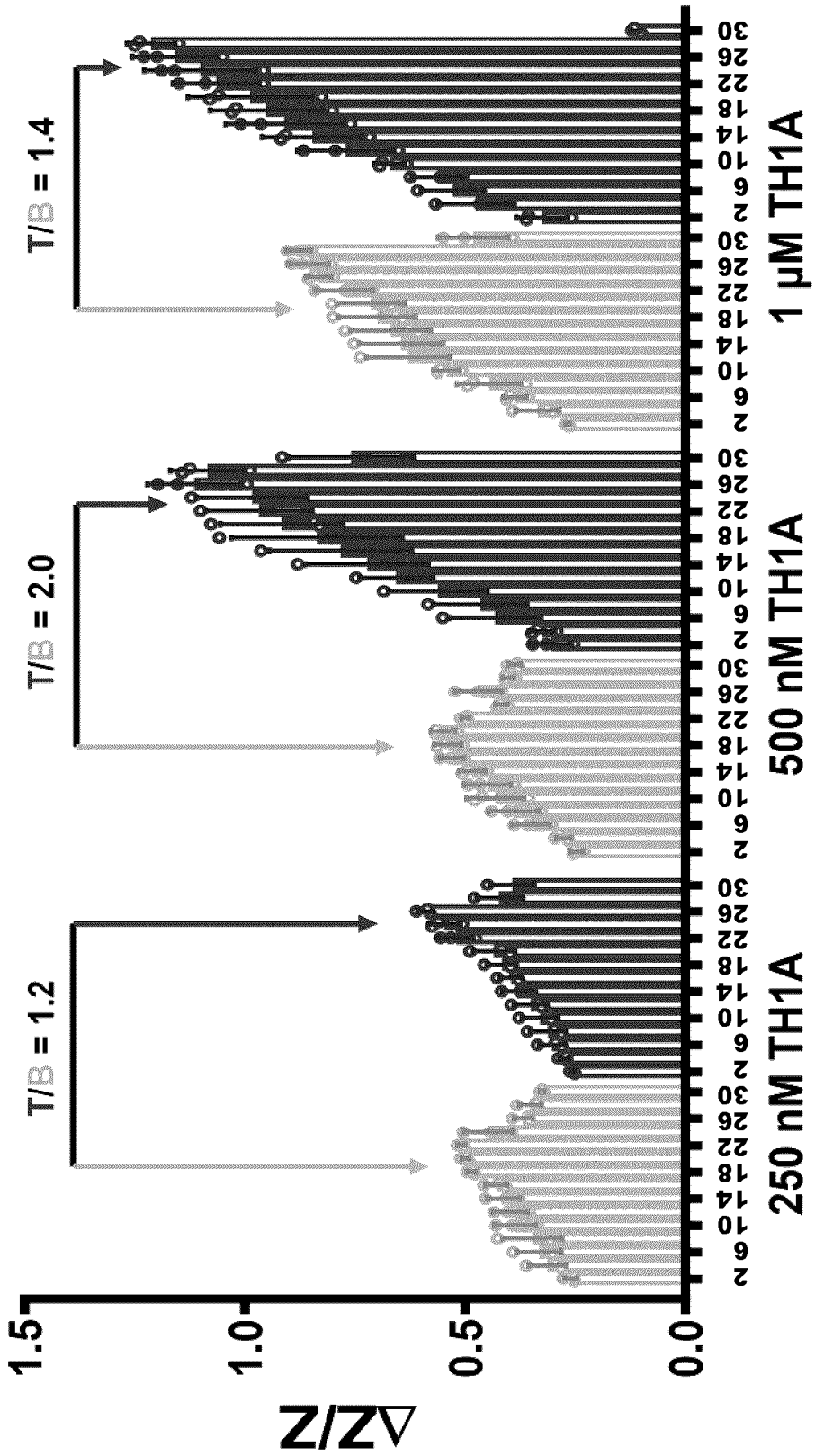
ΔZ/Z
1.5
1.0
0.5
0.0
T/B = 1.2
T/B = 2.0
T/B = 1.4
250 nM TH1A
500 nM TH1A
1 µM TH1A
2 6 10 14 18 22 26 30
Time (min)

FIG. 15

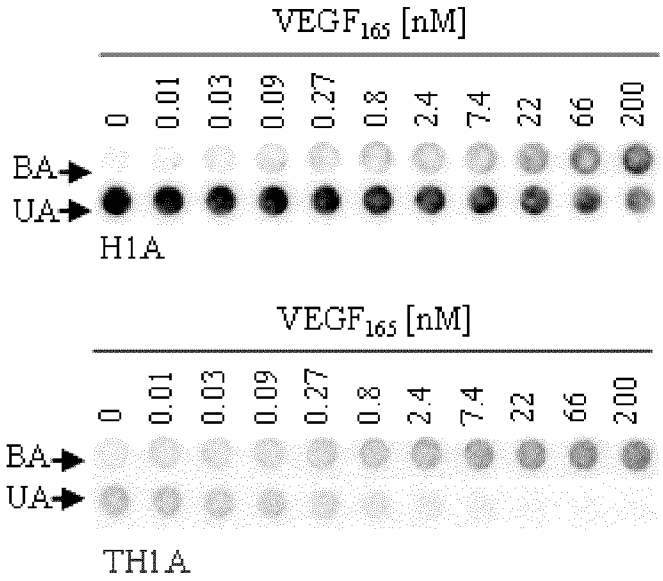

FIG. 16A

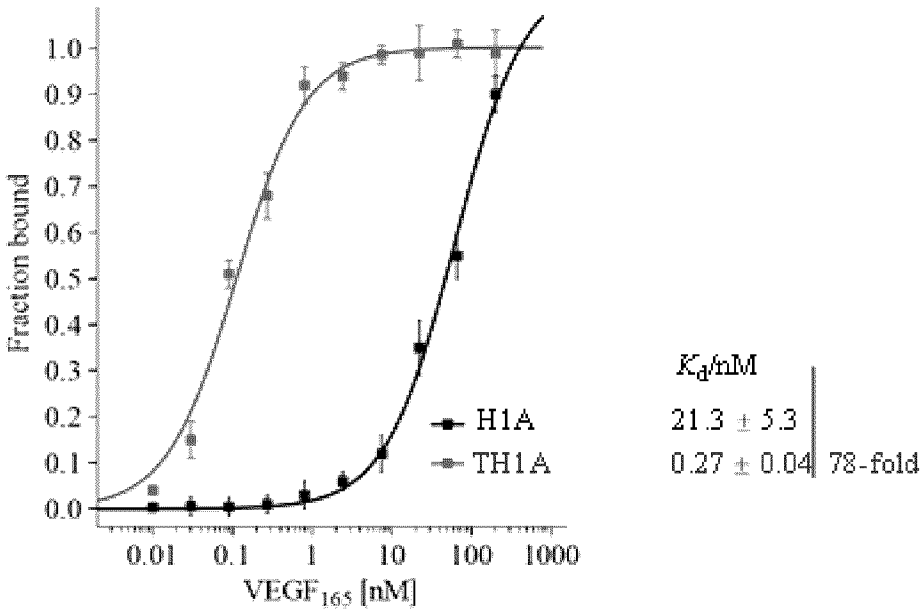

FIG. 16B

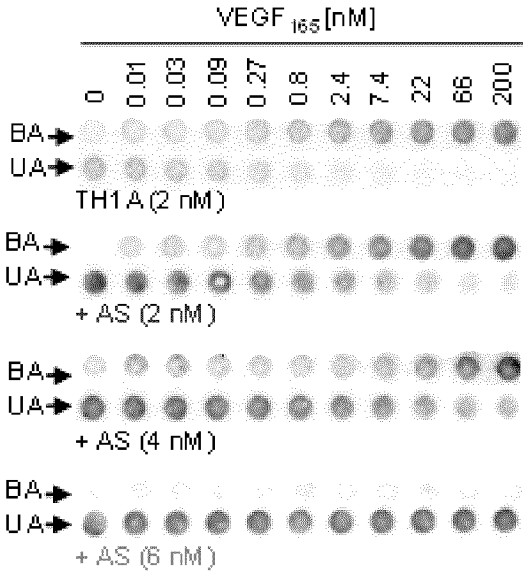

FIG. 17A

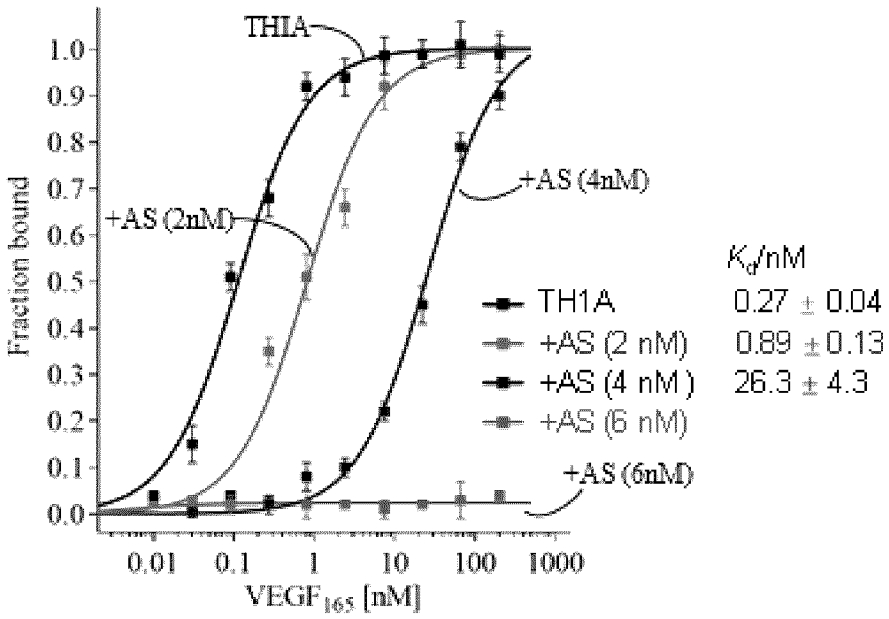

FIG. 17B

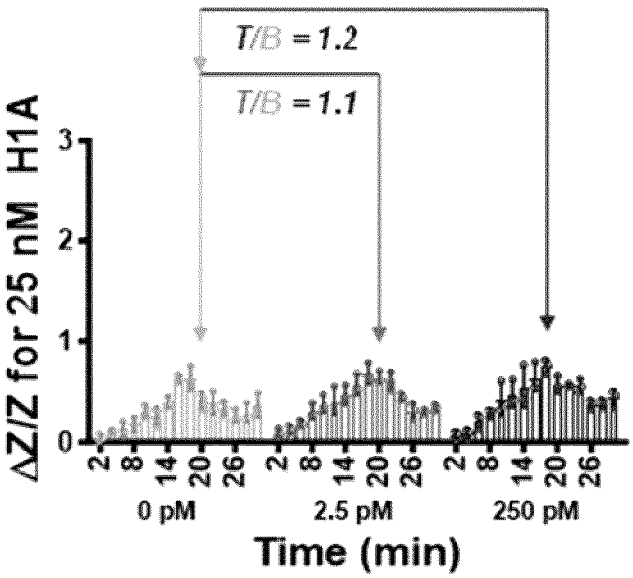

FIG. 18A

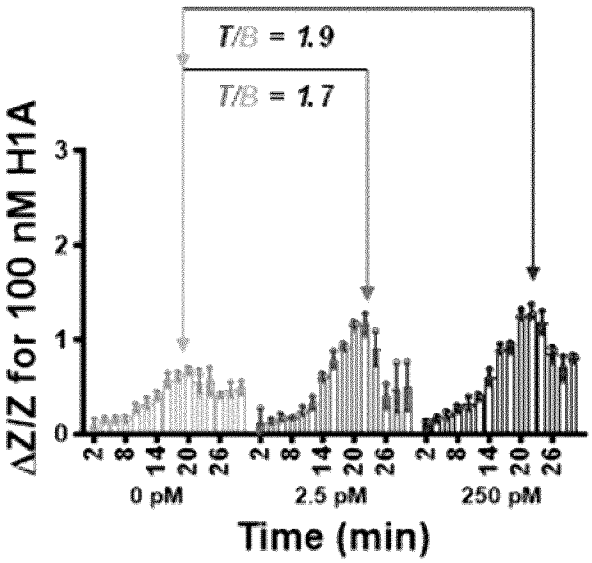

FIG. 18B

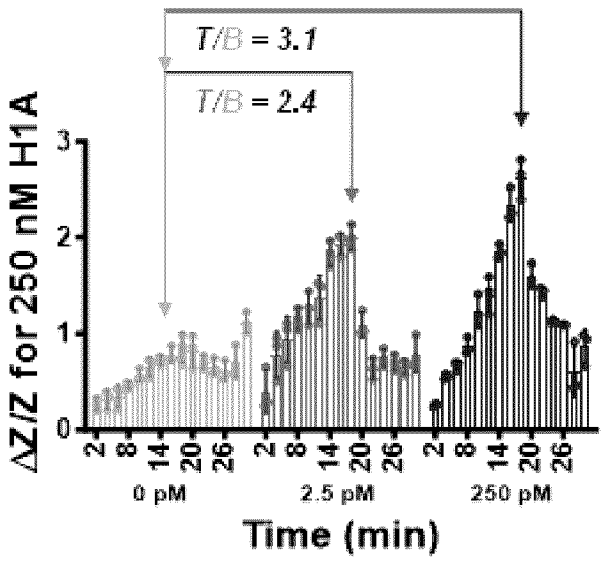

FIG. 18C

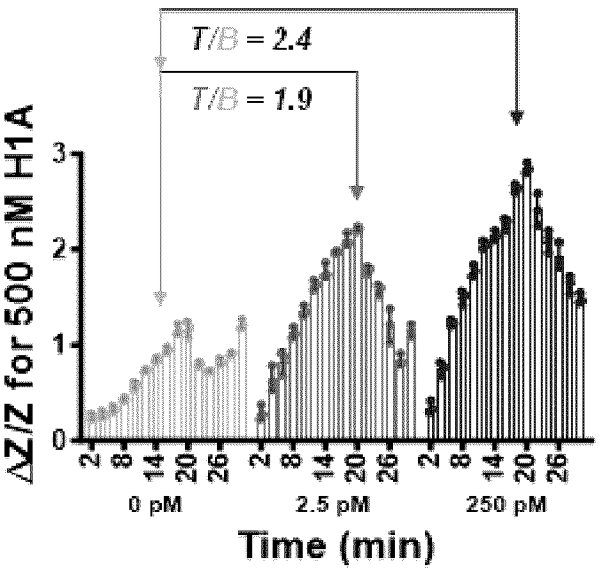

FIG. 18D

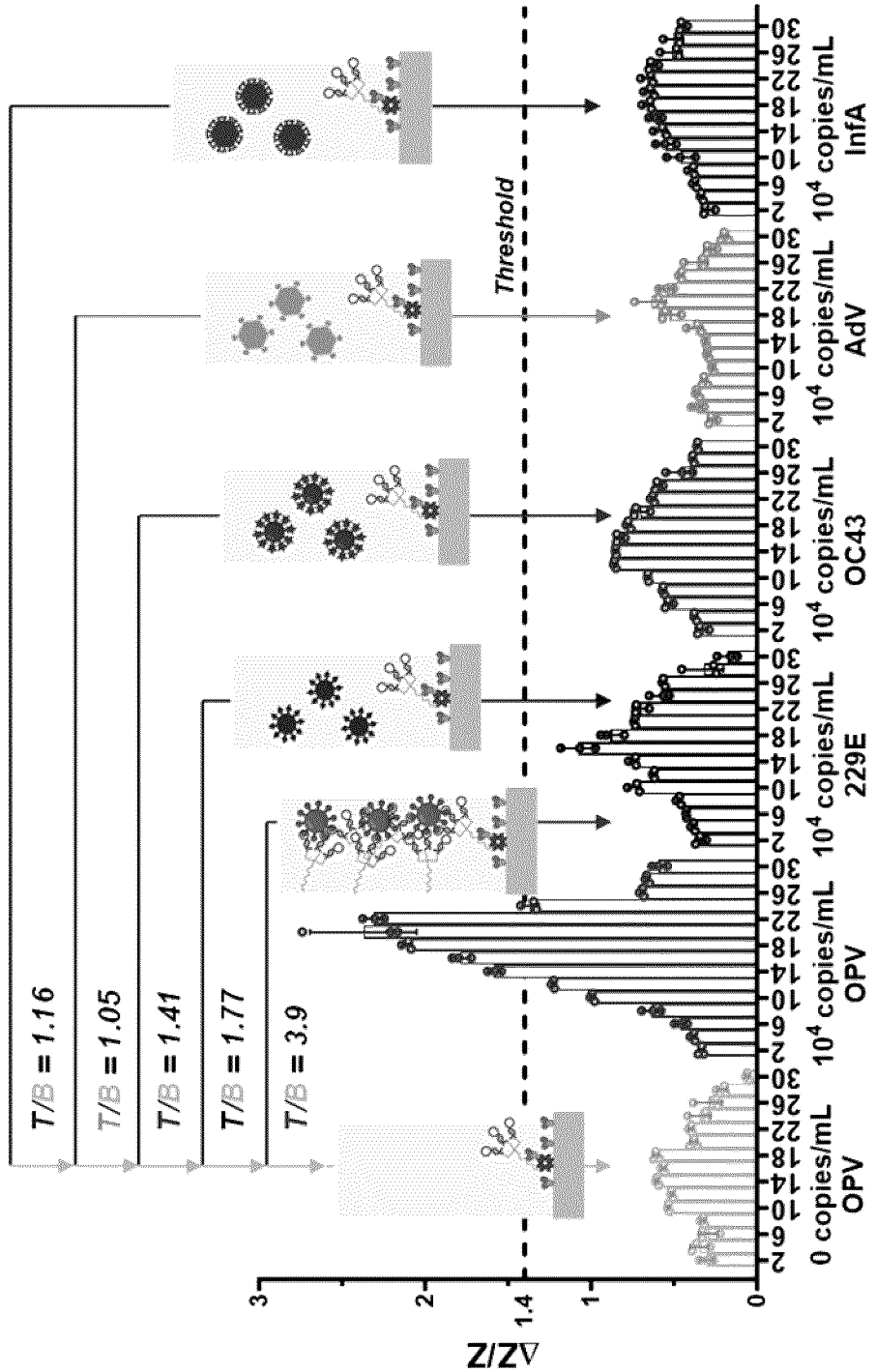
T/B = 1.16
T/B = 1.05
T/B = 1.41
T/B = 1.77
T/B = 3.9
Threshold
Z/Zᵛ
Time (min)
0 copies/mL OPV
10⁴ copies/mL OPV
10⁴ copies/mL 229E
10⁴ copies/mL OC43
10⁴ copies/mL AdV
10⁴ copies/mL InfA

FIG. 19A

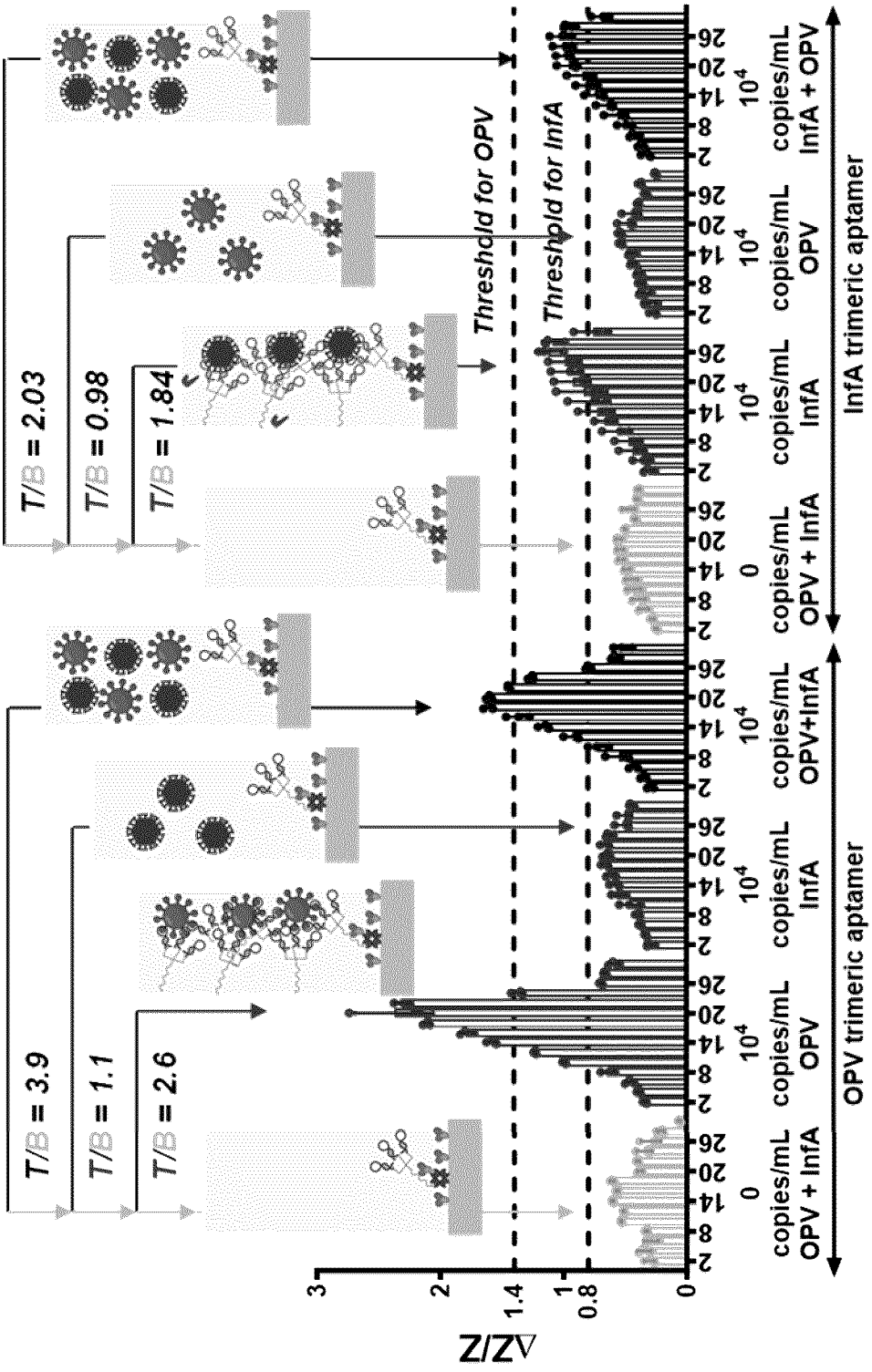
T/B = 3.9
T/B = 1.1
T/B = 2.6
T/B = 2.03
T/B = 0.98
T/B = 1.84
Threshold for OPV
Threshold for InfA
ΔZ/Z^V
Time (min)
OPV trimeric aptamer
InfA trimeric aptamer
copies/mL OPV + InfA
copies/mL OPV
copies/mL InfA
copies/mL OPV+InfA
0
10^4

FIG. 19B

INTERNATIONAL SEARCH REPORT

International application No.
PCT/CA2024/051053

A. CLASSIFICATION OF SUBJECT MATTER

IPC: ***G01N 27/26*** (2006.01), ***G01N 27/327*** (2006.01)

CPC: G01N 27/26 (2020.05), G01N 27/3275 (2013.01)

According to International Patent Classification (IPC) or to both national classification and IPC

B. FIELDS SEARCHED

Minimum documentation searched (classification system followed by classification symbols)
IPC: ***G01N*** (2006.01) (using keywords)

Documentation searched other than minimum documentation to the extent that such documents are included in the fields searched

Electronic database(s) consulted during the international search (name of database(s) and, where practicable, search terms used)

Canadian Patent Database, Google, Questel Orbit, United States Patent Database (USPTO).
Keywords: aptamer, biosensor, electrochemical, frequency, impedance, label, multimeric, potentiostat, spectroscopy.

C. DOCUMENTS CONSIDERED TO BE RELEVANT

Category*	Citation of document, with indication, where appropriate, of the relevant passages	Relevant to claim No.
Y	CA 3144887 A1 (ROZLOSNIK ET AL.) 14 January 2021 (14-01-2021) - abstract - page 1, line 5 - page 2, line 24 - page 3, lines 6-13; page 4, lines 2-9 - page 6, lines 5-12; page 10, line 8 - page 12, line 25 - page 17, lines 19-30; page 18, lines 11-34 - page 21, lines 1-27; page 23, lines 1-10 - page 24, lines 9-15	1, 13, 14, 16, 17, 27-31, 36

☒ Further documents are listed in the continuation of Box C. ☒ See patent family annex.

*	Special categories of cited documents:	"T"	later document published after the international filing date or priority date and not in conflict with the application but cited to understand the principle or theory underlying the invention
"A"	document defining the general state of the art which is not considered to be of particular relevance	"X"	document of particular relevance; the claimed invention cannot be considered novel or cannot be considered to involve an inventive step when the document is taken alone
"D"	document cited by the applicant in the international application	"Y"	document of particular relevance; the claimed invention cannot be considered to involve an inventive step when the document is combined with one or more other such documents, such combination being obvious to a person skilled in the art
"E"	earlier application or patent but published on or after the international filing date	"&"	document member of the same patent family
"L"	document which may throw doubts on priority claim(s) or which is cited to establish the publication date of another citation or other special reason (as specified)		
"O"	document referring to an oral disclosure, use, exhibition or other means		
"P"	document published prior to the international filing date but later than the priority date claimed		

Date of the actual completion of the international search 04 October 2024 (04-10-2024)	Date of mailing of the international search report 04 October 2024 (04-10-2024)
Name and mailing address of the ISA/CA Canadian Intellectual Property Office Place du Portage I, C114 - 1st Floor, Box PCT 50 Victoria Street Gatineau, Quebec K1A 0C9 Facsimile No.: 819-953-2476	Authorized officer Tung Nguyen (819) 639-8246

C (Continuation). DOCUMENTS CONSIDERED TO BE RELEVANT

Category*	Citation of document, with indication, where appropriate, of the relevant passages	Relevant to claim No.
Y, &	WO 2022261776 A1 (LI ET AL.) 22 December 2022 (22-12-2022) - paragraphs [0005]-[0019], [0084]-[0093] - paragraphs [0108], [0119], [0123], [0129], [0133], [0137]-[0139] - paragraphs [0142]-[0147], [0157], [0161]-[0167], [0173], [0175] - paragraphs [0180]-[0186], [0194], [0197]-[0199] - paragraphs [0200], [0204]-[0206], [0213], [0215], [0220]-[0223] - paragraphs [0225], [0227]-[0230]; [0237], [0239], [0254]-[0257]	1-18, 21, 24, 27-36
A	US 20020012943 A1 (FOWLKES ET AL.) 31 January 2002 (31-01-2002) - See entire document	1-36
A	CA 2763842 A1 (KRAATZ ETAL.) 16 December 2010 (16-12-2010) - See entire document	1-36
A	WO 2022020202 A1 (WU ET AL.) 27 January 2022 (27-01-2022) - See entire document	1-36

INTERNATIONAL SEARCH REPORT

International application No.
PCT/CA2024/051053

Box No. I **Nucleotide and/or amino acid sequence(s) (Continuation of item 1.c of the first sheet)**

1. With regard to any nucleotide and/or amino acid sequence disclosed in the international application, the international search was carried out on the basis of a sequence listing:

   a. ☒ forming part of the international application as filed.

   b. ☐ furnished subsequent to the international filing date for the purposes of international search (Rule 13*ter*.1(a)),

      ☐ accompanied by a statement to the effect that the sequence listing does not go beyond the disclosure in the international application as filed.

2. ☐ With regard to any nucleotide and/or amino acid sequence disclosed in the international application, this report has been established to the extent that a meaningful search could be carried out without a WIPO Standard ST.26 compliant sequence listing.

3. Additional comments:

INTERNATIONAL SEARCH REPORT
Information on patent family members

International application No.
PCT/CA2024/051053

Patent Document Cited in Search Report	Publication Date	Patent Family Member(s)	Publication Date
CA3144887A1	14 January 2021 (14-01-2021)	EP4004531A1	01 June 2022 (01-06-2022)
		IL289593A	01 March 2022 (01-03-2022)
		KR20220028052A	08 March 2022 (08-03-2022)
		US2022260567A1	18 August 2022 (18-08-2022)
		WO2021004812A1	14 January 2021 (14-01-2021)
WO2022261776A1	22 December 2022 (22-12-2022)	None	
US2002012943A1	31 January 2002 (31-01-2002)	AU6651798A	26 August 1998 (26-08-1998)
		AU729118B2	25 January 2001 (25-01-2001)
		CA2279571A1	13 August 1998 (13-08-1998)
		CN1249815A	05 April 2000 (05-04-2000)
		EP0970375A2	12 January 2000 (12-01-2000)
		JP2002524021A	30 July 2002 (30-07-2002)
		KR20000070821A	25 November 2000 (25-11-2000)
		NO993764D0	03 August 1999 (03-08-1999)
		NO993764L	28 September 1999 (28-09-1999)
		NZ336910A	28 September 2001 (28-09-2001)
		WO9835232A2	13 August 1998 (13-08-1998)
		WO9835232A3	04 March 1999 (04-03-1999)
CA2763842A1	16 December 2010 (16-12-2010)	CN102460139A	16 May 2012 (16-05-2012)
		CN102460139B	30 April 2014 (30-04-2014)
		EP2440911A1	18 April 2012 (18-04-2012)
		EP2440911A4	13 February 2013 (13-02-2013)
		US2012073987A1	29 March 2012 (29-03-2012)
		WO2010142037A1	16 December 2010 (16-12-2010)
WO2022020202A1	27 January 2022 (27-01-2022)	US2023264192A1	24 August 2023 (24-08-2023)